5-2007

REAL TIME PROGNOSTIC STRATEGIES APPLICATION TO GAS TURBINES

Rajat Sekhon
Clemson University, rsekhon@clemson.edu

REAL TIME PROGNOSTIC STRATEGIES: APPLICATION TO GAS TURBINES

A Thesis
Presented to
the Graduate School of
Clemson University

In Partial Fulfillment
of the Requirements for the Degree
Master of Science
Mechanical Engineering

---

by
Rajat Sekhon
May 2007

Accepted by:
Dr. John Wagner, Committee Chair
Dr. Eric Austin
Dr. Ardalan Vahidi

ABSTRACT

Gas turbines are increasingly deployed throughout the world to provide electrical and mechanical power in consumer and industrial sectors. The efficiency of these complex multi-domain systems is dependant on the turbine's design, established operating envelope, environmental conditions, and maintenance schedule. A real-time health management strategy can enhance overall plant reliability through the continual monitoring of transient and steady-state system operations. The availability of sensory information for control system needs often allow diagnostic/prognostic algorithms to be executed in a parallel fashion which warn of impending system degradations. Specifically, prognostic strategies estimate the future plant behavior which leads to minimized maintenance costs through timely repairs, and hence, improved reliability. A health management system can incorporate prognostic algorithms to effectively interpret and determine the healthy working span of a gas turbine. The research project's objective is to develop real-time monitoring and prediction algorithms for simple cycle natural gas turbines to forecast short and long term system behavior.

Two real-time statistical and wavelet prognostic methods have been investigated to predict system operation. For the statistical approach, a multi-dimensional empirical description reveals dominant data trends and estimates future behavior. The wavelet approach uses second and fourth-order Daubechies wavelet coefficients to generate signal approximations that forecast future plant

operation. To complement the empirical models, a real-time analytical, lumped parameter mathematical model has been developed that describes normal transient and steady-state gas turbine system operation. The model serves as the basis to understand a simple cycle gas turbine's operation, and may be utilized in model-based diagnostic algorithms.

To validate the model and the prognostic strategies, extensive data has been gathered for a 4.5 MW Solar Mercury 50 and a 85 MW General Electric 7EA simple cycle gas turbine. For the dynamic gas turbine model, the comparison between the field data and simulation results for five Mercury 50 gas turbine signals (e.g., shaft speed, power, fuel flow, turbine rotor inlet temperature, and compressor delivery pressure) demonstrate a high degree of correspondence. Although there are some deviations between the analytical and experimental results during the transient phase, the estimated steady state results are within 2.0% of the actual data. The direct comparison of the two forecasting methods revealed that the wavelet method is superior since the forecasting error is 2.4% versus 4.0% for the statistical method on the Mercury 50 simple cycle gas turbine steady-state signals (e.g., compressor delivery pressure and turbine rotor inlet temperature). Similarly, the General Electric 7EA steady-state signal (e.g., turbine inlet temperature) offered a forecasting error of 9.23% for the wavelet and 11.47% for the statistical methods, respectively. The developed approaches successfully estimate and predict the system operation and may be used with a diagnostic algorithm to monitor gas turbine system health.

ACKNOWLEDGEMENTS

First and foremost, I would like to express my sincere thanks to my advisor, Dr. John R. Wagner. His guidance and patience during the course of my graduate experience have been invaluable. His discipline, attention to details, and emphasis on clear communication, are a few qualities that I hope, I have adopted during our association. I am grateful to Dr. Eric Austin and Dr. Ardalan Vahidi for serving on my research committee.

It gives me great joy to thank my family who has supported me in all my endeavors with love and pride. I am forever indebted to my friends and colleagues who have provided the memories of a lifetime. Special thanks to Mr. Hany Bassily for his guidance and help during my research.

I would like to acknowledge the support of Mr. Jeff Hinson and Mr. Kenny McDowell from the Clemson University Facilities staff for their assistance in experimental data logging. Additional thanks are in order to the gentlemen at the Rainy power generation station for providing extensive experimental data. The research team would also like to thank Dr. Ting Wang from the Energy Conversion and Conservation Center, University of New Orleans, New Orleans, LA.

TABLE OF CONTENTS

Table of Contents (Continued) Page

LIST OF TABLES

LIST OF FIGURES

List of Figures (Continued)

List of Figures (Continued)

List of Figures (Continued)

NOMENCLATURE

Symbol	Units	Description
A	m^2	compressor annular area
A_χ	-	signal approximation
a	-	polynomial coefficient
C_A	m/s	axial velocity of flow in compressor
C_{W1}	m/sec	whirl velocity at rotor inlet
C_{W2}	m/sec	whirl velocity at rotor outlet
c_{pa}	J/kg-K	specific heat at constant pressure, air
c_{pg}	J/kg-K	specific heat at constant pressure, gas
$\vec{D}$	-	sum of squares of deviations
d	-	scaling coefficient
d_χ	-	signal details
E	-	statistical operator for mean
e	-	scaling coefficient index
F	rad/s	function frequency
f	-	length of semi major axis
f_1, f_2	-	foci of the ellipse
h	-	length of semi minor axis
h_{03}	J/kg	combustion chamber inlet total enthalpy

Nomenclature (Continued)

Symbol	Units	Description
I_m	A	starter motor current
i	-	time index
J_c	kg-m^2	compressor inertia
J_{Eq}	kg-m^2	lumped inertia
J_L	kg-m^2	load inertia
J_M	kg-m^2	starter motor inertia
J_T	kg-m^2	turbine inertia
j	-	selected output signal number
K_t	N-m/A	torque constant
k	-	selected input signal number
k_a	-	specific heat ratio of air
k_g	-	specific heat ratio of gas
L	-	signal length
LHV	J/kg	lower heating value of fuel
m	s	final time recorded
$\dot{m}$	kg/s	mass flow rate
m_{cc}	kg	mass inside combustion chamber
$\dot{m}_f$	kg/s	fuel flow rate
$\dot{m}_3$	kg/s	combustion chamber inlet mass flow rate
$\dot{m}_4$	kg/s	combustion chamber outlet mass flow rate

Nomenclature (Continued)

Symbol	Units	Description
N	RPM	shaft speed
n	-	input signals selected
n_s	-	compressor stages
P_{0Sin}	Pa	stager inlet total pressure
P_{0Sout}	Pa	stager outlet total pressure
P_{Sout}	Pa	stager outlet static pressure
P_{01}	Pa	compressor inlet total pressure
P_{02}	Pa	compressor outlet total pressure
P_{03}	Pa	recuperator outlet total pressure
P_{04}	Pa	combustion chamber total outlet pressure
P_{05}	Pa	turbine outlet total pressure
ΔP	%	recuperator pressure drop
p	-	output signals selected
Q	kJ/kWh	heat rate
q	-	regression order index
R	J/kg-K	gas constant for air
r	-	regression order
s	-	signal component
s^2	-	variance
T_{Sout}	K	stage outlet static temperature

Nomenclature (Continued)

Symbol	Units	Description
T_{02}	K	compressor outlet total temperature
T_{03}	K	recuperator outlet total temperature
T_{04}	K	turbine inlet total temperature
T_{05}	K	turbine outlet total temperature
ΔT_{0S}	K	total temperature rise in stage
t	s, minutes	time
t^*	minutes	raw data time
Δt	-	sampling rate
U	-	input signal
U_b	m/s	blade speed
U^*	-	conditioned input signal
u	-	selected input signal
u_{cc}	J/kg-K	combustion chamber internal energy
u_0, v_0	-	wavelet parameters
W_C	KW	compressor power
W_S	KW	compressor stage input power
W_T	KW	turbine power
Y	-	output signal
Y^*	-	conditioned output signal
y	-	selected output signal

Nomenclature (Continued)

Symbol	Units	Description
$\bar{y}$	-	sample mean
$\vec{Z}$	-	regression curve
χ	-	translation variable
ψ	-	mother wavelet
$\hat{\psi}$	-	fourier transform of mother wavelet
η	-	dilation variable
ϕ	-	scaling function
γ	-	input variable detail coefficients
$\hat{\gamma}$	-	output variable detail coefficients
ξ	-	input variable approximation coefficients
$\hat{\xi}$	-	output variable approximation coefficients
κ_d	-	signal disturbance component
κ_n	-	signal noise component
ε	-	forecast error
ϑ	-	wavelet function energy
$\Re$	-	correlation coefficient
ς	-	admissibility constant
σ	-	standard deviation
α	deg	air angle
η	-	dilation variable
η_C		compressor isentropic efficiency
η_R	-	recuperator isentropic efficiency

Nomenclature (Continued)

Symbol	Units	Description
η_s	-	stage isentropic efficiency
η_T	-	turbine isentropic efficiency
τ_C	N-m	compressor torque
τ_{Fric}	N-m	friction torque
τ_L	N-m	load torque
τ_M	N-m	starter motor torque
τ_T	N-m	turbine torque
ω	rad/s	shaft speed
ξ_b	s	combustion chamber time constant
ψ	-	temperature coefficient
ρ_{Sout}	kg/m^3	density of stage mass flow

CHAPTER 1

INTRODUCTION

Gas turbines are a vital part of world industry, by providing mechanical power for transportation, power generation, and manufacturing plants. The world average annual gas turbine market is estimated at 20B Euros of which aviation accounts for 68%, electric production 27%, power drives 3%, and marine gas turbines 2% (Langston, 2005). The growing need for reliable electricity has prompted the design of stationary gas turbines which operate on multiple fuels such as diesel, natural gas, synthetic coal gas, and others. The power generating gas turbines contribute approximately 15% of the world's 16,230 trillion watt hours of annual electricity production. To better monitor and control these complex machines, a complete analysis for prediction of the transient operation is required with accompanying mathematical description.

The reliability, availability, and maintainability technical area of the high efficiency engines and turbines program encompasses the design of gas turbine health management systems. The introduction of real-time diagnostic and prognostic capabilities on gas turbines can provide increased reliability, safety, and efficiency. The diagnostic module is responsible for the prompt detection of system degradations. Prognostic activities are focused on the prediction of anomalous plant behavior such that maintenance measures may be performed to permit continued operation.

The two primary monitoring approaches for dynamic systems (including stationary gas turbines) can be classified as model-based and model-free. For the model- based approach, a real-time mathematical model based on laws of thermodynamics and physics is required to simulate a system's operation. However a mathematical model's behavior estimation and predictions often deviate from the experimental data. Hence, model-free approaches were adopted for system behavior predictions. Methodologies have been developed which use statistical and wavelet analysis to find system trends and make valid predictions based on observed trends.

Research Objectives and Goals

The main objective of this research was to develop a real-time health management system for gas turbines to improve turbine reliability and allow higher availability levels. The formulation and implementation of real-time diagnostic and prognostic strategies, which detect and predict the onset of system degradation and maintenance needs, will constantly monitor the overall system performance to reduce operation and maintenance costs. A series of four goals were identified.

Analytical Modeling of the Turbine System

A model-based system health management approach requires the existence of a real-time mathematical model that describes the turbine system using differential and algebraic equations. The model should depict the "normal" turbine system behavior. This research has developed a transient gas turbine model. The major components have been modeled as subsystems and linked together to create

a simulation tool. The model simulates a Mercury 50 gas turbine located at Clemson University.

Real-Time Turbine Sensor Experimental Data Streaming

Real-time experimental data has been collected and recorded from the Mercury 50 gas turbine located at the Clemson University main campus. The performance of the Mercury 50 can be evaluated using this streamed data. The benefit of such a data collection connection is that it can be used to formulate a database for turbine health management systems. Further, extensive data sets have been obtained from a General Electric 7EA gas turbine. The periodic experimental data recorded from the Mercury 50 gas turbine runs has been used to validate the mathematical model. The diagnostic/prognostic algorithms have been validated using data from both of the above mentioned gas turbines.

Sensor Fusion for Data Analysis

Initially a set of twenty-eight plant signals was selected to be monitored and recorded from the Mercury 50. The total available number of signals is 180. This smaller subset of signals is being recorded in real-time and can be fused to monitor the system. These signals include key temperature and pressure measurements which will be used for model validation and in the diagnostic/prognostic module. Similar procedure was adopted for the General Electric 7EA gas turbine as well.

Prognostic Module Design

Prognostic methods using statistics and wavelet transforms have been developed to analyze a given population of experimental data points. The

statistical method visually presents the data in multi-dimensional views and incorporates regression to predict. Furthermore the method gives a clear visual representation of the variability of the data. The second method uses wavelet transforms to remove noise from the signal and then a least square fit is performed for prediction, this prognostic module has been implemented in real time to predict system degradation.

Thesis Organization

Chapter 2 presents a literature review which examines the recent advancement in system health management and mathematical modeling of stationary gas turbines. Chapter 3 establishes the analytical modeling technique to formulate a mathematical description of a Mercury 50 stationary gas turbine for diagnostic/prognostic methodologies. Chapter 4 presents two real-time prognostic strategies, which monitor and predict the behavior of a stationary gas turbine system. Chapter 5 gives a description of the experimental setups used to obtain field data. Chapter 6 presents the experimental and numerical results. Conclusions and reccomendations will be presented in Chapter 7. Appendix A gives the details of the real-time mathematical model. Appendix B presents the data acquisition algorithm for the Mercury 50 gas turbine. The statistical and prognostic algorithm codes have been presented in Appendix C. Appendix D presents the statistical and the wavelet coefficients used for forecasting the selected turbine output signals.

CHAPTER 2

LITERATURE SURVEY

Prognostics

To introduce the work in the field of system health management and prognostics, a list of references is presented which offers insight into the past and current work. Prognostic strategies attempt to diagnose machine/component impending failure conditions, and estimate the remaining useful lifetime using statistical approach for enhanced equipment availability while minimizing maintenance costs (Roemer *et al.,* 2001). Traditional health management systems have been mainly concerned with diagnostics, but in the past decade, considerable work has taken place on prognostics. It has increasingly been recognized that the prognostics module may be integrated with existing diagnostic system architectures (Roemer and Kacprzynski, 2000). Efforts to automate plant monitoring using a novel approach which integrates neural networks with rule extraction has been demonstrated by Brotherton *et al.* (2000). Jaw (1999) presented a methodology using artificial neural networks to capture the time varying behavior of complex systems to improve the fidelity of models used for real time prognostic algorithms in aircrafts.

DePold and Gass (1998) proposed a prognostic system for gas turbines using statistical analysis to improve data quality, neural networks to detect trends to classify system changes, and an expert system to rank maintenance action. Real time statistical prognostics, in conjunction with sensor based diagnostics have

been used in industry to predict turbine critical component life. An implementation of this prognosis approach to predict the remaining useful life of gas turbine engine bearings has been examined by Orsag *et al.* (2004). Kacprzynski *et al.* (2002) investigated the application of stochastic failure models, calibrated for current state information, to assess current and future system health. Greitzer and Ferryman (2003) developed a generic prognostic and diagnostic integrated module for mechanical systems. The technology was explored on land/naval gas turbines to decrease the short and long term operating and logistic costs. The inherent uncertainties of prognostics have been addressed through probabilistic architectures. Compressor fouling, an inevitable deterioration mode in gas turbines, occurs at different rates for different turbine systems. Gulen *et al.* (2002) investigated an on-line real time prognostic strategy which can manage maintenance (e.g., washing) costs to reduce compressor fouling by as much as 20%. Similar work has also been carried out for offshore gas turbines by Veer *et al.* (2004).

Friend (2000) demonstrated the integration of intelligent processing and data fusion to obtain valuable information for system diagnostics and prognostics. Correlation of data from key sensors is used to derive actual life consumed and the remaining useful life. Pawlowski *et al.* (2002) have made efforts to apply real time prognostics to diesel engines using an architecture similar to the gas turbine prognostics for M1 Abrams tanks. Finally, prognostics can be applied to most mechanical systems for condition based maintenance and prediction of future health using wavelets. A generic framework using wavelet neural networks has

been developed and validated by Wang and Vachtsevanos (2001). Process prognostics is always associated with uncertainties; therefore, confidence bounds need to be defined for predictions. A method to estimate confidence bounds and reduce uncertainties in real-time has been established by Barlas *et al.* (2003). An opportunity exists to directly compare the estimation performance of prognostic strategies on a common problem.

Gas Turbine Mathematical Models

Aggarwal and Younis (1982) proposed a mathematical model to simulate the startup of gas turbines. The starting characteristics were estimated to asses the overall performance of a starting system for an aircraft engine. Rowen (1992) modeled a single shaft gas turbine used in variable speed mechanical drives. The model was integrated into a complex simulation involving driven equipment and controlled processes. Crosa *et al.* (1996) proposed a simulator for estimating the off-design and dynamic behavior of a heavy duty gas turbines used in combined cycles, using Simulink/Matlab. Camporeale *et al.* (1998) introduced a simulation model of a multi-shaft regenerative gas turbine. This model was used for the synthesis of system controllers and analysis of critical operating conditions for a counter-flow regenerator. Transient response of regenerative gas turbines was also investigated by Korakiantitis *et al.* (1993) using instantaneous and transient flow component models.

Vroemen *et al.* (1998) applied model based predictive control (MPC) to laboratory gas turbines, nonlinear extensions were made to linear model predictive control. This process uses a model of a gas turbine to predict future

system response. Fortunato *et al.* (2002) investigated a real-time high fidelity code for simulating the operation of a double shaft industrial gas turbine. The lumped parameter, non-linear model was used for designing and testing control systems for gas turbines. Further applications for design and optimization of control structures using a dynamic model simulating a wide range of operating scenarios for a cogeneration nuclear gas turbine power plant have been introduced by Kikstra and Verkooijen (2002).

CHAPTER 3

A REAL-TIME GAS TURBINE DYNAMIC MODEL

Gas turbines are a vital part of world industry by providing mechanical power for transportation, power generation, and manufacturing plants. To ensure the dependability of these complex multi-domain systems, a health monitoring system can be attached to the controller in a parallel manner. The growing demand for reliable electricity has prompted the design of stationary gas turbines which operate on multiple fuels such as diesel, natural gas, synthetic coal gas, and others. To better monitor and control these complex machines, a complete analysis to predict the transient operation is required with accompanying mathematical description. Gas turbines undergo transient operations due to startups, changing loads, and sudden shutdowns which may lead to system degradation over a period of time. To understand the turbine dynamic behavior, these transient conditions have to be analyzed.

Often it is not possible to perform test bed experiments on turbine systems due to safety and cost related issues. Therefore, physical models of these complex systems must be developed which simulate the actual turbine system operation over a range of different operating scenarios. Many different dynamic models for gas turbines have been developed in the past (e.g., Szuch 1978, Bettocchi *et al.*, 1996, and Crosa *et al.*, 1996). These models capture the dynamics of the turbine systems with varying degree of accuracy. Although various models have been created for gas turbine system, they are mostly used to simulate the steady state

operation, and hence, overlook the fact that cost and safety related issues are strongly influenced by a turbine's transient operation.

As many concerns arise within the gas turbine industry concerning performance and emissions related issues, it is important to develop efficient health monitoring solutions for the future to limit degradations in system performance and enhance overall plant operations. A nonlinear dynamic model has been developed for a gas turbine. The model simulates the transient and steady state gas turbine's nominal operating conditions. The development of the model presented in this chapter is a part of a strategy aimed at the introduction of on-line diagnostic and prognostic capabilities to the stationary gas turbine operations which would provide increased reliability, safety, and efficiency in gas turbine operations. Model-based diagnostic methods eliminate the need for redundant hardware through the use of analytically estimated plant output for comparison. In creating a mathematical model which can successfully detect and alert system administrators that a problem exists, the need for plant or system maintenance can be reduced.

Analytical Gas Turbine Model

The reliability of a physical system simulation is dependent the model's accuracy. The quantitative modeling of a dynamic process requires knowledge of the process, and ability to mathematically represent it using differential and algebraic equations, and availability of system parameters. A real-time nonlinear mathematical model, based on analytical and empirical relations, has been created to estimate a "normal" turbine system's operation. A nonlinear approach was

adopted to model the dynamics due to transients during start up, load changes, and shutdown. The thermodynamic model presented in this section was developed as a sequence of interconnected subsystems (refer to Figure 3.1).

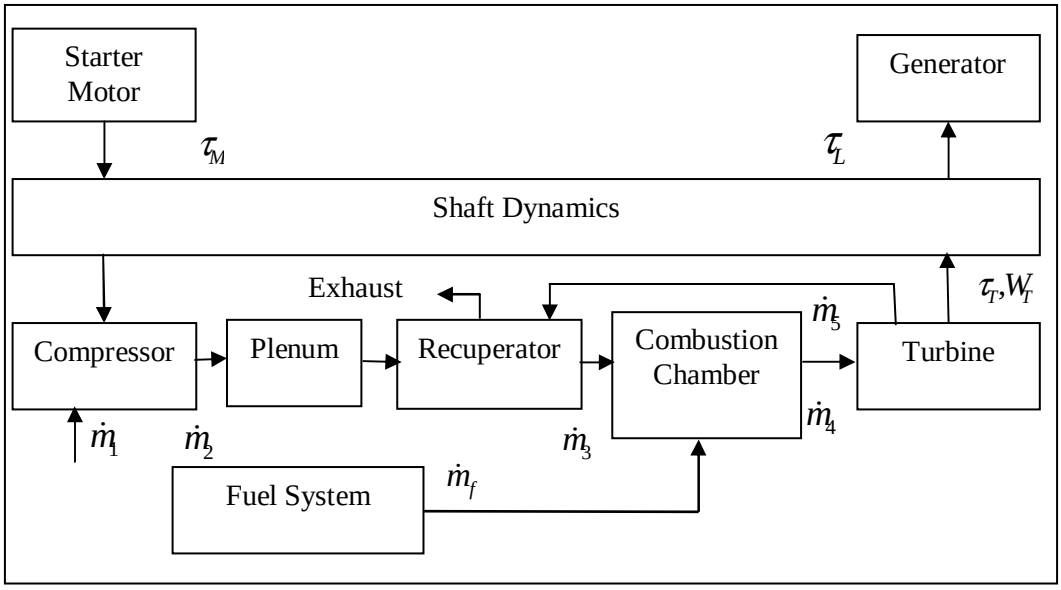

Figure 3.1 Turbine subsystems diagram which reflects the components with signal flow direction

These subsystems model the basic components of a stationary gas turbine. Physical and thermodynamic laws (Howell and Buckius, 1987) have been used to describe the system dynamics. The dynamic balance of the rotating shaft has also been modeled. This mathematical model has been transformed into a computer algorithm in the MATLAB/Simulink environment. As the model has a modular structure, additional subsystems can be incorporated to model a different system configuration (e.g., Rowen, 1992).

The proposed gas turbine system model takes a transient approach to mathematical modeling. Figure 3.1 shows the basic components of a stationary gas turbine which have been used for modeling. Each subsystem of the gas turbine plant was modeled separately including the starter motor, compressor,

combustion chamber, turbine, fuel input, and the electrical power generator. Inlet air is compressed in the compressor and is then passed through the recuperator where it gains heat energy from the turbine exhaust gases. The combustion chamber imparts additional energy to the flow mass, which is utilized in the turbine to obtain work. The system load and starter motor are both connected to the system shaft. The system receives initial inputs of ambient pressure and temperature. Using these system inputs the model simulates the initial cold start of the gas turbine system to steady state operation.

Thermodynamic Analysis

The model is based on a modified Brayton cycle. A temperature-entropy diagram is shown for a Brayton cycle (Sarvanamutto *et al.*, 2001) in Figure 3.2. The air mass enters the system at Station 1 (refer to Figure 3.3). The compressor performs work on the air mass and increases its pressure and temperature adiabatically to the compressor's exit at Station 2. The vertical line 1 to 2 depicts ideal isentropic compression. In reality, there is an increase in the entropy of the process flow. The compression is not isentropic and the process may be depicted by the line 1 to 2A. Heat addition takes place in the recuperator as depicted by line 2A to 3. Additional heat is added to the flow at constant pressure in the combustion chamber depicted by line 3 to 4. Further isentropic expansion of the air mass takes place in the turbine as work is done by the flow (line 4 to 5). Again, the process is not ideally isentropic so the process line leans towards the right. The area under the T-s curve is proportional to the useful work derived from the system.

A series of nine assumptions (e.g., Ailer *et al.*, 2001) have been imposed to model the gas turbine:

A.1 Ideal gas behavior of the working medium

A.2 All the power is absorbed by the rotor. The stator merely transforms the kinetic energy into an increase in static pressure.

A.3 The mass flow rate inside the compressor is constant.

A.4 Compression process is adiabatic.

A.5 Axial velocity of the air mass flow inside the compressor is constant.

A.6 No air bleed occurs from the compressor.

A.7 The combustion chamber is modeled as a pure energy accumulator.

A.8 Expansion process in the turbine is adiabatic.

A.9 Mean value of specific heats for each subsystem.

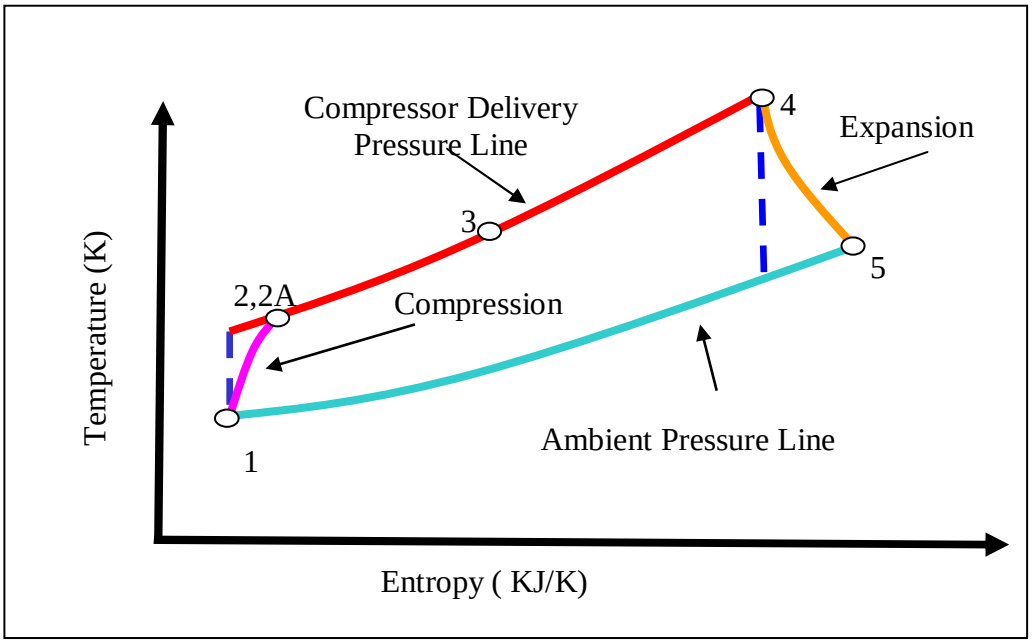

Figure 3.2 Modified temperature versus entropy diagram for the Brayton cycle (Sarvanamutto *et al.*, 2001)

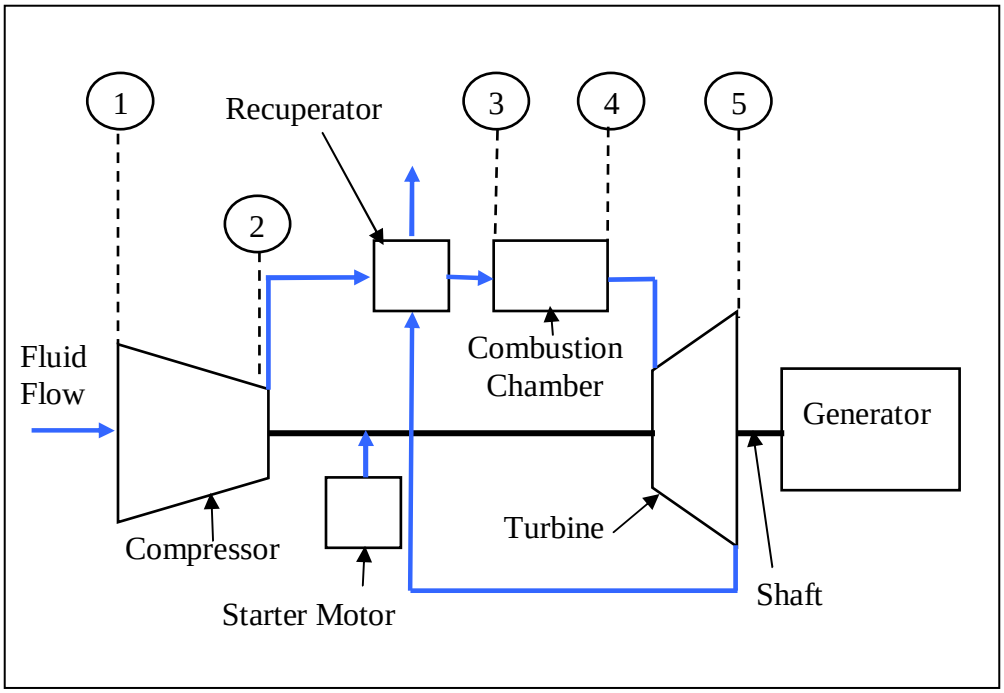

Figure 3.3 Stationary gas turbine system components with five stations identified for analysis

Model Description

The various gas turbine subsystems will be modeled and analyzed in this section with the explicit presentation of the governing differential and algebraic equations.

Compressor

The compressor is modeled as a control volume in which mass and energy flow are conserved. The compressor subsystem's thermodynamic analysis was considered using a control volume with air as the working medium. As shown in Figure 3.4, the boundary conditions include the inlet stagnation pressure, P_{01}, inlet temperature, T_{01} compressor exit pressure, P_{02} and compressor exit temperature, T_{02}.

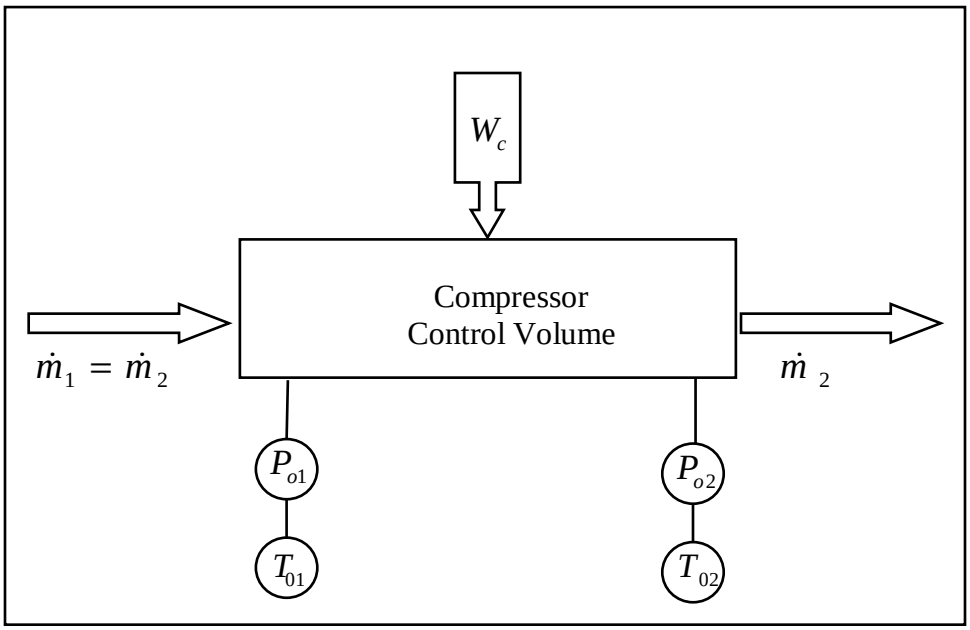

Figure 3.4 Compressor block diagram with input and output variables

Compressor Maps

The compressor mass flow rate has been approximated using variable inlet guide vane angles (VIGV) and flow velocity inside the compressor as compressor maps (Walsh and Fletcher, 2004) are not available for the Mercury 50. The derived mass flow rate is a function of pressure ratio for different rotational speeds. The Mercury 50 gas turbine has a ten stage compressor and a two stage turbine. The typical sketch of a compressor stage is shown in Figure 3.5.

A series of eighth additional assumptions are made for the analysis of the compressor performance, and hence, to draw the compressor maps:

A.10 The increase in the stagnation pressure is accomplished wholly within the rotor.

A.11 The inlet flow angle(α_1) is 11^o and the outlet blade angle (β_2) is 51^o.

A.12 The axial velocity is assumed to be a constant throughout the compressor stage.

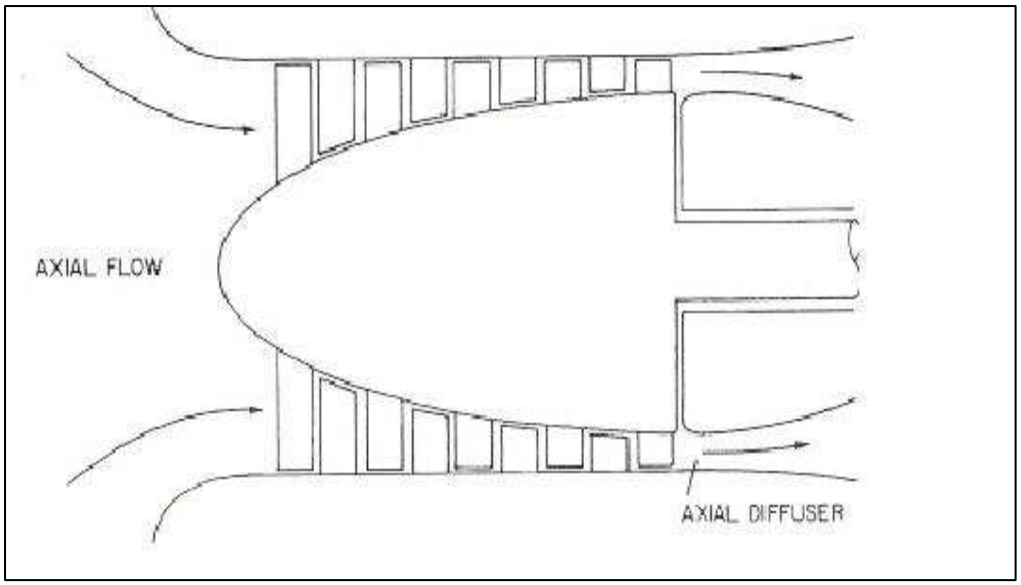

Figure 3.5 Typical cross-sectional view of a compressor stage with the stator and rotor blade profile (Saravanamutto *et al.*, 2001)

A.13 Isentropic process.

A.14 Fluid friction is neglected.

A.15 There is no loss of stagnation pressure in the stator stage.

A.16 One-dimensional flow.

A.17 Stage compression efficiency is 0.9.

The air approaches the rotor with a velocity C_1 at an angle α_1 from the axial direction (refer to Figure 3.6). Velocity relative to the blade at an angle β_1 is determined by combining C_1 vectorially with U. After passing through the rotor, the absolute velocity increases and the air leaves the rotor with a relative velocity V_2 at an angle β_2 determined by the rotor blade outlet angle. Since C_a is kept constant, the value of V_2 is obtained from the triangle relationship. The value of C_2 is determined by combining vectorially V_2 and U at an angle α_2. The air leaving the rotor at α_2, passes to the stator where it is diffused to a velocity C_3 at an angle α_3. Since $\alpha_3 = \alpha_1$ and $C_3 = C_1$, based on similar velocity triangles for each

stage, and since $C_{a1} = C_{a2} = C_a$, and from geometry of triangles as shown in Figure 3.6.

The power input to the compressor stage and change in angular momentum of air passing through the stage are related as

$$W_S = \dot{m}U\left(C_{W2} - C_{W1}\right) \tag{3.1}$$

which may be expressed in terms of the air angles and the axial velocity of flow as

$$W_S = \dot{m}UC_A\left(\tan\alpha_1 - \tan\alpha_2\right) \tag{3.2}$$

Using the steady flow energy equation, the stage temperature difference is given as

$$\Delta T_{0S} = \frac{UC_A}{c_{pa}}\left(\tan\alpha_1 - \tan\alpha_2\right) \tag{3.3}$$

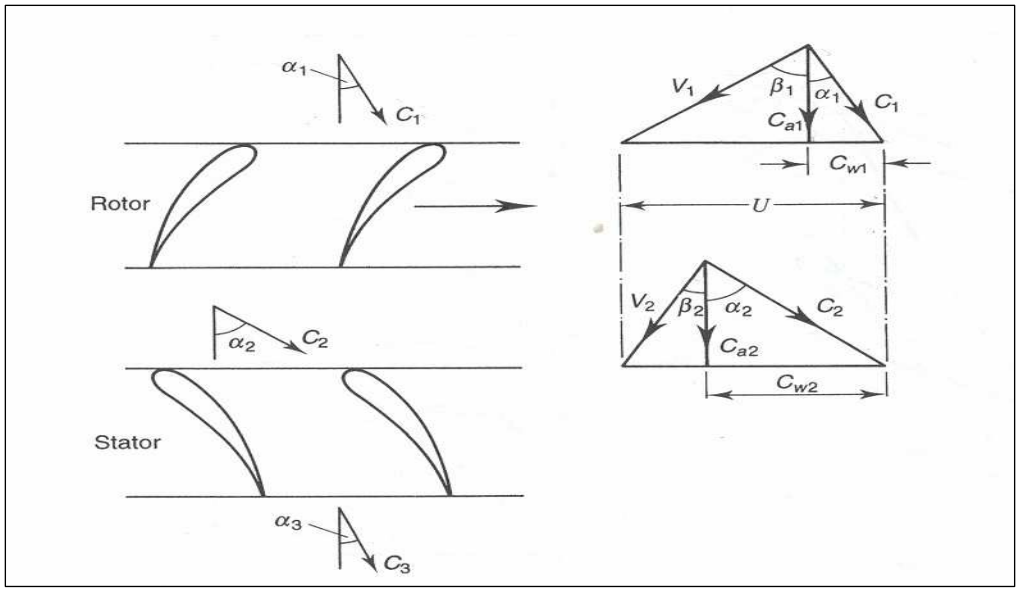

Figure 3.6. Velocity triangles for compressor's single stage (Sarvanamutto *et al.*, 2001)

The pressure ratio for a single stage with a stage isentropic efficiency, η_s, may be obtained as

$$\frac{P_{0Sout}}{P_{0Sin}} = \left[1 + \eta_S \frac{\Delta T_{0S}}{T_{0in}} \right] \tag{3.4}$$

The air mass density at the stage outlet is given as

$$\rho_{Sout} = \frac{P_{Sout}}{RT_{Sout}} \tag{3.5}$$

so that the mass flow rate becomes

$$\dot{m} = \rho_{Sout} A C_A \tag{3.6}$$

The overall temperature rise for the compressor subsystem may be obtained as

$$T_{02} - T_{01} = \frac{n\psi U^2}{c_{pa}} \tag{3.7}$$

Where ψ is the compressor temperature coefficient, and is determined empirically. C_{pa} is the specific heat capacity of the incoming air mass.

The compressor subsystem pressure ratio is given as

$$\frac{P_{02}}{P_{01}} = \left[1 + \eta_c \left(\frac{T_{02} - T_{01}}{T_{01}} \right) \right]^{\frac{k_a}{k_a - 1}} \tag{3.8}$$

Finally, the work input to the compressor subsystem may be given as

$$W_c = \dot{m} c_{pa} \left(T_{02} - T_{01} \right) \tag{3.9}$$

The modeled compressor of a Mercury 50 gas turbine is shown in Figure 3.7. A small compressor torque value is desired since it represents the work performed to

compress the air which reduces the overall efficiency. The compressor torque is dependent on the mass flow rate through the gas turbine, the inlet and outlet temperatures, and the compressor shaft speed.

Plenum

During transient operation of the turbine, the flow rate changes due to variations in the fuel flow rate which is a function of the shaft speed and load. The mass flow rate inside the combustion chamber may be momentarily different than the mass flow rate inside the compressor. To account for this variance, a plenum is introduced in the turbine model which acts as a mass capacitor. The plenum hypothetically releases (or absorbs) air mass to maintain a steady mass flow rate. Hence, the unsteady mass balance is modeled through an adiabatic capacity (plenum) with no energy involved. As shown in Figure 3.8, the plenum is considered as a control volume.

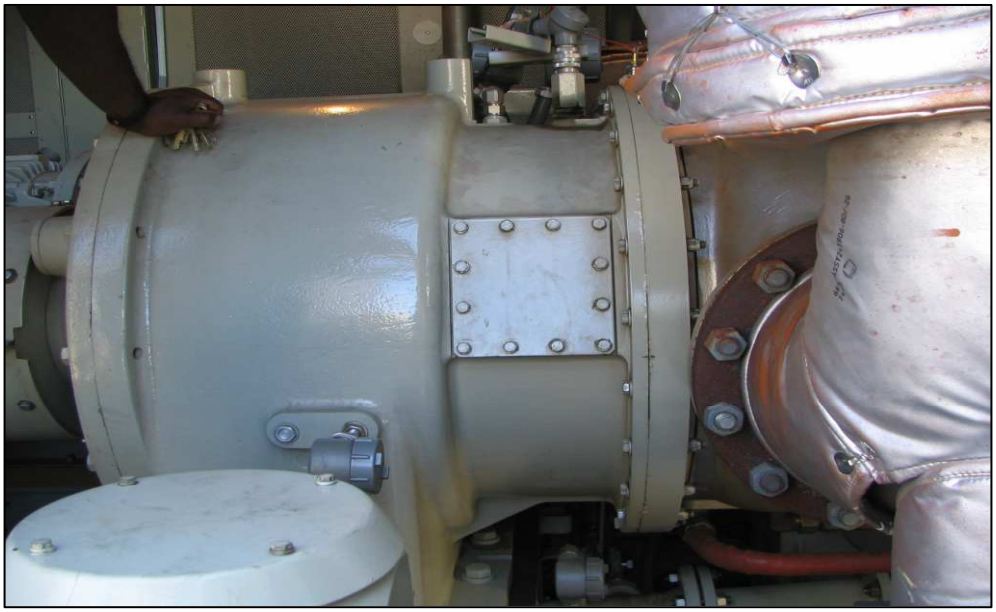

Figure 3.7 Mercury 50 gas turbine compressor located at Clemson University's campus facilities plant

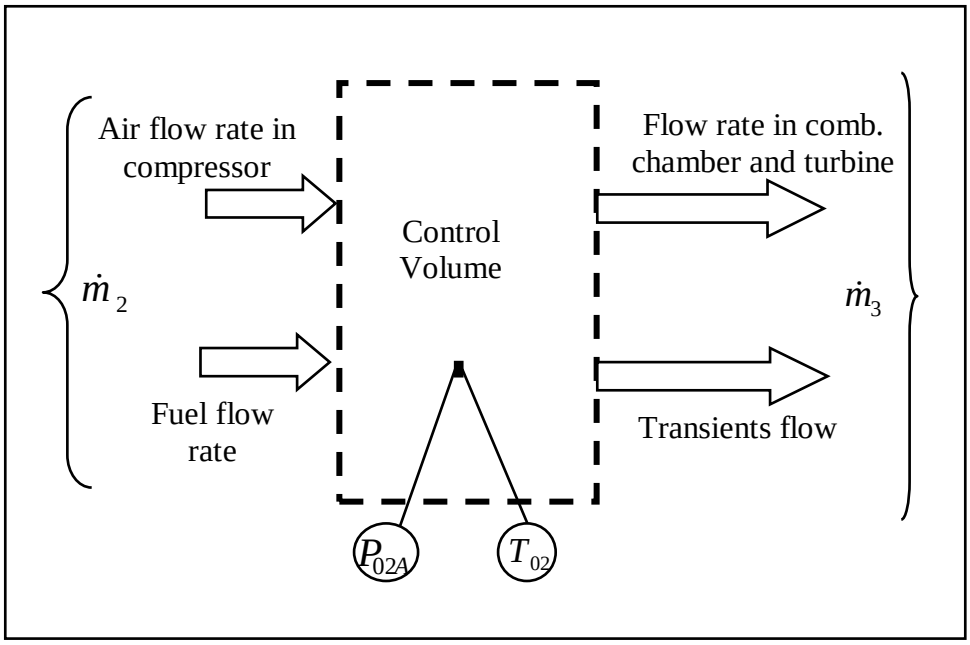

Figure 3.8 Plenum block diagram with input and output variables

The plenum is placed upstream of the combustion chamber to accommodate the unsteady mass balance within the compressor ducts, combustion chamber, and the turbine ducts. The flow velocity is assumed to be negligible inside the plenum .The formulation of the plenum is based on the conservation of mass from which the time derivative of the compressor outlet pressure, P_{02A}, is given as

$$\frac{dP_{02A}}{dt} = \frac{KRT_{02}}{V_P}\left(\dot{m}_2 - \dot{m}_3\right) \tag{3.10}$$

where V_P is the volume of the plenum, $\dot{m}_3$ is the outlet mass flow rate, and R is the gas constant, The pressure differential equation is a function of the mass flow rates $\dot{m}_2$ and $\dot{m}_3$.

Recuperator

Recuperator is the name given to the heat exchanger in a gas turbine, where heat exchange takes place between the hot and the cold stream through a separating wall. The recuperator was modeled as a control volume, with the boundary conditions as shown in Figure 3.9. Here, T_{05} is the inlet turbine exhaust temperature. The variables P_{03} and T_{03} are the exit stagnation pressure and temperature, respectively. Inside the recuperator, the hot turbine exhaust rejects heat and the fresh charge from the compressor absorbs heat. Assuming the mass flow to be constant, the heat exchange rate equation is given as

$$c_{pa}(T_{03} - T_{06}) = c_{pg}(T_{05} - T_{02}) \tag{3.11}$$

where T_{06} is the temperature of the gases exhausted from the recuperator to the atmosphere, and C_{pg} is the specific heat capacity of the exhaust gases. As a result of the heat exchange, the recuperator increases the discharge air temperature exiting the compressor. The outlet temperature for the recuperator may be expressed as

$$T_{03} = T_{02} + \eta_R \left(T_{05} - T_{02}\right) \tag{3.12}$$

where η_R is the recuperator efficiency or the thermal effectiveness. The thermal effectiveness can be increased by increasing the volume of the heat exchanges in order to obtain a higher rate of heat transfer.

There is also a pressure drop, ΔP, in the recuperator and the outlet pressure, P_{03}, is given as

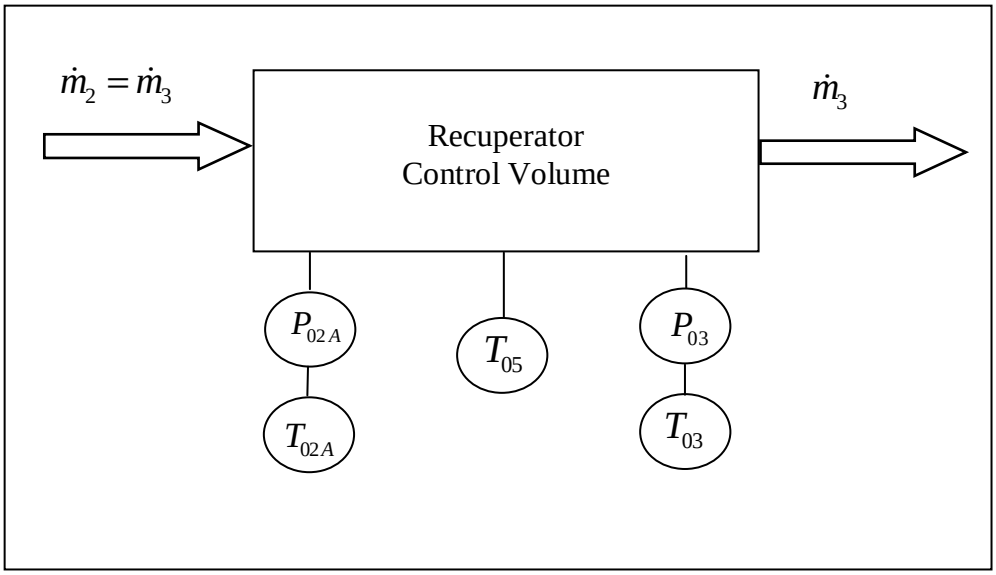

Figure 3.9. Recuperator block diagram with input and output variables

$$P_{03} = P_{02}\left(1 - \frac{\Delta P}{P_{02}}\right) \tag{3.13}$$

The pressure losses inside the recuperator are unavoidable but can be minimized by reducing the flow velocity.

Fuel System

The turbine fuel system model varies the fuel flow rate according to the shaft speed and load. During load applications, transient conditions occur which result in a variation of fuel flow with time, until steady state conditions are attained. The fuel map, shown in Figure 3.10, governs the system fuel flow, based only on the shaft speed and applied electrical generator load. The actual fuel map for the Mercury 50 gas turbine is not readily available. Therefore, this map has been generated empirically using experimental data sets recorded at Clemson University. The fuel used in the Mercury 50 turbine is natural gas with a lower heating value of 61.4 MJ/kg.

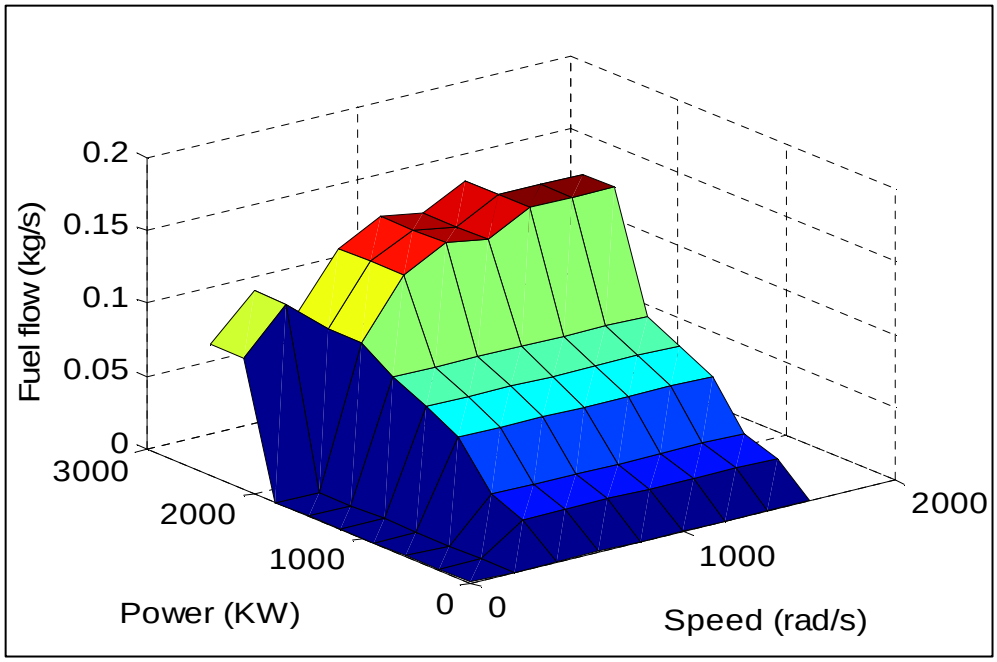

Figure 3.10. Fuel flow map based on system load and speed

Combustion Chamber

The combustion chamber (refer to Figure 3.11) is modeled as a pure energy accumulator. The inside pressure and temperature, P_{04} and T_{04}, have been assumed to be homogeneous and equal to the outlet values. The combustion chamber model is a control volume with mass and energy transfer occurring across the boundaries as shown in Figure 3.12. The energy balance is given as

$$\frac{d\left(m_{cc}u_{cc}\right)}{dt} = \dot{m}_3 h_{03} + \dot{m}_f \left(h_f + \eta_{cc} LHV\right) - \dot{m}_4 h_{04} \tag{3.14}$$

where m_{cc} and u_{cc} are the mass and the specific internal energy, respectively, of the gases inside the combustion chamber, $\dot{m}_4$ is the outlet mass flow rate, $\dot{m}_f$ is the fuel flow rate, η_{cc} is the combustor efficiency, and h_f is the enthalpy of the fuel. The acronym LHV denotes the lower heating value of the natural gas and is defined as the amount of heat released by combusting a specified quantity of the

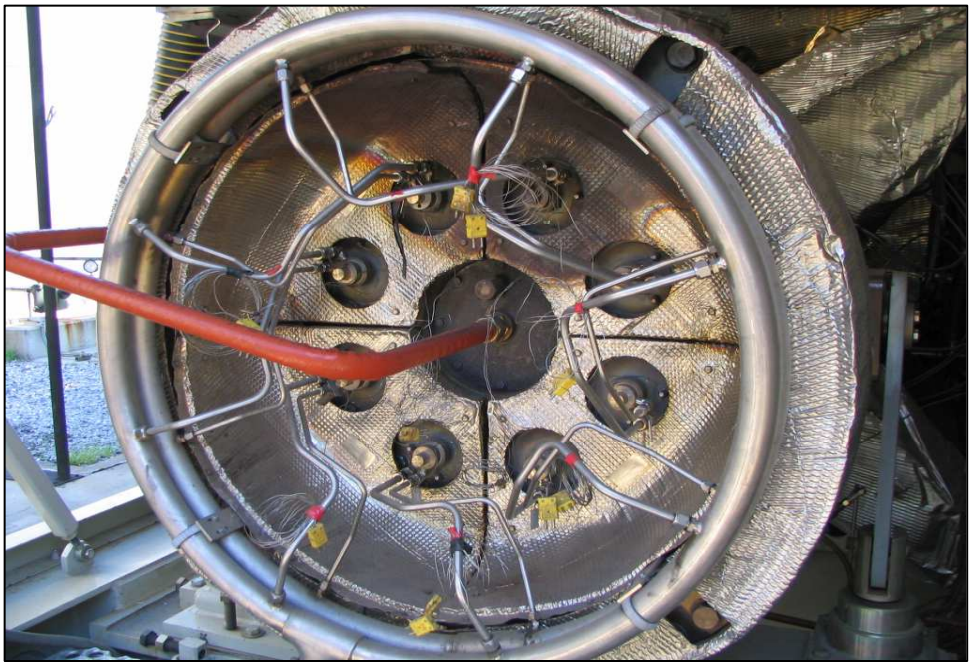

Figure 3.11. Combustion chamber of a Solar Mercury 50 gas turbine located at Clemson University

natural gas, initially at $25^{\circ}C$ and returning the temperature of the combustion products to $150^{\circ}C$.

Assuming negligible variations in the mass and internal energy, equation (3.14) may be written as

$$\xi_b \frac{dT_{04}}{dt} = \frac{\left(\dot{m}_3 h_{03} + \dot{m}_f \left(h_f + \eta_{cc} LHV\right) - \dot{m}_4 h_{04}\right)}{\dot{m}_4 c_{pg}} \tag{3.15}$$

which gives the rate of temperature change inside the combustion chamber. The time constant, ξ_b ,is given by $\xi_b = \frac{m_{cc}}{k\dot{m}_3}$. Applying the continuity equation, the exit mass flow rate becomes $\dot{m}_4 = \dot{m}_3 + \dot{m}_f$.

A pressure loss exists in the combustion chamber due to internal aerodynamic resistance and momentum changes produced by the combustion

reactions. This pressure drop was incorporated into the model and was evaluated using the Rayleigh effect, the outlet pressure may be expressed as

$$P_{04} = P_{03} + f\left(T_{04} / T_{03}\right) \tag{3.16}$$

Generally, Rayleigh analysis indicates that whenever the stagnation pressure, T_0, rises in a flow at a given Mach number there must be an associated loss in stagnation pressure, P_0, independent of the frictional losses in the flow. The pressure loss is in proportion to the heating (i.e., the rise in stagnation temperature) and is larger for Mach numbers close to unity.

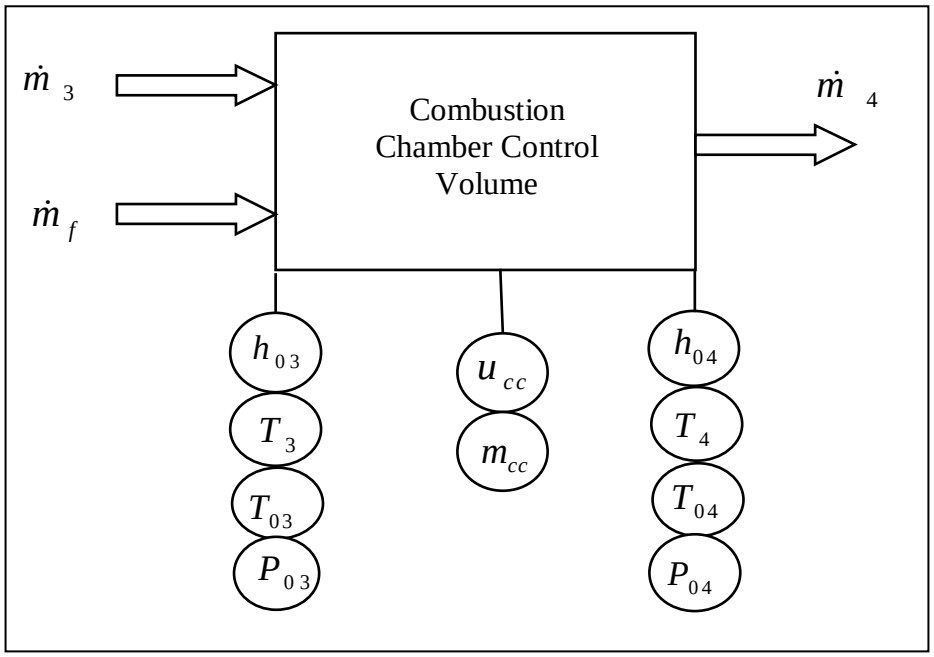

Figure 3.12 Combustion chamber block diagram showing input and output variables

Turbine Subsystem

The Mercury 50 single shaft turbine has two stages with no reheat capabilities. The subsystem was modeled as a single control volume with the boundary conditions shown in Figure 3.13. Hot gases at pressure P_{04} and

temperature T_{04} are supplied to the turbine where the hot gases expand and do work on the turbine blades. The power produced by the expanding gases is given as

$$W_T = \dot{m}_4 c_{pg} \left(T_{04} - T_{05} \right) \tag{3.17}$$

The turbine outlet temperature is given as

$$T_{05} = T_{04} \left(1 - \eta_T \left(1 - \left(\frac{P_{05}}{P_{04}} \right)^{\frac{k_g - 1}{k_g}} \right) \right) \tag{3.18}$$

The parameter, η_T, is the efficiency of the turbine. The exit pressure P_{05} is considered atmospheric. Per equation (3.18), a greater difference between the turbine inlet and outlet temperatures allows more work to be extracted from the expanding gases. However there is a limit to the value of the turbine inlet temperature due to material and design constraints. Hence, a low exit temperature may be desired.

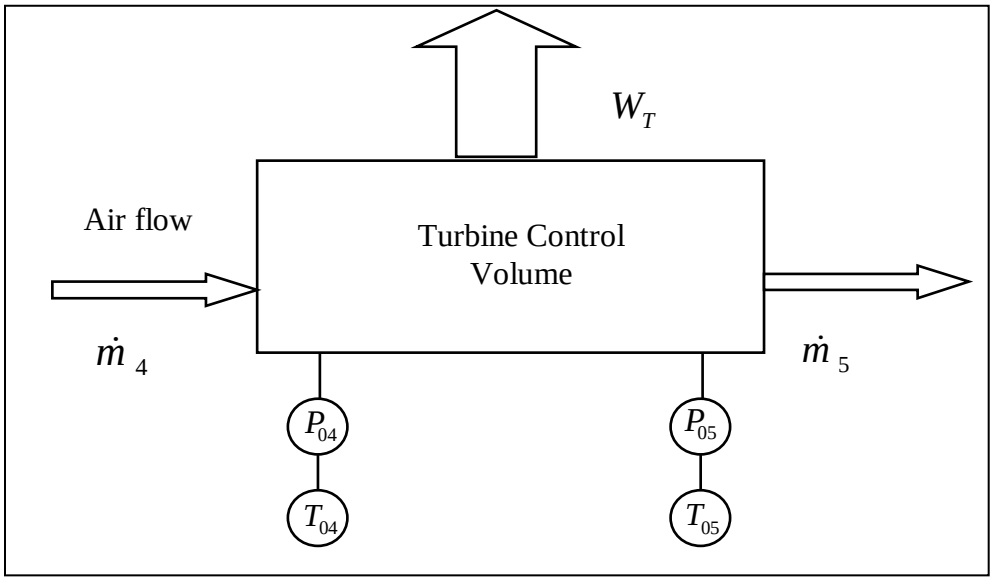

Figure 3.13. Turbine subsystem block diagram with inlet and outlet variables

Shaft Dynamics

The shaft dynamics model considers the torque inputs/outputs from the turbine, compressor, starter motor, the generator, as well as friction. Applying Newton's law to the torque balance offers the equation

$$\frac{d\omega}{dt} = \left(\frac{\tau_T + \tau_M - \tau_C - \tau_{Fric} - \tau_L}{J_{Eq}} \right) \tag{3.19}$$

where $J_{Eq} = J_c + J_T + J_M + J_L$ is the lumped inertia of the compressor, turbine, starter motor, and generator. Figure 3.14 shows the various torques acting on the stationary gas turbine. These moments of inertia are with respect to the centerline of the turbine shaft.

Starter Motor and Generator Load

For the normal gas turbine start up process which brings the turbine shaft to a nominal angular velocity, the starter motor model was introduced. The induction starter motor provides the start up torque to ramp the speed from zero to approximately 67% of the turbine nominal rotational speed (14,800 RPM) at which starter dropout occurs. The starter motor is connected directly to the turbine system shaft. The starter motor also provides necessary torque to drive the compressor during the purge crank phase. This cycle occurs at 27% of the turbine nominal rotational speed and helps to drive out any residual fuel from the exhaust system.

The torque generated by the starter motor is given as

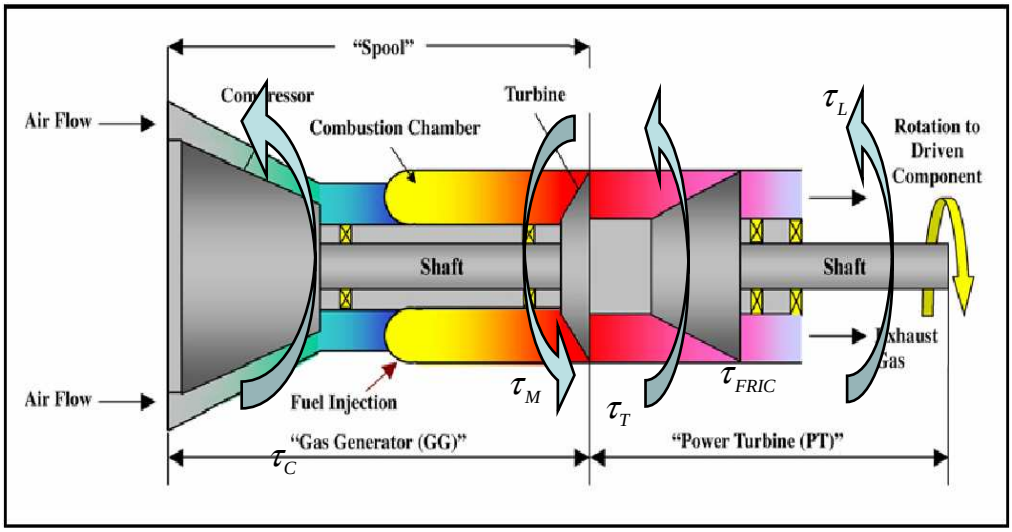

Figure 3.14 Torques acting on a stationary gas turbine during its operation

$$\tau_M = K_t I_M \tag{3.20}$$

where I_M is the armature current given as

$$\frac{dI_M}{dt} = \frac{1}{L}(-R_A I + V_S - K_B \omega) \tag{3.21}$$

To determine the usable power that is obtained from the gas turbine engine the power generator subsystem of the gas turbine was modeled. This in effect converts the usable torque created by the turbine subsystem, torque not used to power the compressor, into electrical energy. For this model the generator portion of the gas turbine is modeled as the load subsystem where the load is applied at different times. The generator load is an input to the dynamic model and can be adjusted based on power generation needs. In other words the variation of the load input allows the model to be adapted to different operating conditions.

Symbol	Value	Units
A	0.19	m^2
c_{pa}	1005	J/kg-K
c_{pa}	1148	J/kg-K
C_A	150	m/s
h_f	4.6e03	J/kg
I_M	25	Amp
J_{Eq}	0.4	kg-m^2
k_a	1.4	
k_g	1.33	
LHV	61e06	J/kg
m_{cc}	1	kg
n	10	
P_{01}	101.3	KPa
ΔP	3 %	
T_{01}	298	K
R	287.4	J/kg-k
U	250	m/s
η_c	0.9	
η_{cc}	0.95	
η_R	0.85	
η_T	0.9	
η_S	0.9	
τ_{Fric}	30	N-m
ψ	0.35	

Table 3.1 Summary of model parameters for the Mercury-50

A variety of model input/output signals have been considered including the generator power, shaft speed, fuel flow, compressor outlet pressure, and combustion chamber outlet temperature. A list of model parameters is provided in Table 3.1. To validate the mathematical model, comparisons between the analytical model and the experimental results from the Mercury 50 gas turbine have been studied and are presented in Chapter 6.

CHAPTER 4

REAL-TIME PROGNOSTIC STRATEGIES

Health monitoring strategies estimate the current and future conditions of a system to increase performance, reliability, and reduce maintenance and replacement costs. Prognostic is a key component of these strategies and operates in parallel with diagnostic modules to monitor and predict plant behavior. The analysis of system health and prediction of remaining useful life may be classified as prognostics. Prognostics use past and current system operation data, individual system histories, and system response characteristics to forecast behavior, hence, providing a reliable health monitoring methodology (Greitzer and Ferryman, 2003). The research project's objective is to develop real-time monitoring and prediction algorithms for stationary gas turbines to forecast short and long term system health and readiness using behavior models, sensor fusion, and statistical analysis.

Gas turbines can experience various system faults during their operating schedules. These complex multi-domain turbine systems operate under varying conditions and locations which demand high reliability so unscheduled "down time" must be minimized by reducing susceptibility to degradations and breakdowns. A health management system can incorporate prognostic algorithms to effectively interpret and determine the healthy working span of a gas turbine. Compressor fouling due to the deposition of inlet air particles is a common problem encountered in normal operation. Some of the other typical system

degradations include fuel nozzle erosion, nozzle choke, and compressor surge (Boyce, 2005). System anomalies such as air intake clogging, inlet guide vane distortion, and oil blockage are less common but can lead to serious system damage and need to be avoided (McAlpin *et al.,* 2003). During the past few years, turbine faults including blade failure and recuperator leaks have occurred in the Mercury 50 gas turbine located at Clemson University.

To successfully control a gas turbine, from a maintenance perspective, the critical operating scenarios such as compressor surge, excessive turbine inlet temperature, flame out, and high rotational shaft speed must be avoided. A health management system is typically a combination of diagnostic and prognostic modules which complement the plant controller in a parallel manner (refer to Figure 4.1).

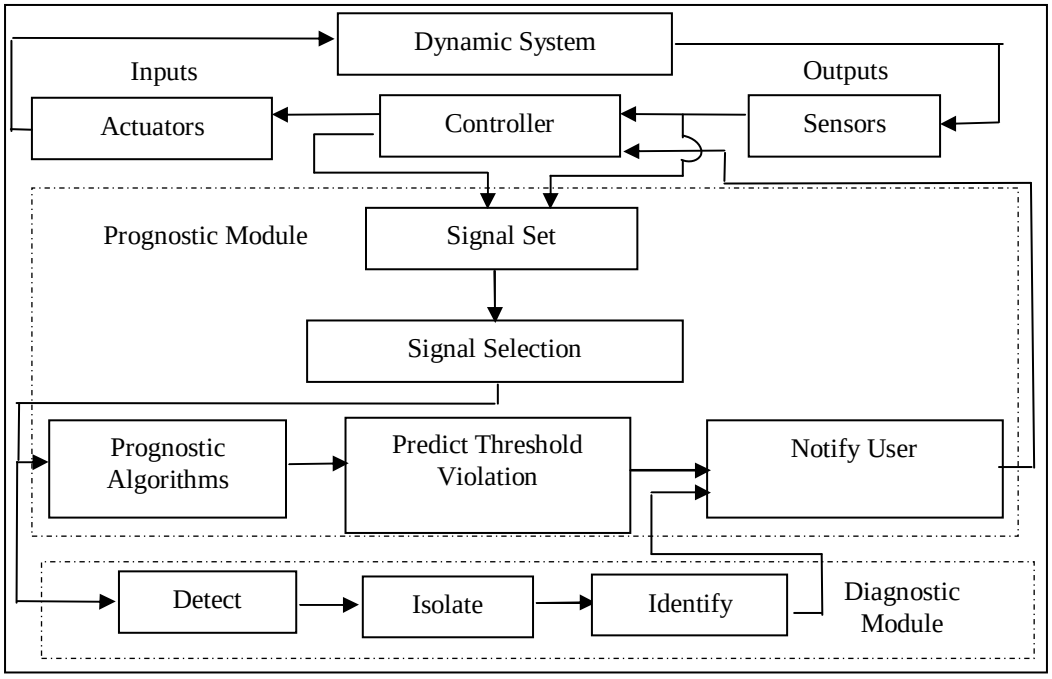

Figure 4.1. Integration of prognostic and diagnostic module with the plant controller for predictive calculations

The implementation of these real-time modules allows the detection and prediction of abnormal system behavior. Diagnostic strategies utilize hardware and software to detect, isolate, and identify a deviation from the normal plant behavior. Prognostic algorithms focus on the estimation of the current health and may predict critical component life. Prognostic strategies predict the future health state of a system (or component) from the present operating conditions and historical data.

The application of prognostics to a dynamic system can be based on different methods including physical and empirical models. The mathematical models can simulate the dynamic system behavior at a future time for a given set of inputs. The reliability of a model based prognostic strategy is dependent on the model's accuracy which requires an adequate understanding of the process and its mathematical representation. Other approaches may incorporate the formulation of rules based on data gathered from practical experience, and the creation of statistical models which determine behavioral trends. Developing these rules and statistical models often requires extensive data for healthy as well as faulty dynamic system operation. One drawback of these approaches is that acquiring a vast experimental database is not always feasible. The selection of a specific strategy is dependent on factors such as the availability of sensor data, frequency of system or component failure, severity of failure, financial constraints, and impact of system failures (Byington *et al.*, 2002).

A statistical and a wavelet approach have been investigated for gas turbine health prognostics (refer to Figure 4.2). The real-time statistical strategy uses the

logged sensor data to identify trends. Short and long time trends are computed using regression analysis. This technique predicts the time to failure, or threshold violation, by forecasting system health at any desired future time. The second strategy is based on wavelet analysis. Wavelet transforms of real-time data are used to compute the wavelet coefficients for a given turbine signal. A regression analysis of these coefficients can be performed to forecast these coefficients for the desired prediction time. The new set of coefficients obtained can be used to reconstruct the signal, and hence, obtain the prediction of the signal values for future times.

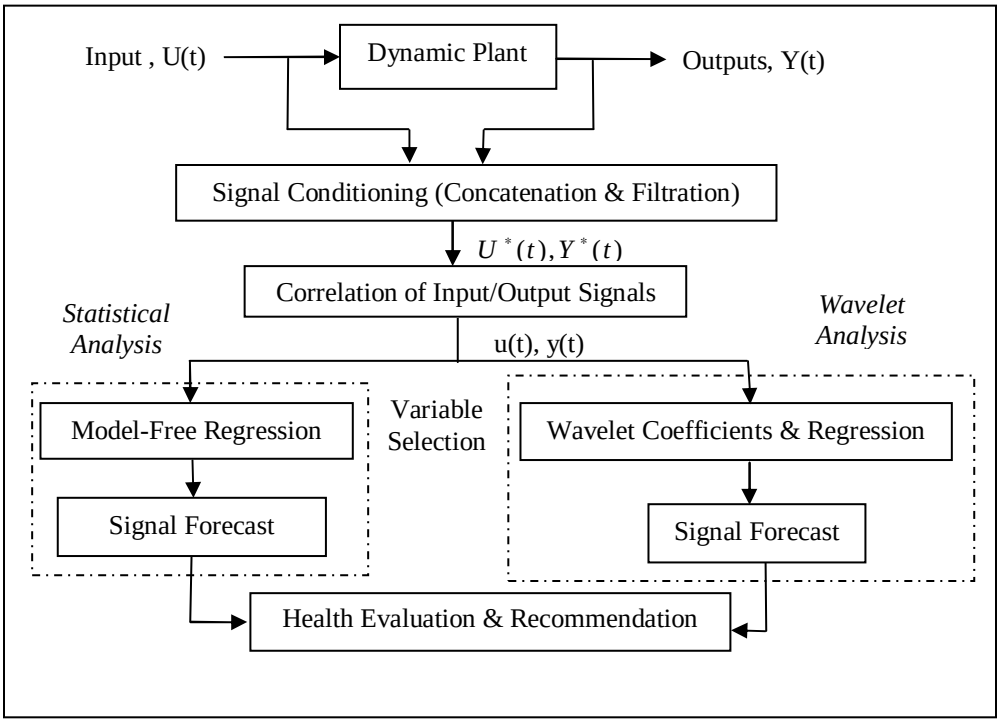

Figure 4.2. Statistical and wavelet prognostic strategies with forecasting

Statistical Prognostic Strategy

A variety of statistical methods have been applied to predict the useful life of plant equipment and general dynamic systems (e.g., Mannapov, 1999, Kim and Mead, 1999, Dong and He, 2004). In general, prognostic methods, including

statistical techniques, rely on historical data to identify system trends and predict future behavior. Several statistical techniques have been investigated to characterize the data including moving mean and least-squares methods. However, the latter method offers minimum error between the estimated and the experimental data. The method weighs large errors more than small errors and positive errors equally with negative errors. Typically, the least-squares method uses polynomial curves to describe the data. Hence, system characteristics may be described using regression analysis methods and extended in time to forecast plant behavior. A three step process is recommended for this prognostic method: signal selection, regression statistics, and signal forecasting.

Signal Selection Using A Correlation Method

Dynamic systems may have a variety of input (e.g., force, heat, voltage) and output (e.g., acceleration, vibration, current) signals that can be measured using appropriate sensors. Let these system input and output vectors be represented by $U(t) \in R^g$ and $Y(t) \in R^h$, respectively. It is likely that these signals may be discontinuous or arise from different operating modes. Hence, these signals may need to be filtered, concatenated, and normalized such that the input and output vectors become $U^*(t) \in R^g$ and $Y^*(t) \in R^h$. A smaller set of input and output vectors, $u(t) \in R^n$ and $y(t) \in R^p$, may be selected to investigate the system health based on a correlation analysis. For this study, the correlation between the system inputs and outputs is given as

$$\Re_{jk} = \frac{\sum_{i=1}^{m} Y_j^*(t_i) U_k^*(t_i) - \left(\sum_{i=1}^{m} Y_j^*(t_i)\right)\left(\sum_{i=1}^{m} U_k^*(t_i)\right)/m}{\left(\sum_{i=1}^{m}\left(Y_j^*(t_i)\right)^2 - \left(\sum_{i=1}^{m} Y_j^*(t_i)\right)^2/m\right)^{0.5}\left(\sum_{i=1}^{m}\left(U_k^*(t_i)\right)^2 - \left(\sum_{i=1}^{m} U_k^*(t_i)\right)^2/m\right)^{0.5}} \quad (4.1)$$

As a general rule, the system outputs with a correlation $\left|\Re_{jk}\right| > 0.80$ for the given inputs are selected.

Model-Free Regression Description

A multi-regression empirical model, based on the selected sensor signals, may be created to describe the system's behavior. Although these signals may be affected by noise, it has been assumed that the noise may be negligible. However, this assumption will be removed for the wavelet prognostic method. For degraded plant operation, the system's steady-state output should change so that time dependent trends may be observed while the system's inputs remain constant (Suleiman *et al.,* 2001). Hence, time will be included in the prediction model. The derived regression model, $\vec{Z}_{ji}$, for the j^{th} signal from the plant output vector y(t) and the identified input signals may be expressed as

$$\left|\vec{Z}_{ji}\right| = \left(\sum_{k=1}^{n}\sum_{q=0}^{r}\left(a_{j_{qk}} t_i^{\,q}\right)^2\right)^{0.5} \qquad \text{(i=1,2,…,m)} \quad (4.2)$$

where the parameters n and r denote the number of selected independent variables (input signals) and the regression order. The polynomial coefficients $a_{j0k}, a_{j1k}, ..., a_{jrk}$ correspond to of the r^{th} regression order.

The sum of squares of the deviations, $\vec{D}_j$, between m time samples in the composite sample data, $V_{j_k}(t_i) = [y_j(t_i) \vdots u_k(t_i)]^T$., and the regression curve, $\vec{Z}_{ji}$, becomes

$$\left|\vec{D}_j\right| = \sum_{i=1}^{m}\left[\left(\sum_{k=1}^{n}\left(V_{j_k}(t_i)\right)^2\right)^{0.5} - \left|\vec{Z}_{ji}\right|\right]^2 = \sum_{i=1}^{m}\left[\left(\sum_{k=1}^{n}\left(V_{j_k}(t_i)\right)^2\right)^{0.5} - \left(\sum_{k=1}^{n}\sum_{q=0}^{r}\left(a_{j_{qk}} t_i^q\right)^2\right)^{0.5}\right]^2 \quad (4.3)$$

where the equation (3) which may be minimized, $\frac{\partial \vec{D}_j}{\partial a_{j_{qk}}} = 0$ for q = (0,1,…,r), to obtain the regression curve by solving the (r+1) equations numerically as

$$\frac{\partial}{\partial a_{j_{q\in[0,r]k}}}\left\{\sum_{i=1}^{m}\left[\left(\sum_{k=1}^{n}\left(V_{j_k}(t_i)\right)^2\right)^{0.5} - \left(\sum_{k=1}^{n}\sum_{q=0}^{r}\left(a_{j_{qk}} t_i^q\right)^2\right)^{0.5}\right]^2\right\} = 0 \quad (4.4)$$

Signal Forecasting

The motivation for a prognostic strategy is to predict the turbine's future behavior based on current and historical data. After developing a method to analyze current behavior, a need existed to forecast system performance. The regression model can predict a variable's value both inside and outside the estimation time interval. The regression coefficients, $a_{j_{qk}}$, should describe the signal trend so that time extension of the regression curve may estimate the system's future behavior. In general, the meaningful prediction time for the regression curve depends on the estimation data. The larger the estimation data sample size, the better the forecast since the curve would be termed "well trained". The dependent variable trends represent the long term signal behavior, rather than fluctuations caused by plant disturbances and load changes. The

forecast curve may be given as

$$\left|\vec{Z}_{ji}\right| = \left(\sum_{k=1}^{n} \sum_{q=0}^{r} \left(a_{jqk}\, t_i^{\,q} \right)^2 \right)^{0.5} \qquad \text{(i=m+1, m+2,…,m+f)} \qquad (4.5)$$

where m+f is the final time value. This forecast, $\vec{Z}_{ji}$, has an error of $\varepsilon_j = \left\{ \sum_{i=1}^{m} \left\| \left[\vec{Z}_{ji} - y_j(t_i) \right] \right\| / m - 1 \right\}$ which can be used for comparison purposes.

For the Mercury 50 simple cycle gas turbine twenty-eight signals are recorded at regular intervals. The signals include observed measurements such as vibration amplitudes, temperatures, pressures, and flow rates (refer to Table 1). The data is stored into the array *y(t)* described as

$$y(t) = \begin{bmatrix} y_1(t_1) & y_1(t_2) & \cdots & y_1(t_m) \\ y_2(t_1) & y_2(t_2) & \cdots & y_2(t_m) \\ \vdots & \vdots & \ddots & \vdots \\ y_n(t_1) & y_n(t_2) & \cdots & y_n(t_m) \end{bmatrix} \qquad (4.6)$$

As in this case one input and one output are selected the regression curve equation becomes

$$\vec{Z} = \sqrt{\sum_{j=1}^{n} \sum_{k=0}^{r} \left(a_{kj}\, t_i^{\,k} \right)^2} \qquad (4.7)$$

The sum of squares of the deviations between m points in the sample data and the regression curve, $\vec{D}$, is given as

$$\vec{D} = \sum_{i=1}^{m} \sum_{j=1}^{n} \left(y_j(t_i) - \vec{Z} \right)^2 = \sum_{i=1}^{m} \left[\sqrt{\sum_{j=1}^{n} \left(y_j(t_i) \right)^2} - \sqrt{\sum_{j=1}^{n} \sum_{k=0}^{r} \left(a_{kj} t_i^{\,k} \right)^2} \right]^2 \qquad (4.8)$$

which is minimized to get a regression curve as $\frac{\partial \vec{D}}{\partial a_{kj}} = 0$ for k = (0,1,…,r). The polynomial coefficients can be obtained by solving the (r+1) equations numerically

$$\frac{\partial}{\partial a_{k\in[0,r]j}}\left\{\sum_{i=1}^{m}\left[\sqrt{\sum_{j=1}^{n}\left(y_j(t_i)\right)^2}-\sqrt{\sum_{j=1}^{n}\sum_{k=0}^{r}\left(a_{kj}t_i^{\,k}\right)^2}\right]^2\right\}=0 \qquad (4.9)$$

Finally, the prediction for the regression curve is estimated as

$$\vec{Z} = \sqrt{\sum_{j=1}^{n}\sum_{k=0}^{r}\left(a_{kj}\,t_L^{\,k}\right)^2} \qquad (4.10)$$

such that m<L<m+t_f where t_f is the desired forecast time.

Health Evaluation

A prognostic strategy can estimate the system's future behavior to facilitate maintenance scheduling and component repair. An adjustable set of thresholds may be established for the statistical estimates so that a violation results in appropriate action. Small variations in a system's output signal, without a change in the system inputs, may be due to extraneous noise, load fluctuations, and/or a slowly occurring degradation. In the proposed evaluation method, forecasted signals are acceptable if they lie within established thresholds. For a normally distributed steady-state signal, 95% of the data should lie within two standard deviations, $\sigma_j = \left[\frac{1}{m}\sum_{i=1}^{m}\left(y_j(t_i) - \bar{y}_j\right)^2\right]^{0.5}$, of the sample mean, $\bar{y}_j$. If the system forecast predicts a threshold violation, remedial action should be dependent on the rate and severity of the threshold violation.

Data Enclosure

Often the experimental data points are scattered around the regression line. Ideally, a method may be created to visually represent the data and its variability. To accomplish this, ellipses have been selected. An ellipse is a closed plane curve consisting of all points for which the sum of the distances between a point on the curve and two fixed points (i.e., foci) is the same. As shown in Figure 4.3, the center of an ellipse is the point halfway between its foci f_1 and f_2. The major axis (i.e., 2f) is the chord that passes through the foci; the minor axis (i.e., 2h) is the chord that passes through the center perpendicular to the major axis. The larger axis receives the major designation, while the smaller axis receives the minor designation.

Mathematically, an ellipse can be represented as $\left\{\frac{p^2}{f^2}+\frac{q^2}{h^2}=1\right\}$ where p and q are the coordinates of the two independent variables. A circle is also a form of an ellipse of eccentricity zero, (i.e., one in which the center and the two foci all coincide). An ellipse can have two axes of differing lengths so it is an excellent way to depict the variation in two data signals. One axis can represent the variation in one signal (e.g., fuel flow) while the other axis represents the variation in the other (e.g., power generated). Using standard deviation, $s_{j,}$ to determine the size of each axis, a certain percentage of data can then be hypothetically enclosed within an ellipse. Or in this case, a certain percentage of data can be enclosed within a series of ellipses or *tuples* (set of ordered elements).

The equation of the ellipse allows the tuples to be plotted as $p = \frac{f}{h}\sqrt{(h^2 - q^2)}$. As mentioned previously, a range that lies two standard deviations on either side of the mean of a normally distributed sample encloses 95% of the points in that sample. The standard deviations of the two signals being analyzed were calculated based on the same set of data used to predict the regression curve. The length of the semi-major and semi-minor axis are given as

$$f = 2\sqrt{\frac{\sum_{i=1}^{m}[y_j(t_i) - \bar{y}_j]^2}{m-1}}, h = 2\sqrt{\frac{\sum_{i=1}^{m}[y_{\hat{j}}(t_i) - \bar{y}_{\hat{j}}]^2}{m-1}} \tag{4.11}$$

where j and $\hat{j}$ denote two different turbine signals and p and q should be $p \in (-f, f)$ and $q \in (-h, h)$. Accordingly, a selection of q can be made and the corresponding value of p can be reached with knowledge of f and h as per equation (4.11). The center of each ellipse is set on the regression line $O\left[\vec{Z}(t)\right]$ so that the ellipse signifies two standard deviations of the fuel flow signal and two standard deviations of the power signal on either side of the regression line in the y- and z-directions, respectively.

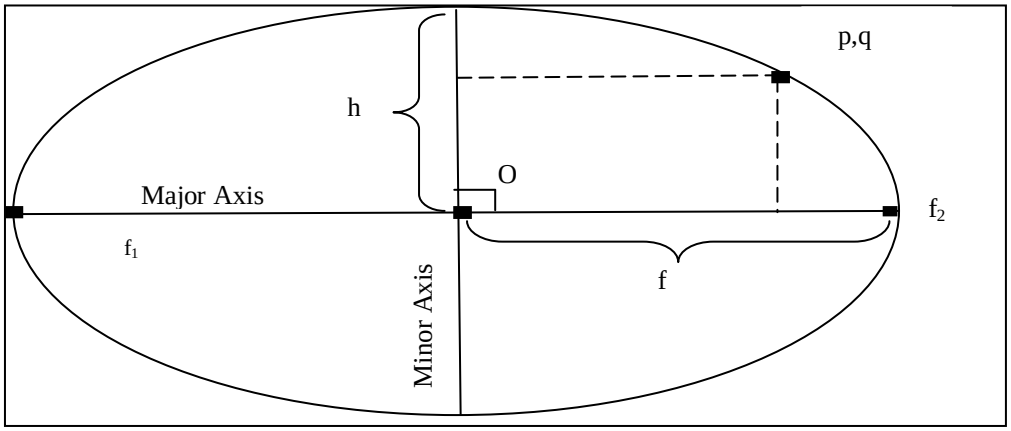

Figure 4.3. An ellipse with its major and minor axis

Wavelet Prognostic Strategy

Wavelet transforms can be applied to time domain plant signals that contain noisy, intermittent, and transient behavior (McAlpin *et al.*, 2003). A wavelet is a waveform of limited duration with a zero average that converts a time domain signal into a magnitude and time function (Aboufadel and Schlicker, 1999, Addison, 2002). Wavelet transforms can be used for multi-dimensional analyses which make them a powerful tool in analyzing and monitoring dynamic systems (Sun *et al*., 2005). For instance, wavelet transforms with neural networks can remove signal noise and predict nonlinear system behavior (Feng *et al.*, 2006). The wavelet transform can also be used to investigate dominant system trends and derive the mean time between hard failures (Guo *et al.*, 2003) within the context of the diagnostic methods.

In this study, the wavelet technique will predict dynamic system operation again using a three step procedure. First, wavelet transforms of the real-time data will compute the wavelet coefficients for a given system signal. Second, a regression analysis of these coefficients can forecast the wavelet coefficients for the desired prediction time. Third, the new set of wavelet coefficients can reconstruct the signal, and hence, obtain a prediction.

Wavelet Description

Any waveform function, $\psi(t)$, can be selected for a wavelet transform if it satisfies the condition of finite energy and admissibility. The finite energy condition (Daubechies, 1992) states that the energy, ϑ, of the wavelet function, $\psi(t)$, should be limited as

$$\vartheta = \int_{-\infty}^{\infty} |\psi(t)|^2 dt < \infty \qquad (\vartheta < \infty) \tag{4.12}$$

The admissibility condition states that the wavelet function has a zero mean, $E(\psi(t)) = 0$, and that the Fourier Transform of the wavelet function with frequency F cannot be zero, $\hat{\psi}(F) \neq 0$, within the support of the wavelet. The admissibility constant for the wavelet function has a finite value

$$\varsigma = \int_0^{\infty} \frac{|\hat{\psi}(F)|^2}{F} dF \qquad (\varsigma < \infty) \tag{4.13}$$

In this expression, $\hat{\psi}(F) = \int_{-\infty}^{\infty} \psi(t) e^{-i(2\pi F)t} dt$ represents the Fourier transform of $\psi(t)$. The value of the admissibility constant is dependent on the wavelet function. A discrete wavelet transform uses an orthonormal wavelet basis with the wavelet function, $\psi(t)$, to obtain the wavelet function, $\psi_{\chi,\eta}(t)$, at a given scale and time as

$$\psi_{\chi,\eta}(t) = \frac{1}{\sqrt{u_0^{\chi}}} \psi\left(\frac{t - \eta v_0 u_0^{\chi}}{u_0^{\chi}} \right) \tag{4.14}$$

The parameters $\chi \in R$ and $\eta \in R$ denote the dilation (scale) and translation (time) variables, respectively. The symbols u_0 and v_0 are wavelet control parameters.

The term “translation” refers to delaying or hastening the onset of a wavelet (i.e., a shift in time). The term “dilation” denotes wavelet scaling (i.e., stretching or compressing). Low and high scales are associated with compressed and stretched wavelets. The scaling function, $\phi(t)$, is any waveform function that

satisfies the condition $\int_{-\infty}^{\infty} \phi(t)dt = 1$. The scaling function at a given scale and time becomes

$$\phi_{\chi,\eta}(t) = \frac{1}{\sqrt{u_0^{\chi}}}\phi\left(\frac{t - \eta v_0 u_0^{\chi}}{u_0^{\chi}}\right) \tag{4.15}$$

Wavelet Coefficient Signal Processing

In some instances, the plant output signals may be affected by disturbances, κ_d, and noise, κ_n. For example, consider $y_j(t) = s(t) + \kappa_d + \kappa_n$ which is composed of signal characteristics, s(t), and additive components κ_d and κ_n. A wavelet transform addresses signal noise by computing two sets of wavelet coefficients: detail and approximate. Signal details refer to the high frequency content of the signal which may be noise and disturbances. Signal approximations are the low frequency signal content. If the high frequency components of the signal are removed, then the signal still retains some characteristics which can be forecasted. However, if the signal approximations are removed, then the signal may loose its primary characteristic and the residual would likely be noise.

The detail and approximation coefficients, $\hat{\gamma}_{\chi,\eta_j}$ and $\hat{\xi}_{\chi,\eta_j}$, were generated on a dyadic scale (i.e., based on powers of two). The given discrete wavelet transform of the learning window may be computed to obtain the detail and the approximation coefficients as

$$\hat{\gamma}_{\chi,\eta} = \int_{-\infty}^{\infty} y_j(t)\frac{1}{\sqrt{u_0^{\chi}}}\psi\left(\frac{t-\eta v_0 u_0^{\chi}}{u_0^{\chi}}\right)dt = \left\langle y_j(t), \psi(t)\right\rangle \tag{4.16a}$$

$$\hat{\xi}_{\chi,\eta} = \int_{-\infty}^{\infty} y_j(t) \frac{1}{\sqrt{u_0^{\chi}}} \phi\left(\frac{t - \eta v_0 u_0^{\chi}}{u_0^{\chi}} \right) dt = \left\langle y_j(t), \phi(t) \right\rangle \tag{4.16b}$$

Note that the detail and approximation coefficients are obtained by the convolution of the system signal with the wavelet and scaling functions. The similar analysis of the input signal provides the corresponding detail, $\gamma_{\chi,\eta}$, and approximation, $\xi_{\chi,\eta}$, coefficients as

$$\gamma_{\chi,\eta} = \left\langle u_k(t), \psi(t) \right\rangle, \; \xi_{\chi,\eta} = \left\langle u_k(t), \phi(t) \right\rangle \tag{4.17}$$

Form a practical perspective, the signal vectors $y(t)$ and $u(t)$ may be filtered using the complementary filters in equations (4.16) and (4.17) to realize low and high frequency coefficients. The next step for the algorithm is a least square fit to obtain a regression model of the signal approximation coefficients.

Forecasting Methodology

The prognostic eliminates high frequency signal noise, through wavelet transforms, to predict the system behavior. The wavelet coefficient regression model for the selected variable may be derived from the approximation coefficients. This regression model forecast the system's approximation coefficients by performing a one dimensional inverse wavelet transform on the coefficients so that

$$A_{\chi}(t) = \sum_{\eta=-\infty}^{\infty} \xi_{\chi,\eta} \phi_{\chi,\eta}(t) \tag{4.18}$$

The prognostic algorithm uses a fourth-order Daubechies wavelet (Daubechies, 1992) for both the wavelet and inverse wavelet transforms. The corresponding wavelet and scaling function for the fourth-order Daubechies wavelets become

$$\psi(t) = \sum_{e=1,3} d_e \phi[2t-(e-3)] - \sum_{e=0,2} d_e \phi[2t-(3-e)], \quad \phi(t) = \sum_{e=0}^{3} d_e \phi(2t-e) \quad (4.18)$$

where the parameters d_e and e represent the scaling coefficient and the scaling coefficient index.

CHAPTER 5

EXPERIMENTAL SETUP

The real time prognostic strategies presented in this thesis can be applied to dynamic systems for which input and output sensory information is available. To apply these methodologies, experimental data is required to develop the statistical basis, estimate future behavior, and compare against actual response. Further, the dynamic stationary gas turbine model required experimental results for validation. During this project, extensive efforts were made to obtain physical operating data sets so that the developed methodologies could be tested rigorously. Hence, operational data was obtained from three different gas turbines: a Solar Mercury 50 gas turbine, a General Electric 7EA gas turbine, and a General Electric LM2000 co-generation gas turbine. The developed prognostic methodologies were applied to various plant signals from these turbines, and the numerical results compared.

Introduction to Gas Turbines

Gas turbines can be classified as either stationary or aeronautical propulsion. The stationary gas turbines are primarily used for power (electrical or mechanical) production in domestic and industrial sector, for instance, marine engines for large ships and electrical power turbines. Stationary gas turbines can also be classified based on criteria such as types of compressors (i.e., rotary or axial), turbine cycle (i.e., simple or combined), shaft arrangement (i.e., single or multi spool), with or without heat exchanger etc. Small scale turbines with power

ratings less than 100 kW are called mircoturbines, these turbines are used as supplementary power sources for running heating and cooling systems for buildings.

The aeronautical propulsion gas turbines are used in aviation as jet aircraft engines. These aero gas turbines have had a great impact on the aircraft industry as they are effective, efficient, and capable of operating for long durations. Further the thrust generated by an aeronautical propulsion gas turbine ranges from 40-450 kN. These gas turbine aircraft engines are of three types turbojet, turbofan (where thrust is generated by a nozzle), and turboprop (where the thrust is generated by a propeller). Gas turbines are also used as aircraft auxiliary power units to provide power supply for the electrical, hydraulic, and compression needs while it is stationary.

The land based stationary gas turbines, typically used in power generation, have power range of 2-250 MW. If greater power production is necessary, combined cycle gas turbines may be used with 2,000 MW ratings. For such systems power production capacity of 2,000 MW maybe achieved. A combined cycle uses the energy available in the exhaust of a gas turbine (i.e., energy not converted to shaft power). This exhaust produces steam in a waste heat boiler, or a heat recovery steam generator, to increase the power output from a steam turbine. In a co-generation plant, the exhaust energy may be also used to produce hot water or steam to heat buildings or enhance chemical processes. The generated steam can also be used to operate an absorption refrigerator in water

chilling or air conditioning. Most of the stationary gas turbines used for power generation are designed to run for 100,000 hours without major overhauls.

The Solar Mercury 50 Gas Turbine

The Mercury 50 gas turbine, shown in Figure 5.1, is used by the Clemson University facilities to provide supplemental electrical power to the campus. It is a high- efficiency small-size gas turbine with low emissions. The Mercury 50 gas turbine is run during peak load conditions at the campus during the morning hours in winters and during afternoon hours in summers. The Mercury 50 has a power production capacity of 4.5 MW with a maximum rotational speed of approximately 14,800 RPM. It contains a ten stage compressor and a two stage turbine. It consists of a single shaft recuperated cycle turbine engine, a generator with accessories, and auxiliary systems. The heat rate of a Mercury 50 is 9,359 kJ/kWh with an electrical efficiency of 38.5%. Unlike most low rating gas turbines the Mercury 50 incorporates a heat exchanger and is not an aero-derivative gas turbine. The inlet of the compressor is at the center of the system with the combustion chamber at the end to facilitate maintenance and compressor wash.

The Mercury 50 stationary turbine's operation can be recorded at the Clemson University research facility computer workstations to determine the status of the gas turbine's operation including system temperatures, pressures, vibration levels, and power output. This real time output data is available for observation and use with diagnostic and prognostic modules. The control over the

Figure 5.1. Mercury 50 gas turbine at Clemson University

operating scenarios of this gas turbine enabled the research team to specify its run duration and operating points so that data could be obtained for various scenarios. The Mercury 50 was run for both healthy and faulty operating scenarios; the faulty run data is not readily available from the gas turbine manufacturers as it is proprietary therefore, the turbine was run with seeded faults such as oil cooler and relief valve failure and the data was recorded.

The experimental data from the Mercury 50 gas turbine is recorded using a IPCOS technology OPC for Matlab software. This software connects the Mercury 50 to the computer workstations in the Energy Systems Laboratory at Clemson University through a RSLINX OPC server. At present, twenty eight signals are recorded and transmitted to the Matlab software in real time. Figure 5.2 shows the flow of data for the experimental setup, different sensors are shown with some of the signal recorded from these sensors. This data obtained from the turbine is stored in the form of arrays in Matlab which can be analyzed by relevant

algorithms. The data transmission from the Allen Bradley PLC is one way so that the turbine operation is not affected.

The data acquisition is started by running the initializing Matlab code through the workstation at the Energy System Laboratory which includes specifying the signals to be recorded and the time for which the data has to be acquired. The present data acquisition rate is one second this data acquisition rate can be varied according to the desired rate of sampling. Once initialized the algorithm records and stores the desired data signals. The data is acquired from a set of 180 sensors located at the various points in the Mercury 50 gas turbine. In Figure 5.3, the main sensor locations are displayed in addition to the signals detected at those points.

The General Electric 7EA Stationary Gas Turbine

The second experimental power plant turbine is a GE 7EA (refer to Figure 5.4) mid-size gas turbine located at a Santee Cooper Rainy power generating station in Anderson County, SC. The GE 7EA is used for peak load sharing in a combined cycle power plant throughout the year. The GE 7EA has a power production capacity of 85 MW with a maximum rotational speed of 3,600 RPM. The GE 7EA power generation setup consists of a single shaft, recuperated cycle turbine engine with a sixteen stage compressor having a compression ratio of 12.6:1. The heat rate of a GE 7EA is 10,991 kJ/kWh with an approximate mass flow rate of 292 kg/s, the net efficiency is 50%, when used in a combined cycle plant. The multiple fuel combustion system enables the GE 7EA to be run on a variety of fuels, consequently the GE 7EA can switch from one fuel to another.

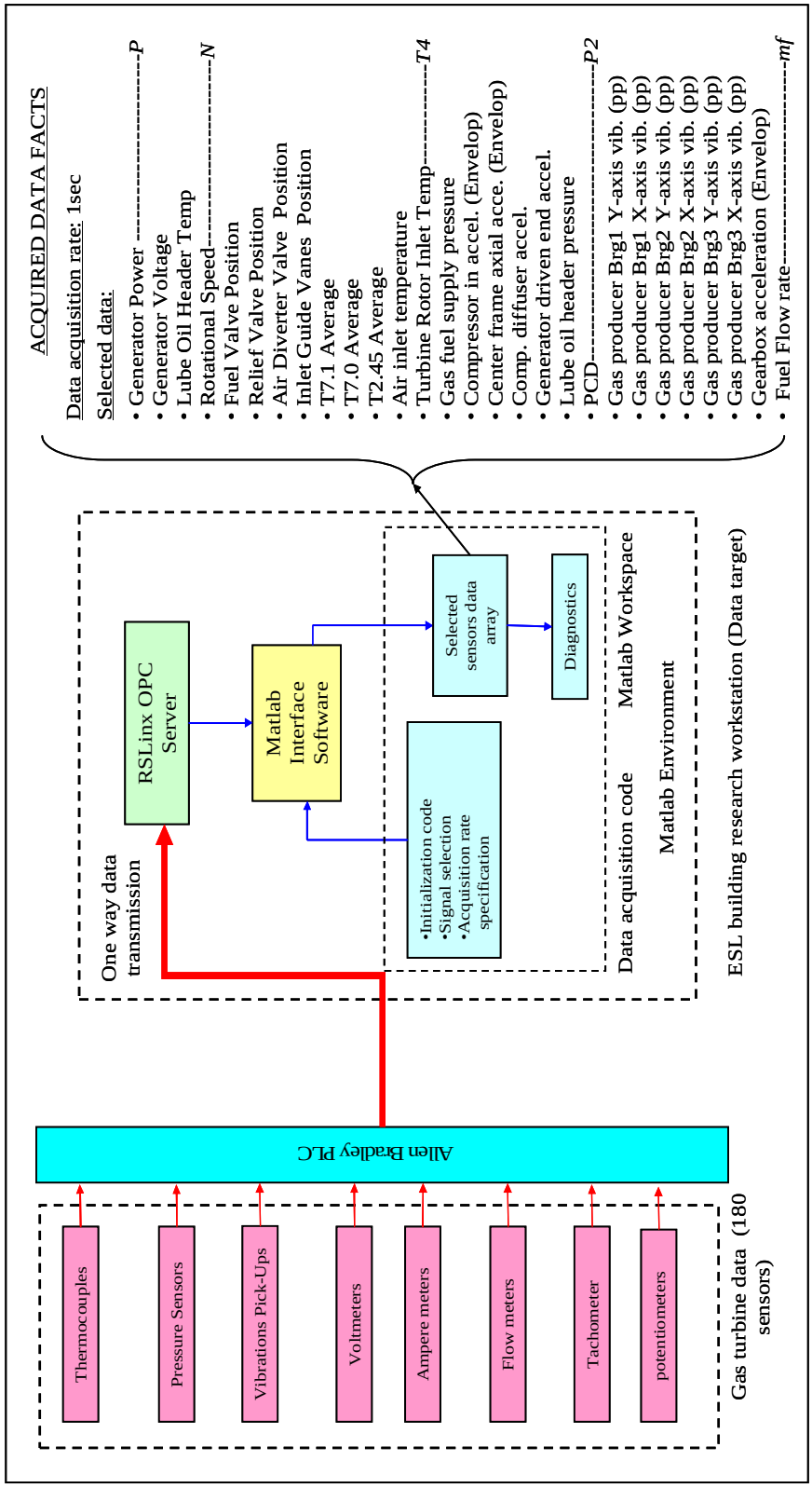

Figure 5.2. Data acquisition diagram for a Solar Mercury 50 gas turbine located at Clemson University

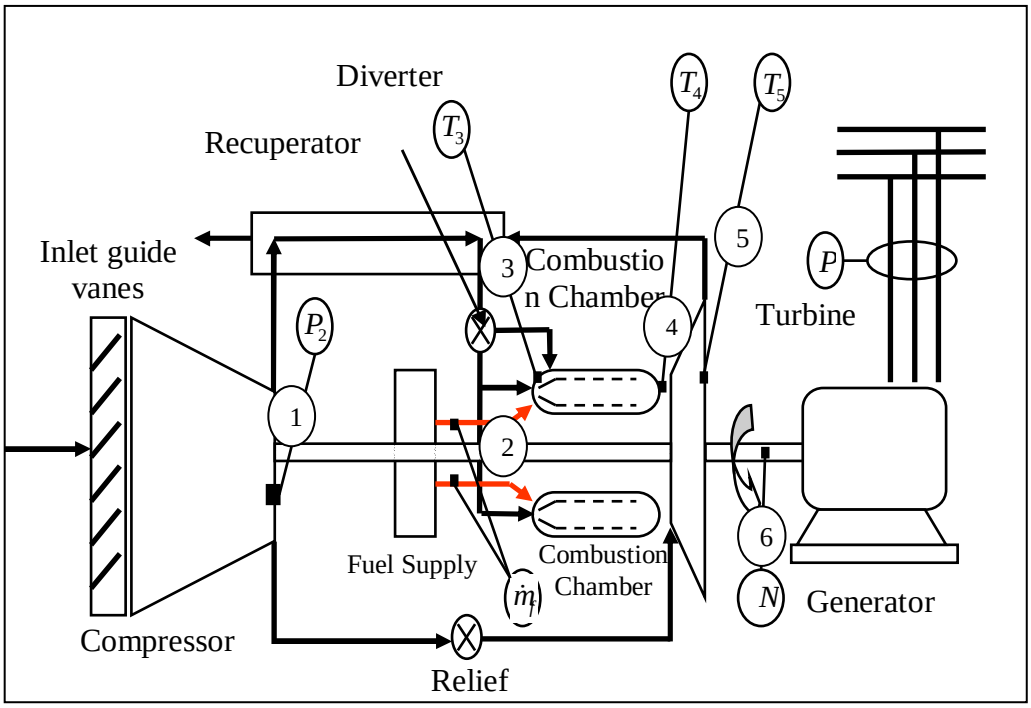

Figure 5.3. Gas turbine primary sensor location points along with the signals recorded

Figure 5.4 . GE 7EA 85 MW gas turbine located at the Rainy power generating station

Real time experimental data can be recorded from this gas turbine at a variable rate using an extensive network of installed sensors; the current sampling rate is one minute. The run time for the gas turbine is based on the power generation and heat needs, the kW of power generated depends on the overall load on the Rainy power generating station. Extensive data sets are available for the GE 7EA gas turbine from the Rainy power generating station. The recorded data represents the operation of this gas turbine over a period of three years.

The General Electric LM2000 Gas Turbine

The third gas turbine from which experimental data has been obtained is the GE 2000LM (refer to Figure 5.5) located at Louisiana State University (Baton Rouge, LA). It fulfills the electricity and waste heat generation requirements of LSU cogeneration plant. It is an aero derivative gas turbine with a maximum power production capacity of 18 MW with a maximum rotational speed of 5,000 RPM. It has a sixteen stage compressor with a compression ratio of 20:1 and a six stage turbine. It has a heat rate of 9,374 kJ/kWh with an overall thermal efficiency of 36.4% and the mass flow rate is 62.72 kg/s. Steady state data for continuous turbine operation up to 24 hours at a sampling rate of five seconds is available from the Louisiana State University cogeneration plant.

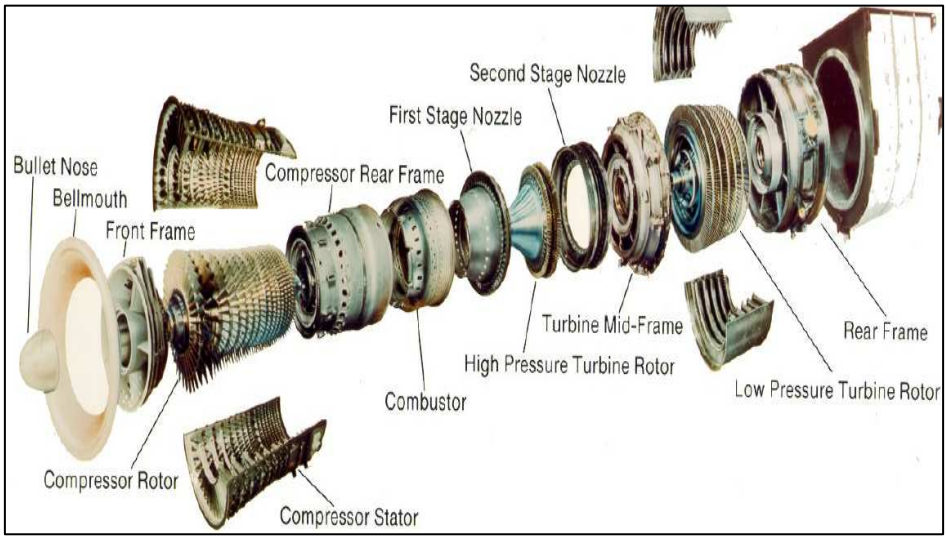

Figure 5.5. Various components of a GE LM 2000 gas turbine

CHAPTER 6

EXPERIMENTAL AND NUMERICAL RESULTS

A variety of signals from the Solar Mercury 50 and the General Electric 7EA were recorded and analyzed. This chapter presents the experimental and numerical results to validate the dynamic turbine model and the proposed prognostic methodologies. First, based on the experimental data from a Mercury 50 the validation results for the mathematical model are presented. Second, the two proposed prognostic methodologies are applied to different data sets collected from the Mercury 50. Third, the prognostic algorithms along with signal conditioning methods are applied to long term data sets from a GE 7EA gas turbine.

Analytical Gas Turbine Model Validation

The dynamic simulation model consists of the differential and algebraic equations presented in Chapter 3. The subsystems have been linked with one another in MATLAB/Simulink to create a simulation tool set that uses the ODE (Dormand-Prince) variable step solver. A variety of model input/output signals have been considered including the generator power, shaft speed, fuel flow, compressor outlet pressure, and combustion chamber outlet temperature. To validate the mathematical model, comparisons between the analytical model and the experimental results from the Mercury 50 gas turbine have been studied. Each of the signals (e.g., shaft speed, power, fuel flow, compressor outlet pressure, and

turbine rotor inlet temperature) were superimposed on their corresponding experimental results graphs.

The model validation of the turbine shaft speed shaft speed is shown in Figure 6.1. Due to fuel flow variations before steady state behavior is obtained, there is some deviation of the model results from the experimental shaft speed. Apart from this discrepancy between 100<t<650s, the model shows close resemblance to the experimentally determined speed for the steady state profile. In Figure 6.2, the validation of the estimated power generated is presented. The model results show good correlation to the experimental results for the start up, the transient and the steady state operation. A good match has been obtained (i.e., within 0.5 % of the experimental data). It can be observed that the model simulates the start of power generation at t= 400s after the initial start up, and sequential loading at 400<t<650s, and the attainment of steady state at approximately at t=650s.

The model validation for fuel flow rate is presented in Figure 6.3. Since no fuel control information is available, fuel flow map has been generated empirically. The model adequately predicts the actual fuel flow during the loading sequence between 200<t< 700s and closely matches the steady state behavior. Figure 6.4 displays the estimated and actual compressor outlet pressure (PCD). Although there are some deviations between the analytical and experimental results during the start up phase, the steady-state results agree closely. Finally, Figure 6.5 presents the comparison between experimentally determined and analytically estimated turbine rotor inlet temperature.

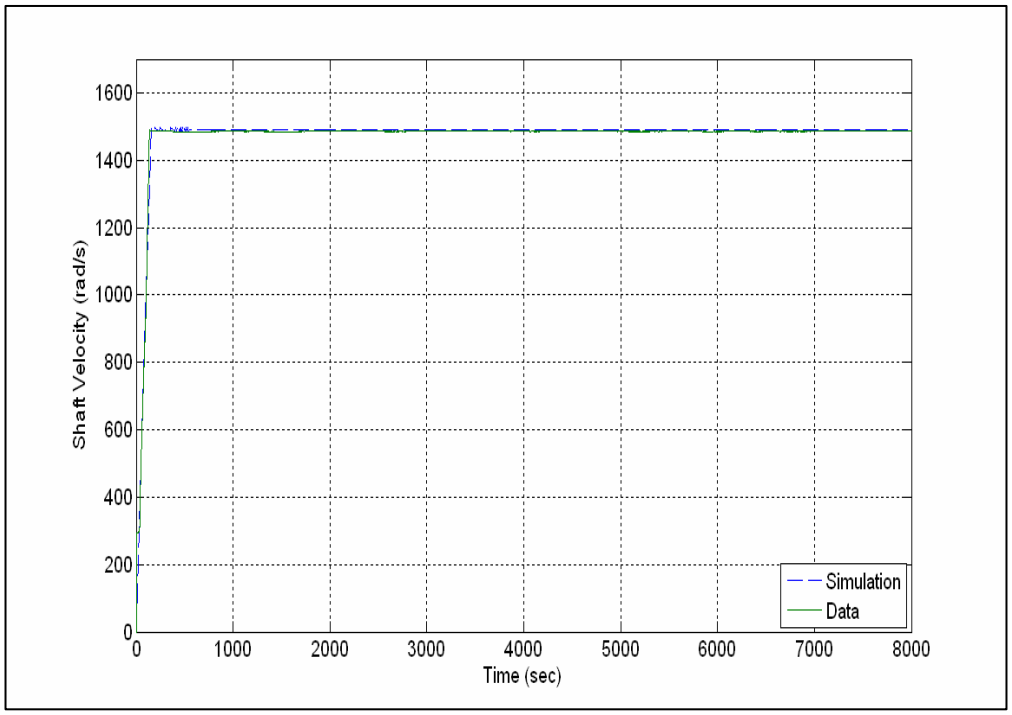

Figure 6.1. Estimated (dashed) and experimental (solid) gas turbine shaft speed versus time

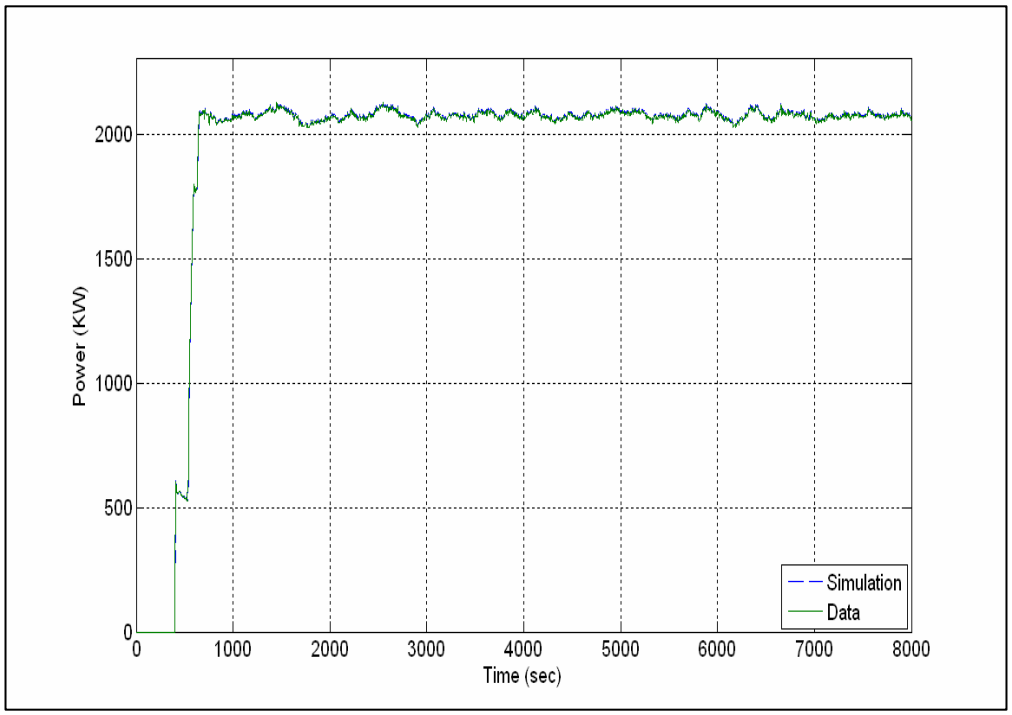

Figure 6.2. Estimated (dashed) and experimental (solid) gas turbine power generated versus time

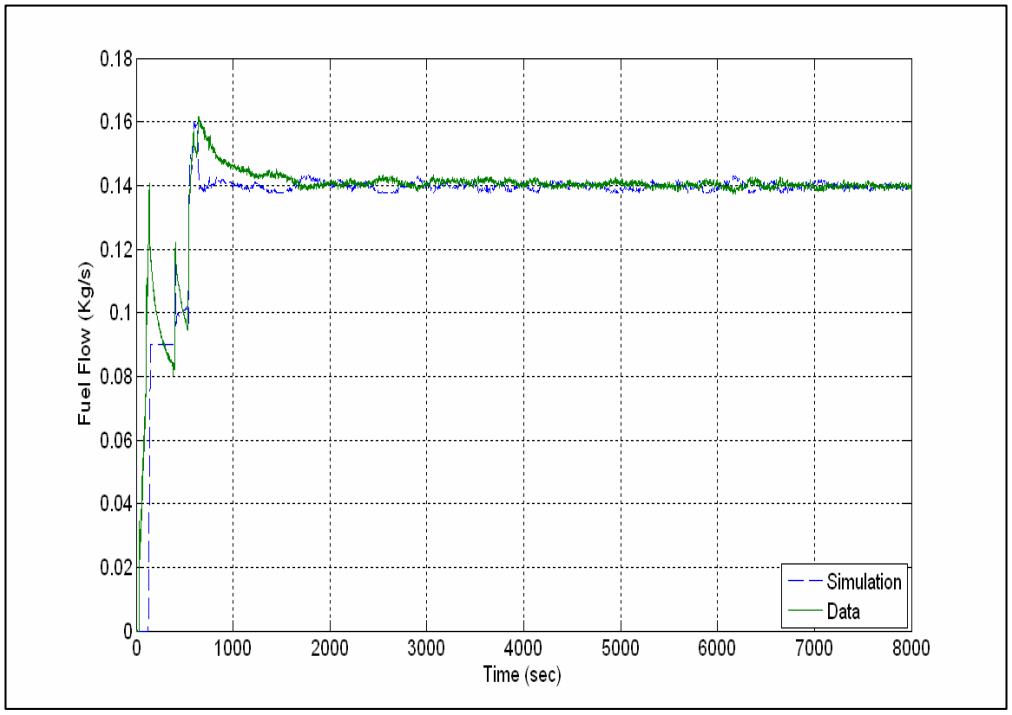

Figure 6.3. Estimated (dashed) and experimental (solid) fuel flow rate versus time

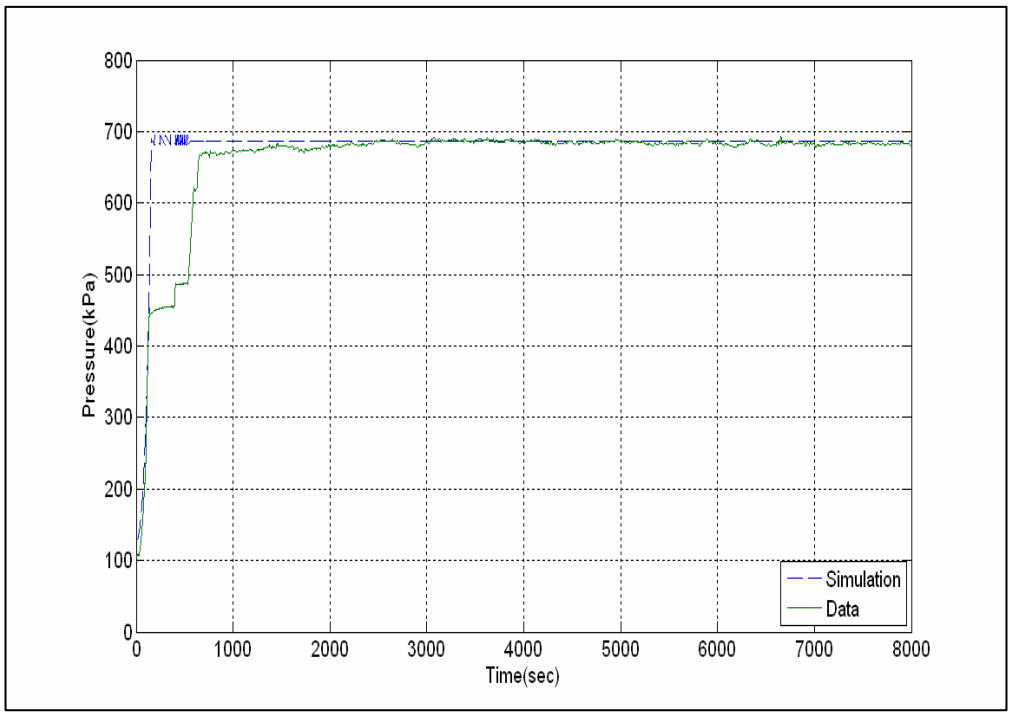

Figure 6.4. Estimated (dashed) and experimental (solid) gas turbine compressor outlet pressure versus time

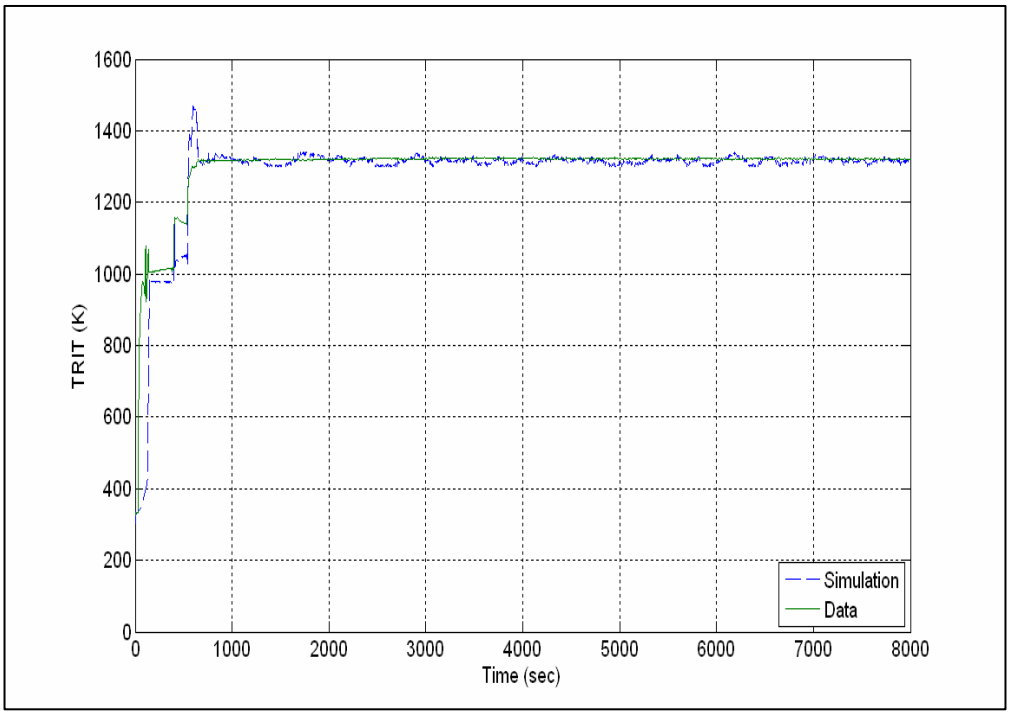

Figure 6.5. Estimated (dashed) and experimental (solid) gas turbine rotor inlet temperature versus time

Prognostic Methods - Application to a Mercury 50 Gas Turbine

In this initial study, two signals were related to time using the least-squares method and a second-order polynomial curve fit. The two signals can be any of the twenty-eight signals listed in Table 6.1. Fuel flow, F1, and power generated, PW, were considered to be suitable for representing some of the characteristic behaviors of the Mercury 50 stationary gas turbine. Figure 6.6 displays a sample of two signals, fuel flow rate (kg/s) and power generated (kW), for a healthy turbine operational run. This data represents steady state behavior which is obtained 4,000s after the initiation of the turbine run and continues till 9,000s. After this period the turbine shutdown process is initiated and the turbine ceases operation at 10,000s. Once the initial cold start is complete, the turbine reaches peak power generation in about 1,000s. The turbine gradually settles into steady state behavior but still there are fluctuations in the power generated for another 3,000s after which the turbine runs smoothly. Hence, the data window from 4,000 to 9,000s is assumed to be a steady state period.

Figure 6.7 displays the computed multiple regression curve based on 4,000 steady state data points for fuel flow and power generated (i.e., $4{,}000<t<8{,}000$s after the initial start up). The algorithm computes the second order multiple-regression curve in real-time. As data is recorded, the regression curve is computed based on the logged data points so that this curve is updated continuously as more data is recorded. The longer the duration of the data recorded, more representative would be the regression curve of the signal trend and turbine behavior. The second order polynomial fit has an error of

approximately 1.4% for both the fuel flow and power generated which is within acceptable limits of $\pm 5\%$.

Figure 6.8 displays tuples plotted with major and minor axes sized as two standard deviation for power and fuel flow signals, $s_j \propto f(F1, PW)$, respectively for a sample of 4,000s after steady state has been achieved. The tuple centers lie on the regression curve shown in Figure 6.7.

Variable	Description of Variable	Units
A1	Compressor inlet acc.	gE
A2	Center frame axial acc.	gE
A3	Compressor diffuser acc.	gE
A4	Generator driven end acc.	gE
A5	Gearbox acc.	gE
B1	Gas producer Brg1 Y-axis	mil pp
B2	Gas producer Brg1 X-axis	mil pp
B3	Gas producer Brg2 Y-axis	mil pp
B4	Gas producer Brg2 X-axis	mil pp
B5	Gas producer Brg3 Y-axis	mil pp
B6	Gas producer Brg3 X-axis	mil pp
C1	Relief valve position	%
C2	Air diverter valve position	%
F1	Fuel flow rate	kg/s
NGP	Turbine shaft speed	%
P1	Gas fuel supply pressure	Pa
P2	Lube oil pressure	Pa
P3	Compressor outlet pressure	Pa
PF	Power factor	
PW	Generated power	kW
T1	Lube oil temperature	˚K
T2	Inlet air temperature	˚K
T3	T7.1 average	˚K
T4	T7.0 average	˚K
T5	T2.45 average	˚K
T6	Turbine inlet temperature	˚K
T7	Enclosure temperature	˚K
V1	Alt average L-L volts	V

Table 6.1. Gas turbine data acquisition signals

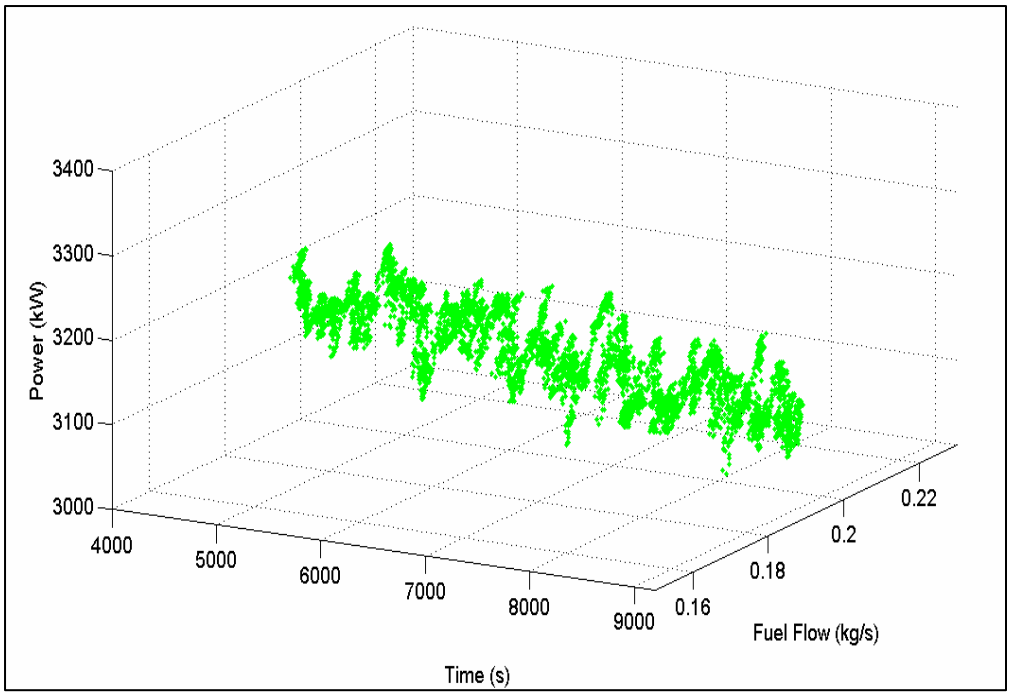

Figure 6.6. Fuel flow and power generated for a Mercury 50 gas turbine in steady state versus time for 4,000<t<9,000s

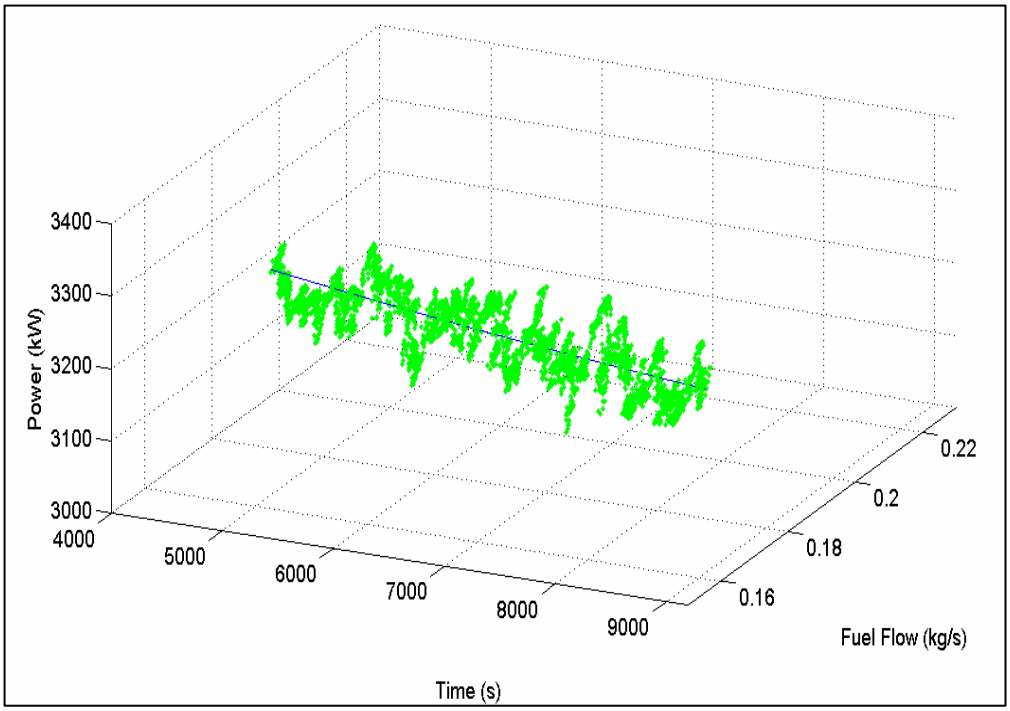

Figure 6.7. Regression curve, $\vec{z}$, for the fuel flow and power generated in a Mercury 50 gas turbine versus time for 4,000<t<8,000s

As the data is updated in real-time, the tuple radius varies with changing standard deviation of the data. These tuples will ideally enclose 95% of the data for a healthy turbine run. These tuples allow one to visualize the behavior of the turbine. The points outside of the tuples represent points occurring during operation that are greater than two standard deviations of the recorded data away from the trend line.

Figure 6.9 shows the forecast between 8,000 and 9,000s for the data in Figure 6.6. A learning window encloses 4,000s of prior data. Ellipses with semi-major and semi-minor axis as two standard deviations for the steady state data for fuel flow and power generated. A comparison between the actual experimental data and the forecast gives an error of approximately 4% which is again within the acceptable limits of $\pm 5\%$.

The signals from a Mercury 50 gas turbine were analyzed using second-order Daubechies wavelets. The initial step computes the discreet wavelet transform of the signal to generate the wavelet coefficients (i.e., a set of detail and approximation coefficients). The gas turbine signal selected was power, PW. As shown in Figure 6.10, the steady state turbine signal (power) for a period of 5,000s was divided into two windows: learning and validation.

Figure 6.11 displays the low frequency approximation wavelet coefficients for the learning window for $4{,}000<t<8{,}000$s. The values of the wavelet coefficients depend on the wavelet function, being used to analyze the signal. Due to “down” sampling the number of wavelet coefficients is exactly half the number of data points in the sampled signal.

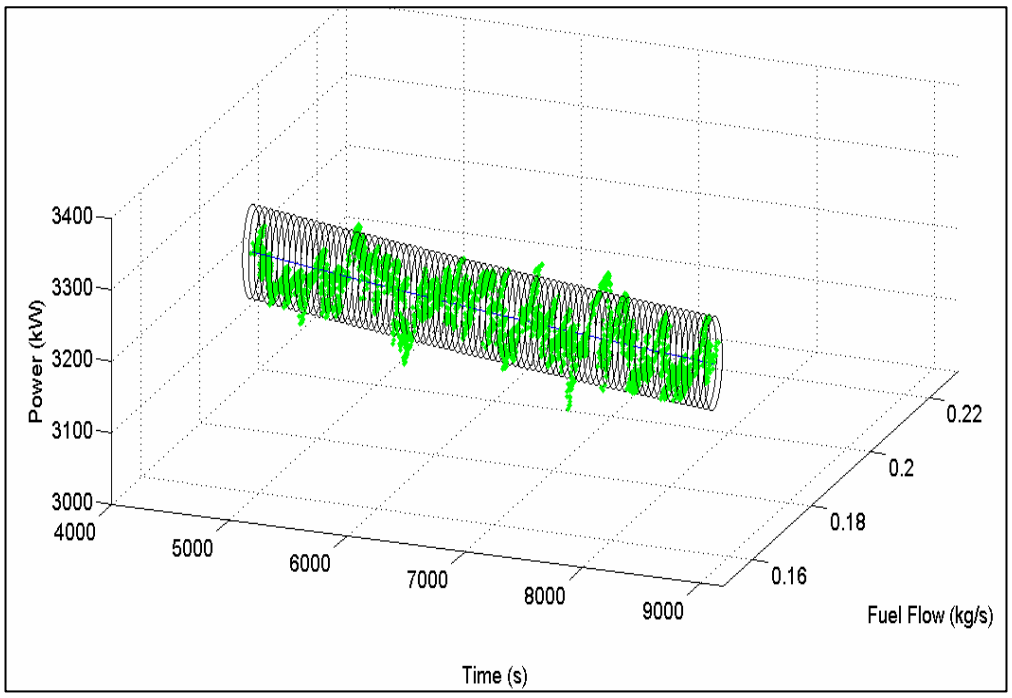

Figure 6.8. Tuples centered on a second order polynomial trend for fuel flow and power versus time for 4,000<t<8,000s

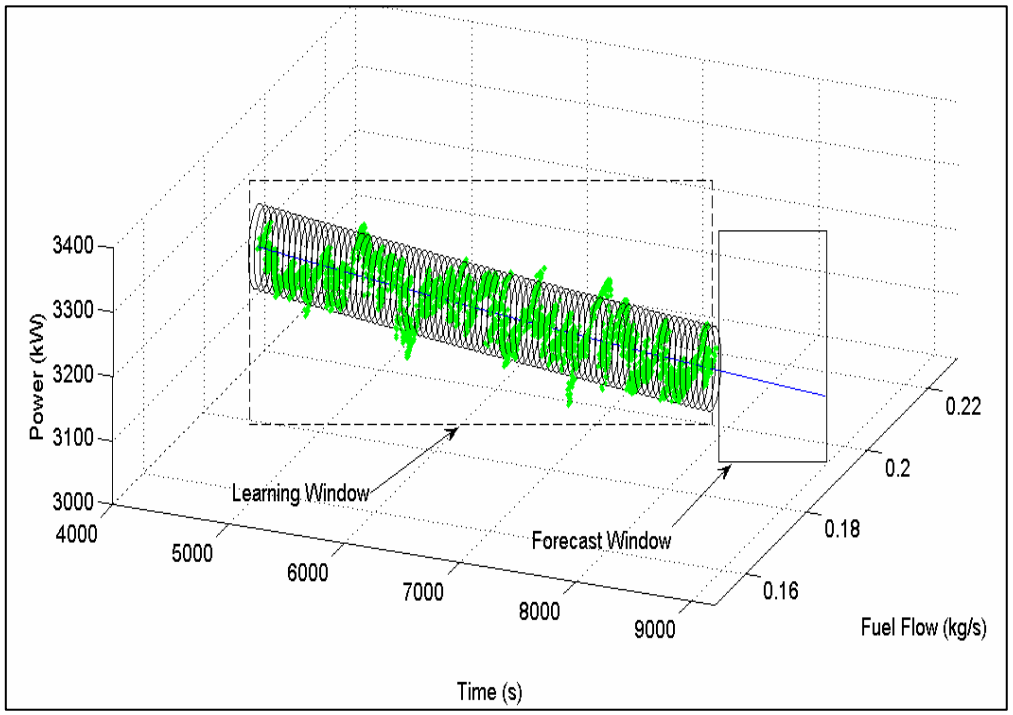

Figure 6.9. Forecast of fuel flow and power generated versus time for a Mercury 50 gas turbine for 8,000<t<9,000s

Figure 6.12 shows the first level wavelet approximation reconstructed from the approximation coefficient vector for the signal. As can be seen, the length of the signal approximation is equal to the sum of the desired forecasted signal (i.e., 8,000<t<9,000s) and the learning window (i.e., 4,000<t<8,000s). The first 4,000s are the signal approximation and the last 1,000s are the forecast approximation. A comparison of the actual signal (refer to Figure 6.10) and the reconstructed signal approximation (refer to Figure 6.12) for the initial 4,000s reveals that the signal approximation does not have the high frequency content of the original signal (i.e., is the signal details). Therefore, the signal details were extraneous and may be filtered out.

Figure 6.13 shows the comparison of the forecast for power generated for the next 1,000s and the corresponding experimental data in the forecast validation window as described earlier. The thick line represents the wavelet forecast which has been superimposed on the experimental data. The forecast does not vary as much as the original signal but can be assumed to represent the mean value of the signal forecast for a given time window. The forecast is within 2.3% of the actual experimental data which is within acceptable limits.

Figure 6.14 shows the wavelet forecast for fuel flow and power generated versus time in three dimensions. The power generated was analyzed as a function of fuel flow and time using two-dimensional discrete wavelet transform. The signal was analyzed for a period of 4,000s to obtain the signal approximation and the signal details were filtered out. Then based on this learning window, an approximation of the signal forecast was obtained for the next 1,000s. This

technique was used for a case study to compare the statistical and the wavelet forecast. The comparison between the forecast approximation and the actual signal for the next 1,000s gave an error of approximately 2.4%.

A case study was conducted in which the two prognostic techniques were applied to two turbine signals. The selected signals were the turbine rotor inlet temperature, TRIT T6, and the compressor outlet pressure, P3. A turbine run window of t=17,000s was selected for the learning data. The forecast was computed using both the statistical and the wavelet method for the next 4,000s. Figure 6.15 shows a comparison between the two techniques along with the respective forecast as labeled. The upper and the lower curves within the forecast window in the figure represent the statistical and the wavelet forecast, respectively.

A comparison was performed between the two forecast curves and the actual experimental data to compute the error, and hence, compare the two methods. It was observed that for rapidly fluctuating data, the wavelet analysis was more stable. The TRIT error, computed in the max norm, was 49°F and 82°F for the wavelet and statistical forecast methods, respectively. The pressure forecast error was approximately 21kPa and 34.2kPa for each method. The forecasting errors for both TRIT and pressure were within the acceptable limits of $\pm 5\%$.

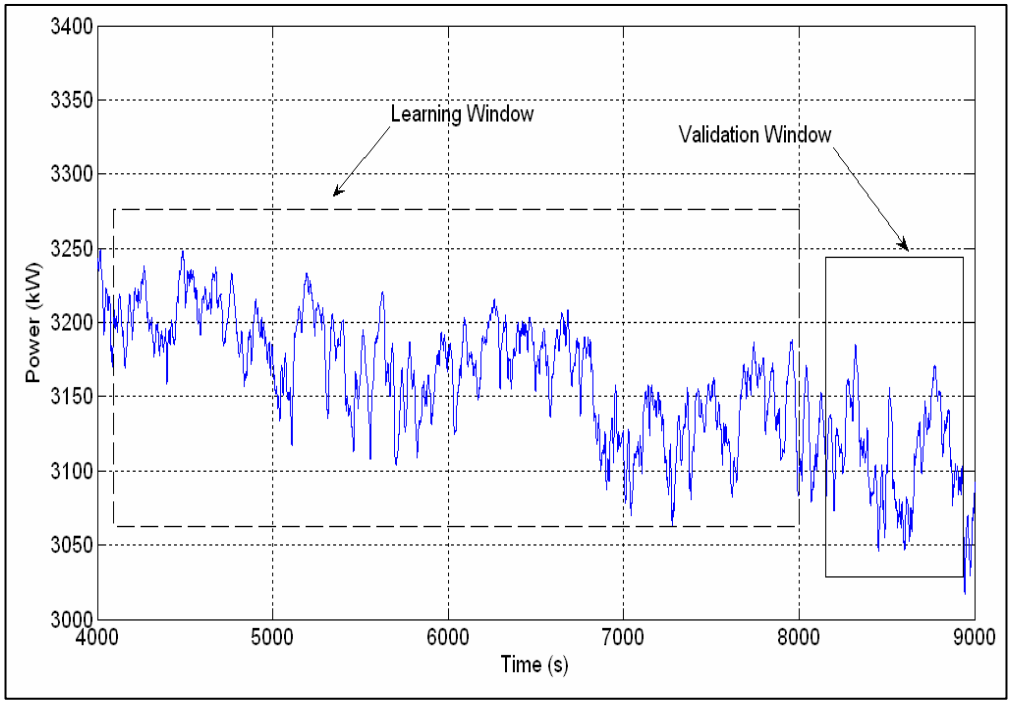

Figure 6.10. Power generation versus time for the steady state of a Mercury 50 gas turbine with learning 4,000<t<8,000s and validation 8,000<t<9,000s windows

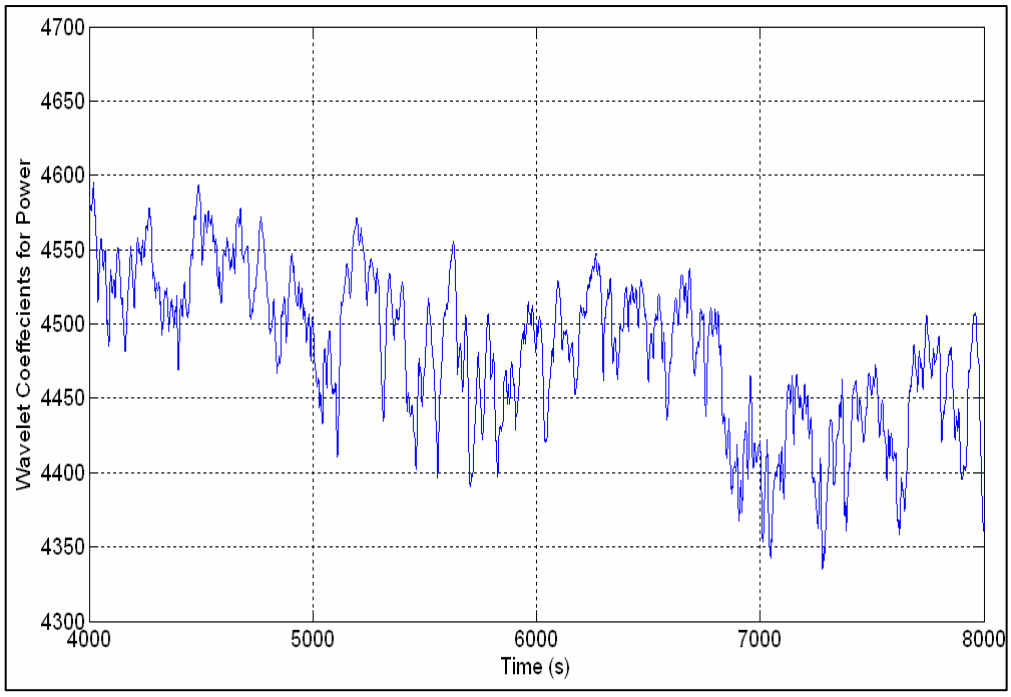

Figure 6.11. Second order approximation coefficients for the learning window 4,000<t<8000 for power generated

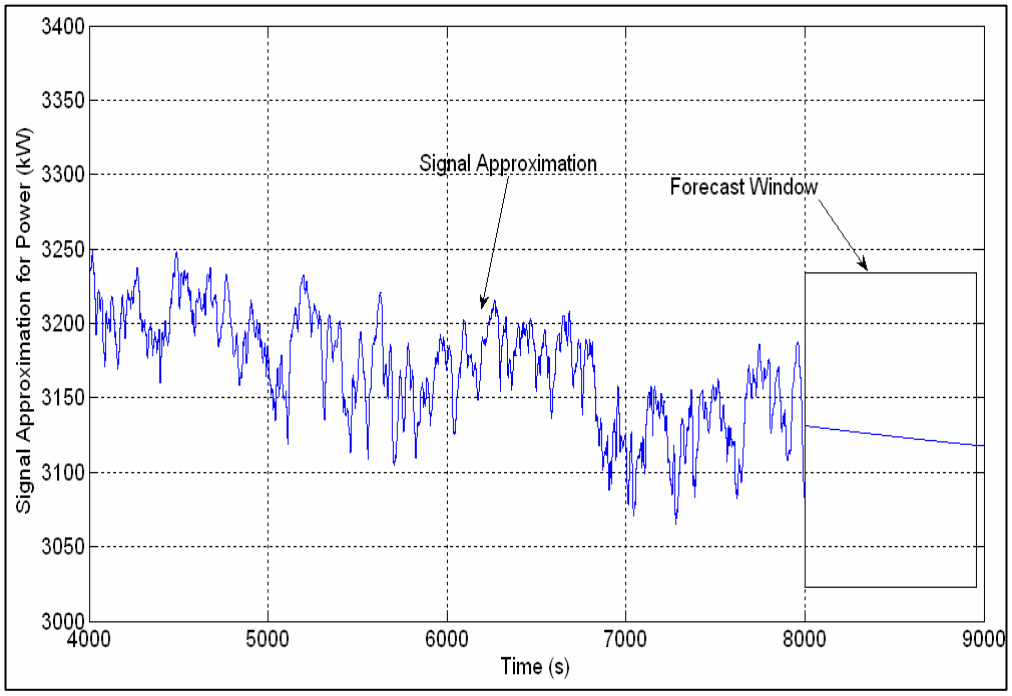

Figure 6.12. Signal approximation for 4,000<t<8,000s and forecast approximation for 8,000<t<9,000s for the steady state operation of a Mercury 50 gas turbine

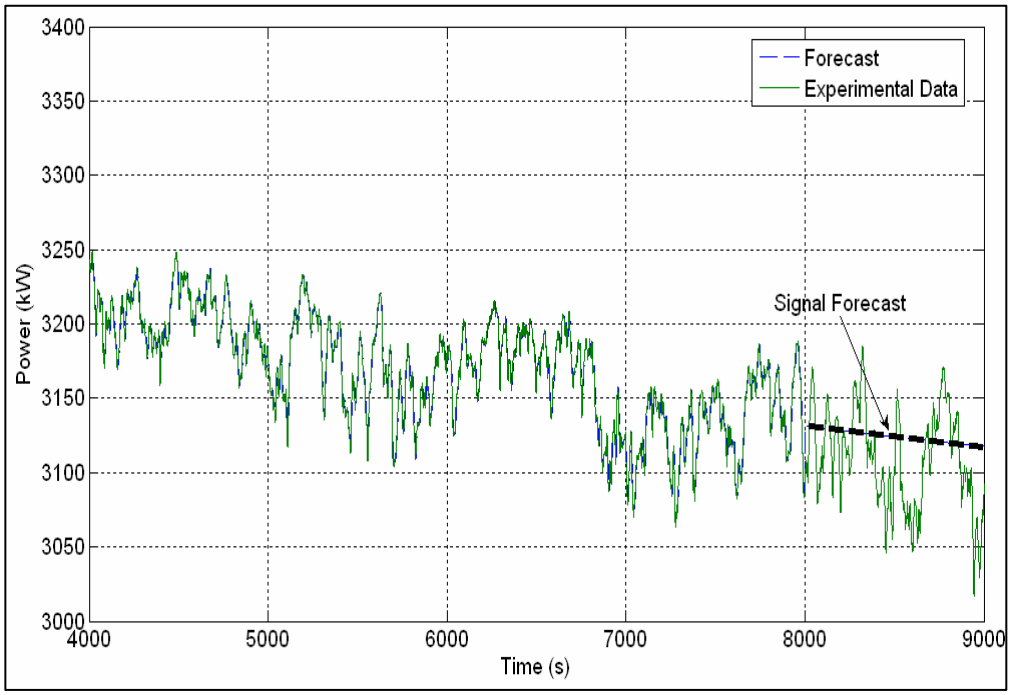

Figure 6.13. Forecast of power generated for a Mercury 50 gas turbine using wavelets for 8,000<t<9,000s

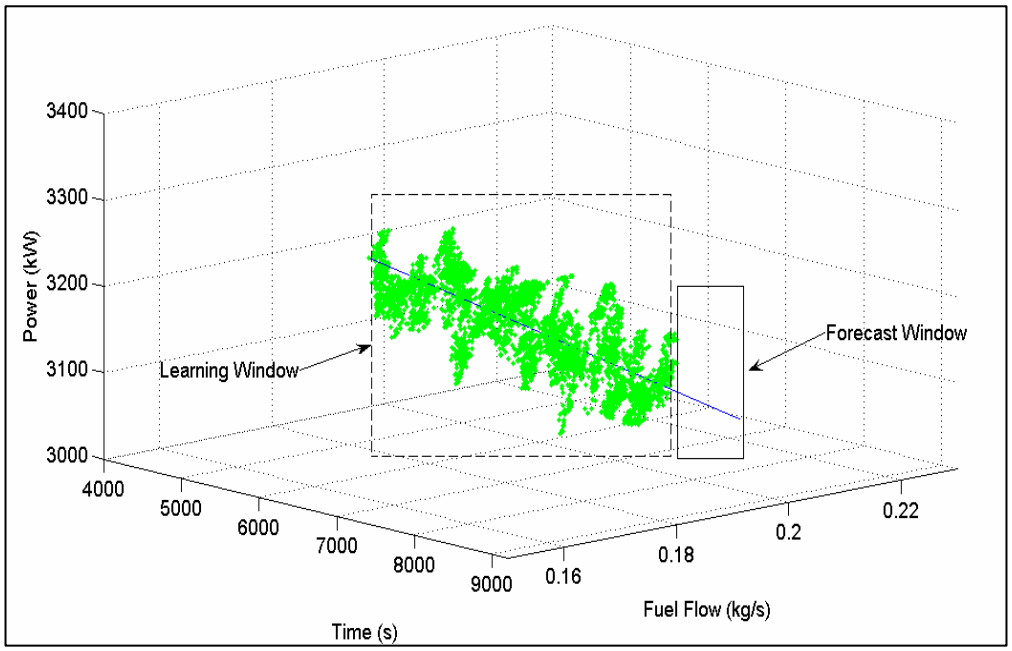

Figure 6.14. Three dimensional wavelet representation for fuel flow and power generated versus time with learning (4,000<t<8,000s) and forecast (8,000<t<9,000s) windows

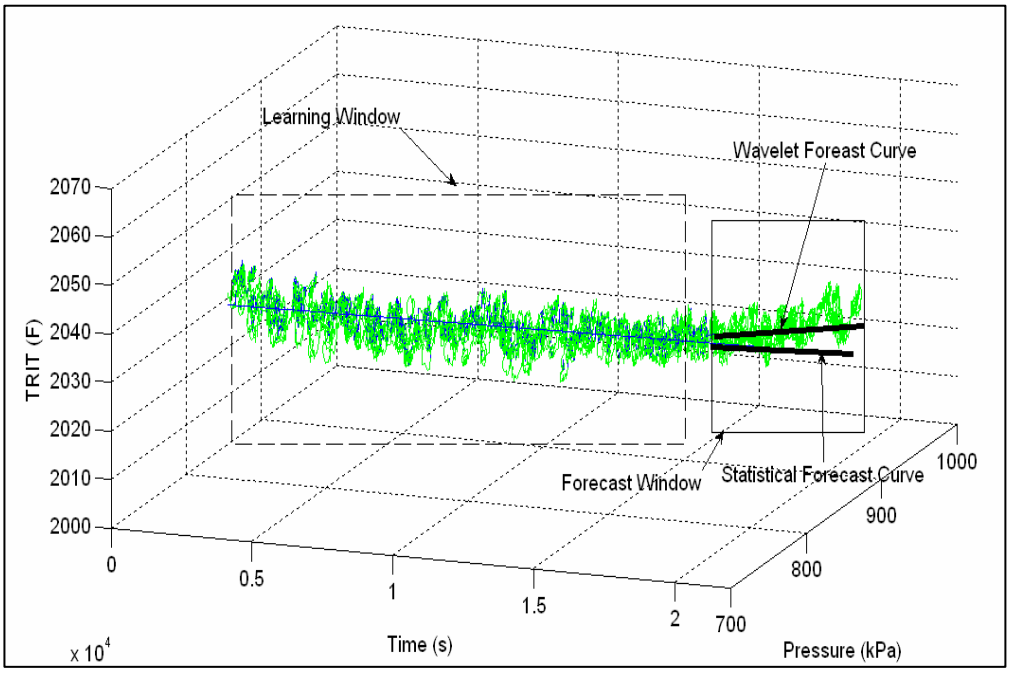

Figure 6.15. Comparison of wavelet and statistical forecast for the steady state operation of the Mercury 50 gas turbine for the forecast window for 17,000<t<21,000s

Prognostic Methods - Application to a General Electric 7EA Gas Turbine

The GE 7EA input signals included power generated (PG), fuel flow rate (FF), and inlet guide vane angle (IGVA). The set of output signals selected to forecast system health consisted of turbine inlet temperature (T_{TT}), compressor delivery pressure (PCD), generator temperature (T_G), exhaust temperature (T_{EX}), compressor discharge temperature (T_{CD}), compressor inlet mass flow (T_{CF}), generator maximum vibration (A_{GV}), and gas turbine maximum vibration (A_{TV}). The output signals were selected based on their high correlations with the three input signals as shown in Table 1. For instance, the turbine inlet temperature has correlation values of $|R_{11}| = 0.83$, $|R_{12}| = 0.83$, and $|R_{13}| = 0.88$ with the PG, FF, and IGVA signals, respectively. Hence, the turbine inlet temperature is selected as a signal to analyze since $|R_{jk}| > 0.80$ for all three input signals.

Prognostic Methodologies

A three step process was followed to analyze the turbine inlet temperature, T_{TT}. First, the steady-state signal was conditioned to obtain a concatenated and filtered signal. Second, the statistical prognostic methodology was applied to obtain the signal forecast. Third, the wavelet method was supplied the same signal to predict the system behavior. Finally, a comparison of the two methods was performed. Note that for real-time applications, the desired system operating mode must be present before signal filtering and analysis; signal concatenation will not occur.

Signal Conditioning

The turbine inlet temperature profile is shown in Figure 6.16a for a period of $t^* = 59{,}000$ minutes. The signal is somewhat oscillatory due to start ups, shut downs, and different operating loads. For a meaningful analysis of the turbine data, three operating ranges (or modes) were identified for the turbine inlet temperature (200-400$^\circ C$, 400-600$^\circ C$, and 600-800$^\circ C$). These operating ranges are user-defined and typically based on turbine operating modes (e.g., light, medium, and heavy loads per electrical power generating demands).

The turbine inlet temperature range of $600 < T_{TT} < 800^\circ C$ was selected since this corresponds to the most common operating mode of maximum turbine load. Specifically, the turbine runs for t=32,200 minutes of the total $t^* = 59{,}000$ minutes in the heavy load mode. In Figure 6.16b, the concatenated data for the turbine inlet temperature has been displayed. The next task was to normalize the concatenated data using a simple filter $Y_j^* = Y_j(i+1) - Y_j(i)$ to further reduce fluctuations. The filtered turbine inlet temperature with a mean value of zero, refer to Figure 6.16c, shows variations about the actual signal mean, $\bar{y}_j$. The data has been divided into the learning (i.e., 0<t<22,200 minutes) and the validation (i.e., 22,200<t<32,200 minutes) windows, W_L and W_V. The prognostic algorithm used the learning window, W_L, as the training data for the regression curve to detect trends. The estimated system forecast was then compared with the experimental data in the validation window, W_V, to gauge the prognostic method accuracy.

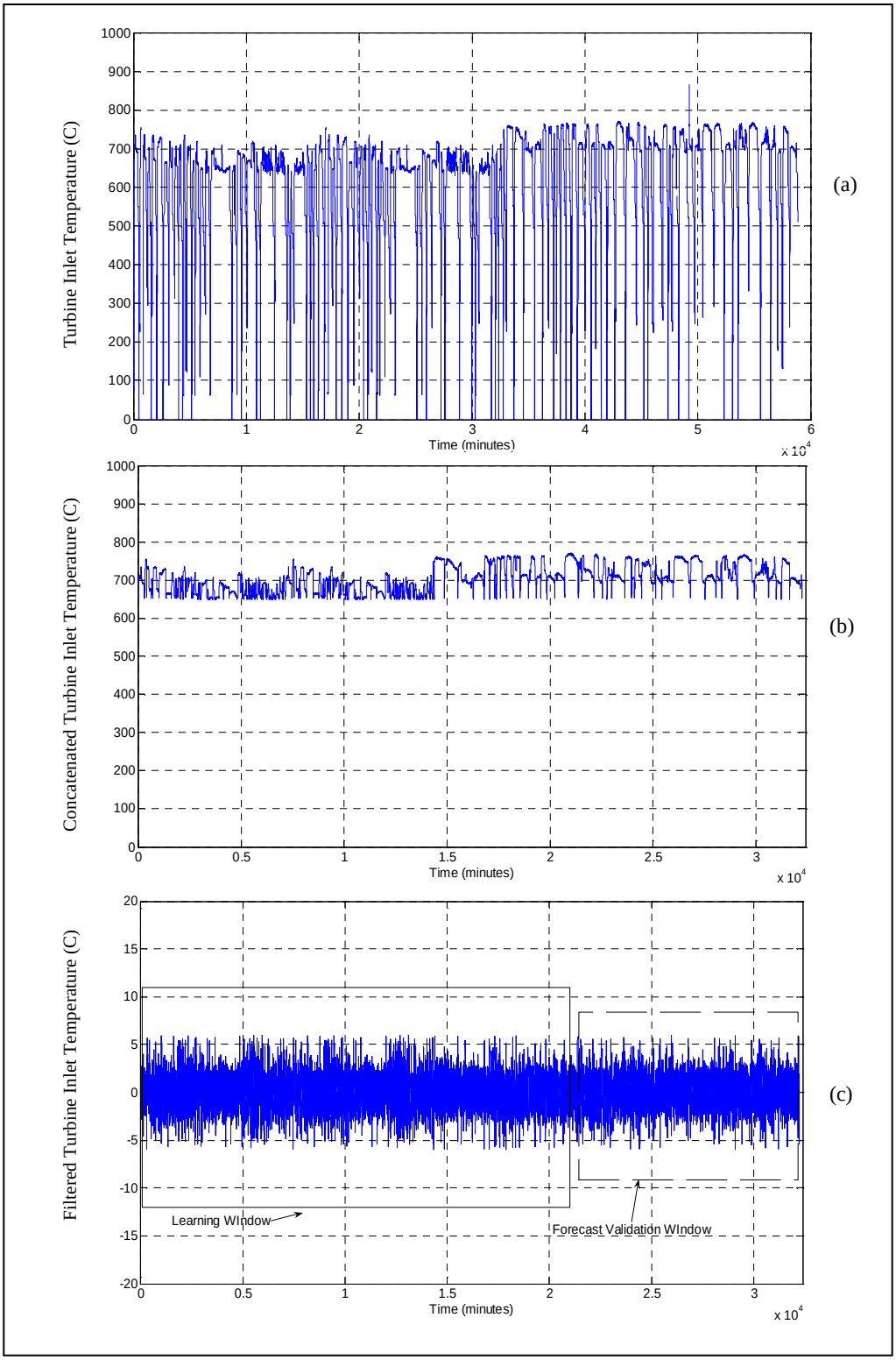

Figure 6.16. GE 7EA stationary gas turbine inlet temperature profile: (a) Raw data signal for $0<t^{*}<59{,}000$ minutes, (b) Restricted operating range of 600-800 $^{\circ}C$ for $0<t<32{,}200$ minutes, and (c) Filtered data showing the learning $0<t<22{,}200$ minutes and validation windows $22{,}200<t<32{,}200$ minutes

Statistical Forecasting

The filtered signal, Y_j^*, was analyzed using the statistical methodology to predict the system behavior. In Figure 6.17a, the regression curve for the initial turbine inlet temperature learning data has been graphed versus time. The derived regression curve, $\vec{Z}_{ji}$, forecasts the system operation for a period of t=10,000 minutes (i.e., 22,200<t<32,200 minutes) as shown in Figure 6.17b. When comparing the predicted and actual data in the validation window the forecast error is 11.47%. The system operation forecast for turbine inlet temperature mapped back into the operating domain along with the forecast error bounds, $\pm\varepsilon$, is shown in Figure 6.17c. Note that the forecasted signal displays a non-fluctuating behavior which predicts the signal mean rather than the specific fluctuations which may be an advantage.

Wavelet Forecasting

The wavelet prognostic algorithm computes the fourth-order wavelet transform of the filtered data, Y_{ji}^*, in the learning window, W_L. This transform yields the low frequency (approximation) and the high frequency (detail) wavelet coefficients. A least squares fit was performed on the approximation coefficients (refer to Figure 6.18a) with the coefficients forecasted for t=10,000 minutes. The signal approximation was reconstructed from the coefficients by taking the inverse wavelet transform. The length of the reconstructed signal approximation was equal to the sum of the desired forecasted signal and the learning window. A comparison between the forecast and experimental for the turbine inlet temperature for 22,000<t<32,000 minutes is shown in Figure 6.18b. The thick line

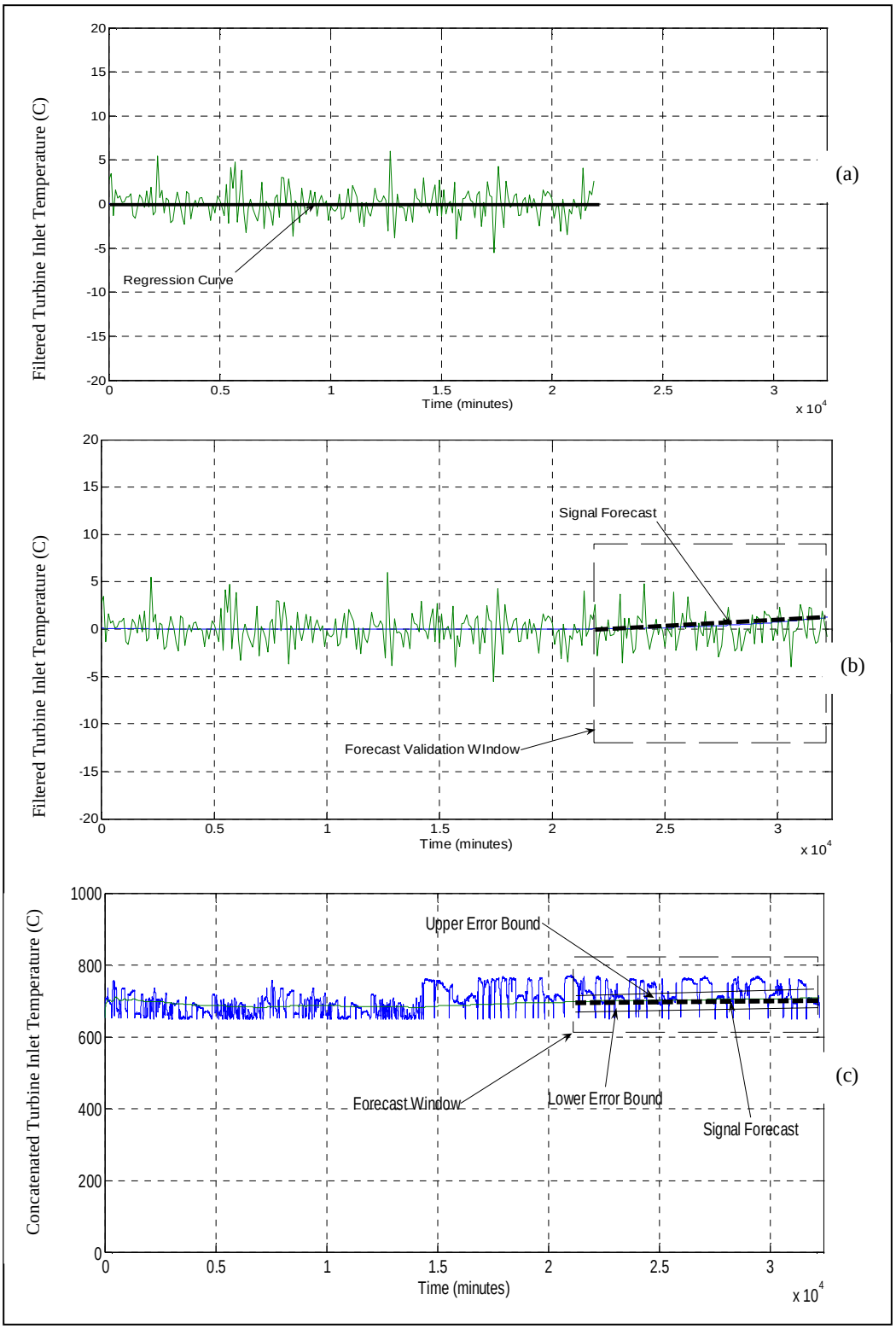

Figure 6.17. Statistical prognostic strategy: (a) Regression curve for turbine inlet temperature during learning window (0<t<22,200 minutes), (b) Statistical signal forecast (22,200<t<32,200 minutes), and (c) Signal and statistical forecast mapped back into the operating domain for 0<t<32,200 minutes

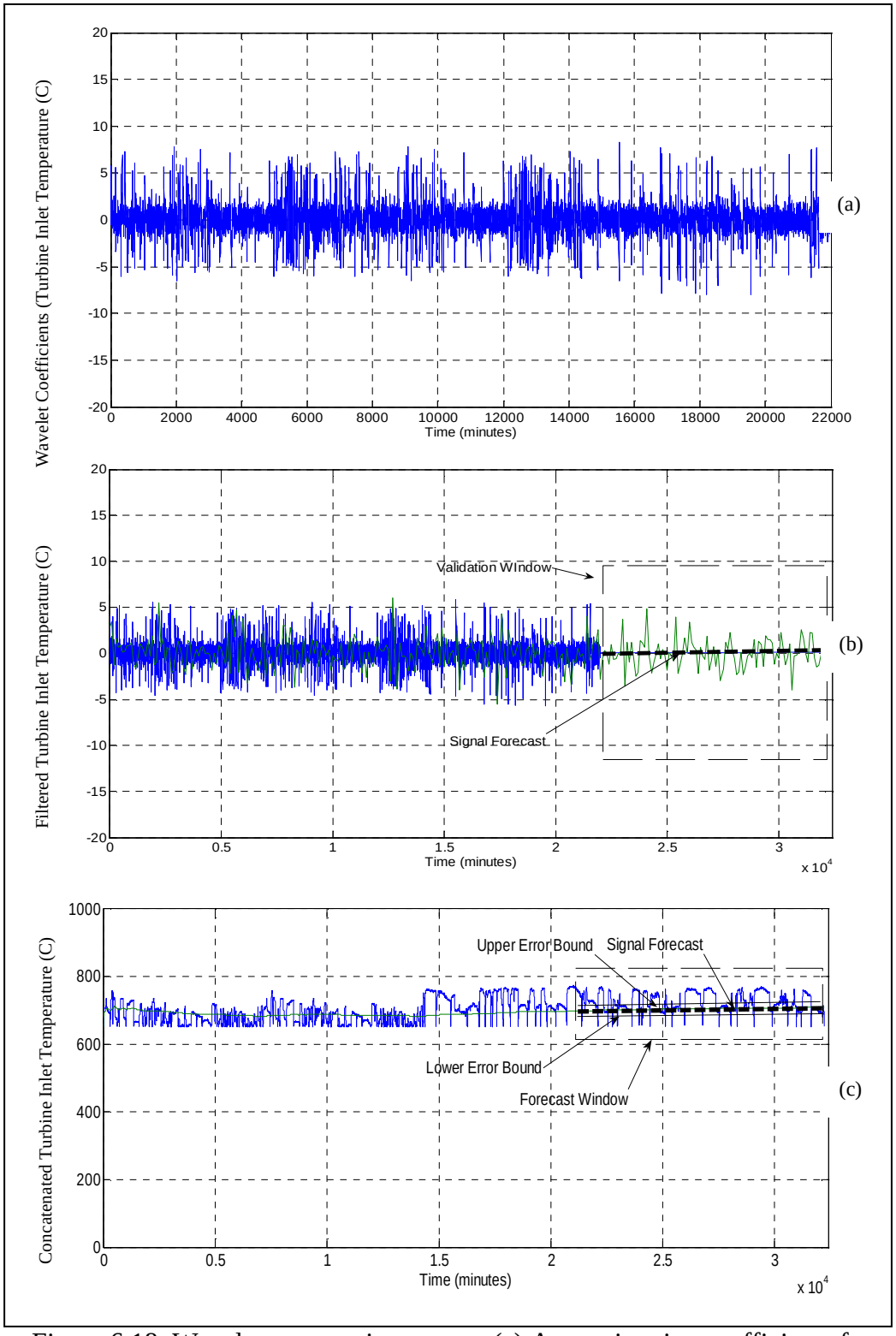

Figure 6.18. Wavelet prognostic strategy: (a) Approximation coefficients for turbine inlet temperature for learning window (0<t<22,200 minutes), (b) Wavelet signal forecast (22,200<t<32,200 minutes) with reduced display density, and (c) Signal and wavelet forecast mapped back into the operating domain for 0<t<32,200 minutes

represents the wavelet forecast which has been superimposed on the experimental data; the forecast error estimation is 9.23%. For a better visual representation, the filtered data and the signal forecast are mapped back into the operating domain along with the error bounds, $\pm\varepsilon$, as shown in Figure 6.18c. A three dimensional representation of the statistical and the wavelet forecast for turbine inlet temperature, T_{TT}, versus the three input signals power generated, inlet guide vane angles, and fuel flow during the forecast window (22,200<t<32,200 minutes) is presented in Figures 6.20-6.25. As shown the turbine inlet temperature is a function of the three input signals.

Comparison of Results

A comparison of the two prognostic techniques, based on the forecast error values, has been presented in Table 6.2. In addition to the turbine inlet temperature, four other plant signals were forecasted and their respective errors computed. In each of the five cases, the wavelet method produced a lower forecast error and may be ranked as the better prognostic strategy. Overall, the forecast errors are acceptable for both the methods, but dependant on steady-state plant operation in well defined modes. To implement the wavelet prognostic strategy in real-time, the general algorithm is shown in Figure 6.19. A variable length user defined window, W_S, must be selected to calculate the wavelet coefficients and predict future plant behavior. At the appropriate time, new data may be obtained and the process continues. Note that in real-time, the forecast error will be small as the signal variations within a user defined window would be negligible and no concatenation would be required.

Signal No.	Signal Description	Correlation, $\lvert\Re_{jk}\rvert$			Forecast Error, $\%\varepsilon$	
		PG	FF	IGVA	Statistical	Wavelet
1	T_{TT}	0.83	0.83	0.88	11.47	9.23
2	T_G	0.83	0.83	0.87	10.40	8.87
3	T_{EX}	0.99	0.99	0.98	9.49	5.24
4	A_{GV}	0.89	0.89	0.87	10.43	9.69
5	A_{TV}	0.82	0.82	0.56	10.89	9.01

Table 6.2. Comparison of statistical and wavelet prognostic forecast for five GE 7EA gas turbine output signals based on the three input signals power generated (PG), fuel flow (FF), and inlet guide vane angle (IGVA); over a 10,000 minutes validation window

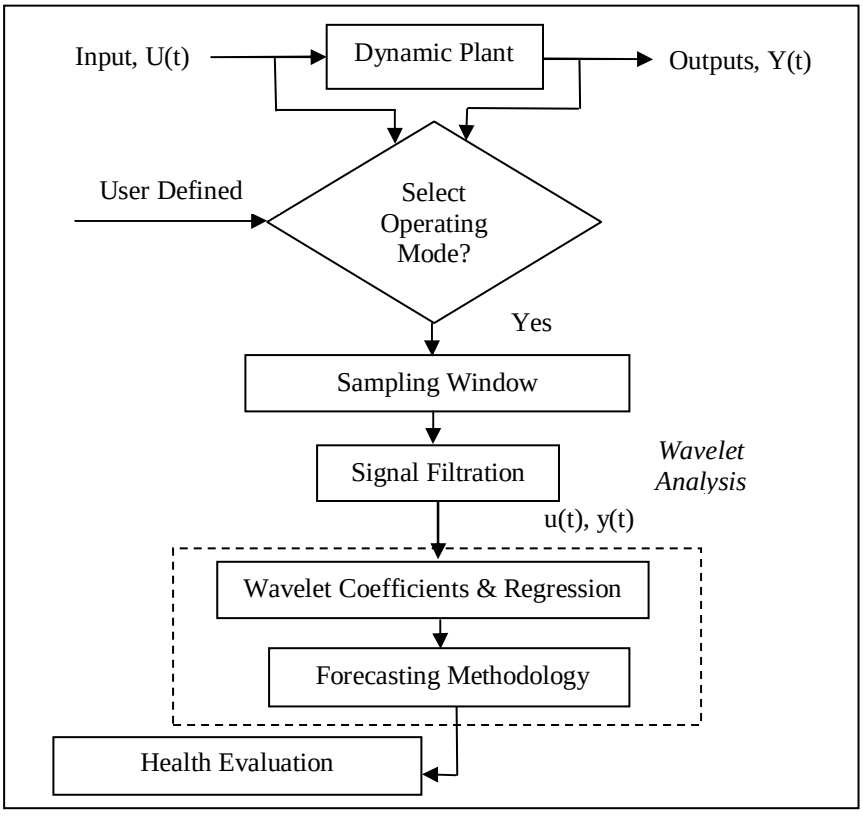

Figure 6.19 Real-time application of the wavelet prognostic methodology

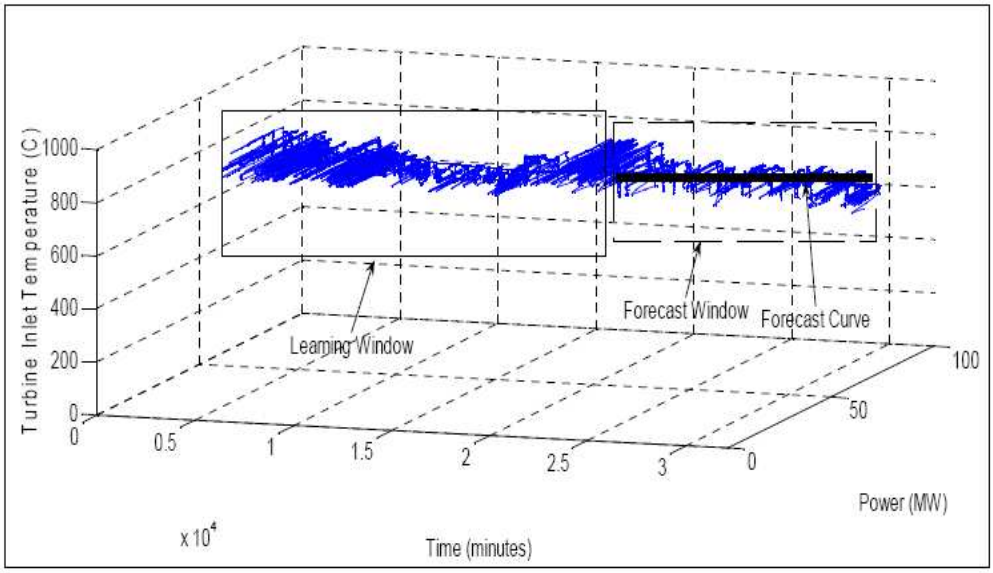

Figure 6.20. Statistical forecast for turbine inlet temperature versus power and time during the forecast window (22,200<t<32,200 minutes)

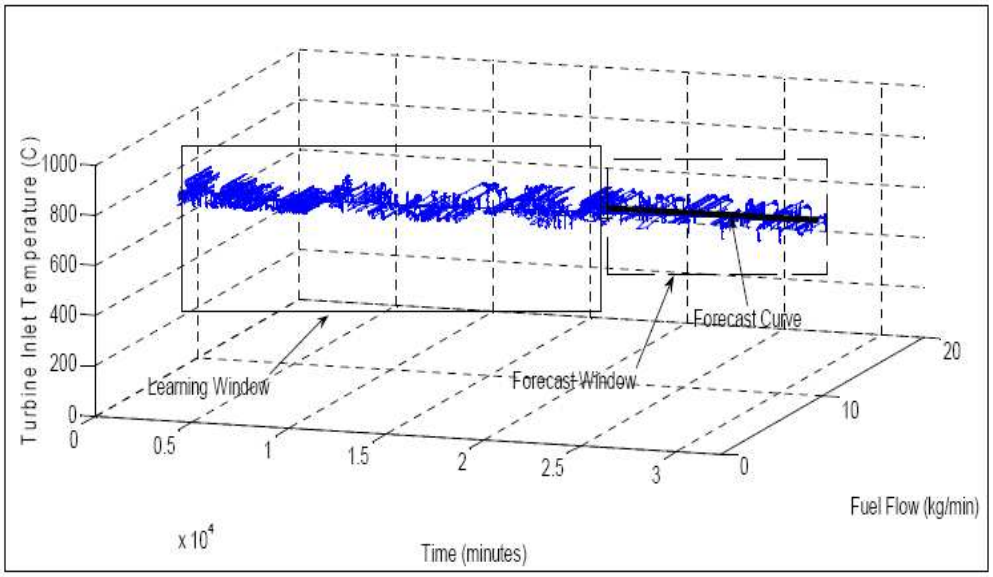

Figure 6.21 Statistical forecast for turbine inlet temperature versus fuel flow and time during the forecast window (22,200<t<32,200 minutes)

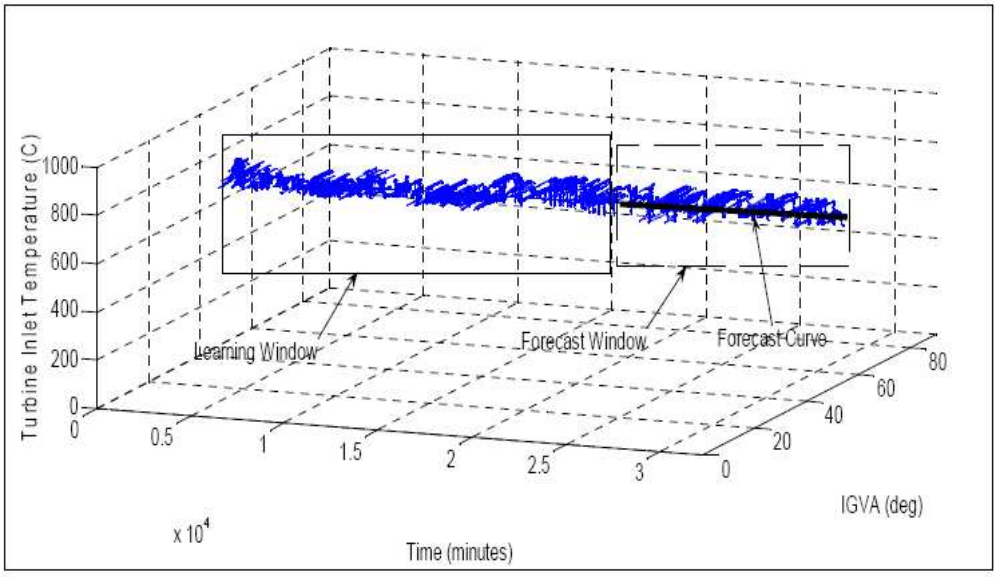

Figure 6.22 Statistical forecast for turbine inlet temperature versus inlet guide vane angle (IGVA) and time during the forecast window (22,200<t<32,200 minutes)

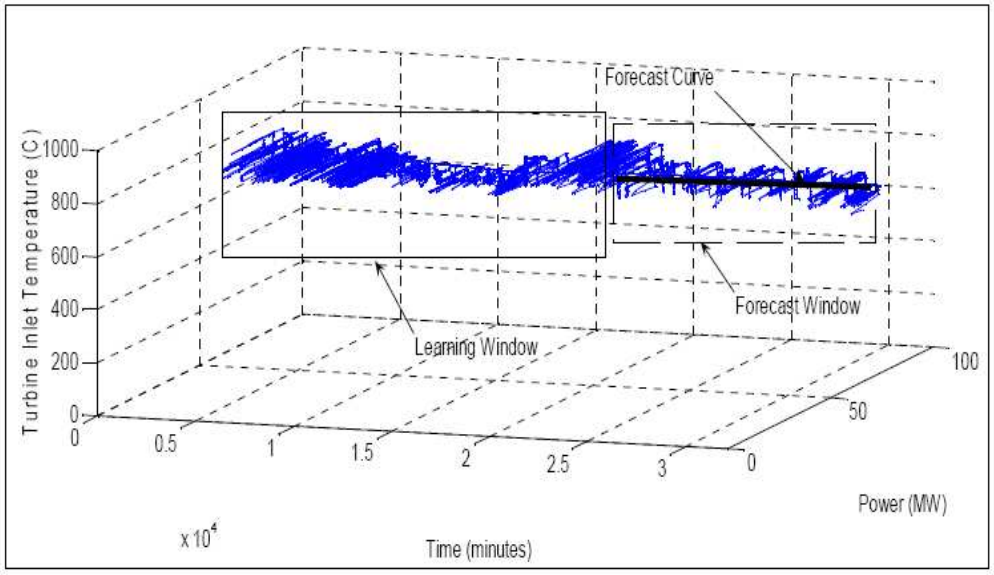

Figure 6.23 Wavelet forecast for turbine inlet temperature versus power and time during the forecast window (22,200<t<32,200 minutes)

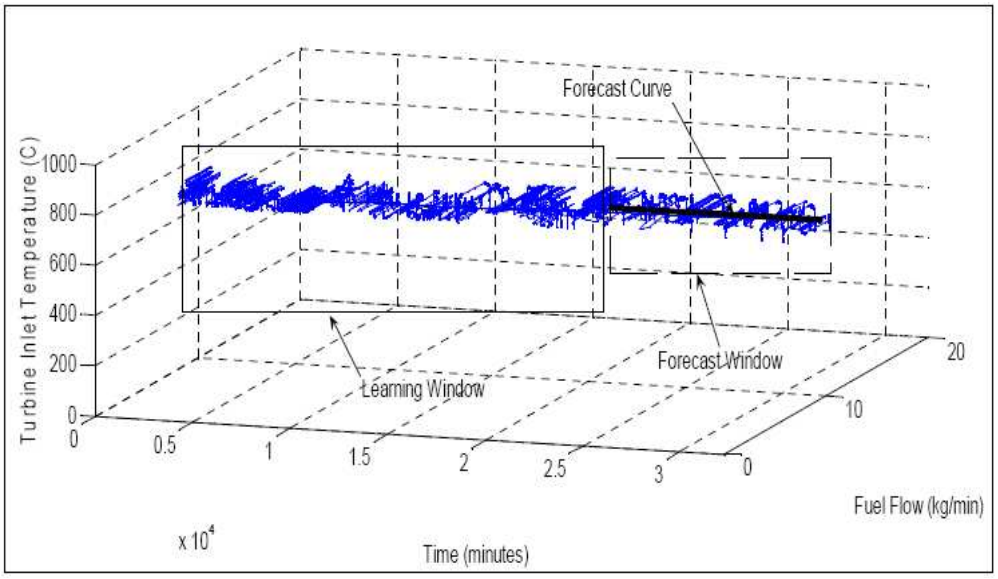

Figure 6.24 Wavelet forecast for turbine inlet temperature versus fuel flow and time during the forecast window (22,200<t<32,200 minutes)

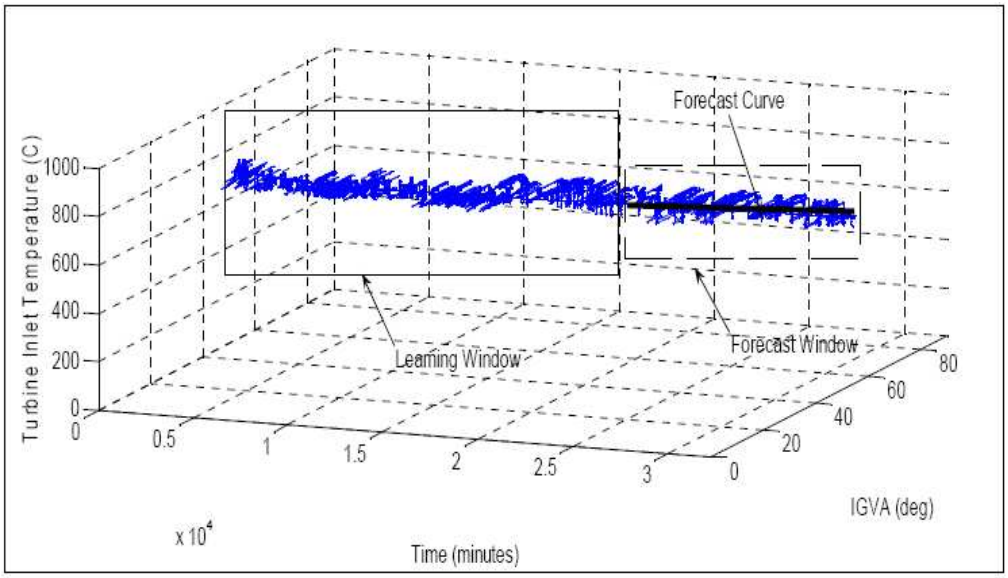

Figure 6.25 Wavelet forecast for turbine inlet temperature versus inlet guide vane angle (IGVA) and time during the forecast window (22,200<t<32,200 minutes)

CHAPTER 7

CONCLUSIONS AND RECOMMENDATIONS

The health monitoring of simple cycle gas turbines requires real-time prognostics strategies to increase performance and reliability, thereby enabling cost savings and increased operator safety. A dynamic mathematical model representing a Mercury 50 gas turbine has been developed and numerical results have been obtained by simulation. Physical and thermodynamic laws have been used to describe the system dynamics. This mathematical model has been transformed into a computer algorithm in the MATLAB/Simulink environment. The simulation results have been compared with representative experimental data gathered for a standard turbine. The estimated turbine behavior compares well with the actual data. This model can be used in a Model-based process diagnostic strategy and represents a key contribution to the field of real-time simple cycle gas turbine health management systems.

Two model-free real-time prognostic strategies with applications to stationary gas turbine have been presented. Representative experimental results have been compared to validate the accuracy of the proposed approaches. The estimated forecast for different turbine signals compares well with the actual test data. It can be concluded that the wavelet transform based method is better, as the forecasting error is less for the former for each of the signals studied. This can be attributed to the “de-noising” of the actual learning signal, as the high frequency content of the signal (i.e., the signal details) is filtered when the wavelet

coefficients are computed. This filtering helps to identify the hidden trend of the signal and the corresponding forecast follows the trend and hence a good forecast is obtained. For the statistical method, no filtering is applied which leads to greater forecasting errors. The developed approaches may be used in parallel for a diagnostic algorithm to monitor stationary gas turbine system health.

Recommendations

The future work for the research team is to extend the developed methodologies to other gas turbine configurations such as the combined cycle systems. On the basis of the research conducted, a few recommendations have been suggested. For the turbine dynamic model, new subsystems need to be included to represent a combined cycle gas turbine. System parameters will have to be adjusted and model validation performed. For the prognostic strategies, different signal combinations may be investigated to forecast system health. In addition, higher level wavelet decompositions may be performed to compare the forecast results for different transform levels. To predict transient behavior the length of the learning data windows may be made small so that short term forecast is obtained. Finally, the prognostic strategies may be applied to other dynamic systems for which the sensory information is readily available.

APPENDICES

Appendix A Matlab/Simulink Code For The Analytical Model

Matlab Code

```
% Matlab Simulink Model for Mercury 50
% Matlab file: ModelFile
% Simulink File: TurbineModel

clear all
clc
load turjun14;

%Model Parameters

comp_area=0.19;                % Compressor Area
specific_air=1005;             % Specific heat air
specific_gas=1148;             % specific heat gas
specific_ratioair=1.4;         %k
specific_ratiogas=1.33;        %k
lower_heatval=61000000;        %LHV
hf=4600                        %Enthaphy
CA=150;                        %Axial velocity
jeq=0.4;
m_cchamber=1;
ns=10;                         % Number of stages
press_inlet=101.3;             %Inlet Pressure
press_drop=3;                  %Pressure Drop
temp_in=298;                   %Inlet Tmperature
R=287.4;
U=250;
%%%%%%%%%%%%%%%%%%%%%%%%%%%%%%%%%%%%%%%%%%%%%%%%
%Various efficiencies
%%%%%%%%%%%%%%%%%%%%%%%%%%%%%%%%%%%%%%%%%%%%%%%%
eff_comp=0.9;                %%% compressor
eff_cchamber=0.95;           %%% combustion chamber
eff_recup=0.85;              %%% recuperator
eff_turbine=0.9;             %%% turbine
eff_stage=0.9;               %%% stage
fric_tor=30;                 %%% friction torque
temp_coeff=0.35              %%% temperature coefficient

%%%%%%%%%%%%%%%%%%%%%%%%%%%%%%%%%%%%%%%%%%%%%%%%%%
%Data conversion
%%%%%%%%%%%%%%%%%%%%%%%%%%%%%%%%%%%%%%%%%%%%%%%%%%%
A=double(temp199);
A=A(807:9402);
A=A/1500;
T=[1:8596];
V1=[T;A]';


%Plots for the model and the experimental data
sim('turbinemodel2');
figure(1)
```

```
plot(TM,CompressorMflow)       % plots the mass flow rate versus
time
xlabel('Time(sec)')
ylabel('Mass Flow(Kg/sec)')
axis([-.01,8000,0,18])
grid on


figure(2)  % plots the shaft speed versus time
plot(TM,ShaftSpeed,'--',tt(1:10000)-
338,double(temp_1(1:10000))*1.4862)
xlabel('Time(sec)')
ylabel('Shaft Velocity(rad/sec)')
axis([-.01,8000,0,1700])
legend('Simulation','Data')
grid on

figure(3)   %plots the powere generated versus time
plot(TM,Power,'--',tt(1:10000)-809,double(temp199(1:10000)))
xlabel('Time(sec)')
ylabel('Power(KW)')
axis([-.01,8000,0,3300])
legend('Simulation','Data')
grid on

figure(4) % plots TRIT versus time
plot(TM,CombustionChamberTemp,'--',tt(1:10000)-
338,((double(temp295(1:10000))-32)*.5555)+273.15)
xlabel('Time(sec)')
ylabel('TRIT(K)')
axis([-.01,8000,0,1800])
legend('Simulation','Data')
grid on

figure(5) % plots PCD versus time
plot(TM,CompressorOutletPressure,'--',tt(1:10000)-
338,((double(temp74(1:10000))-6240)*.05526)+100)
xlabel('Time(sec)')
ylabel('Pressure(kPa)')
axis([-.01,8000,0,1100])
legend('Simulation','Data')
grid on

figure(6) % plots fuel flow versus time
plot(TM,FuelFlow,'--',tt(1:10000)-338,(double(temp46(1:10000))-
6240)/89856)
xlabel('Time(sec)')
ylabel('Fuel Flow (Kg/sec)')
axis([-.01,8000,0,.24])
legend('Simulation','Data')
grid on
```

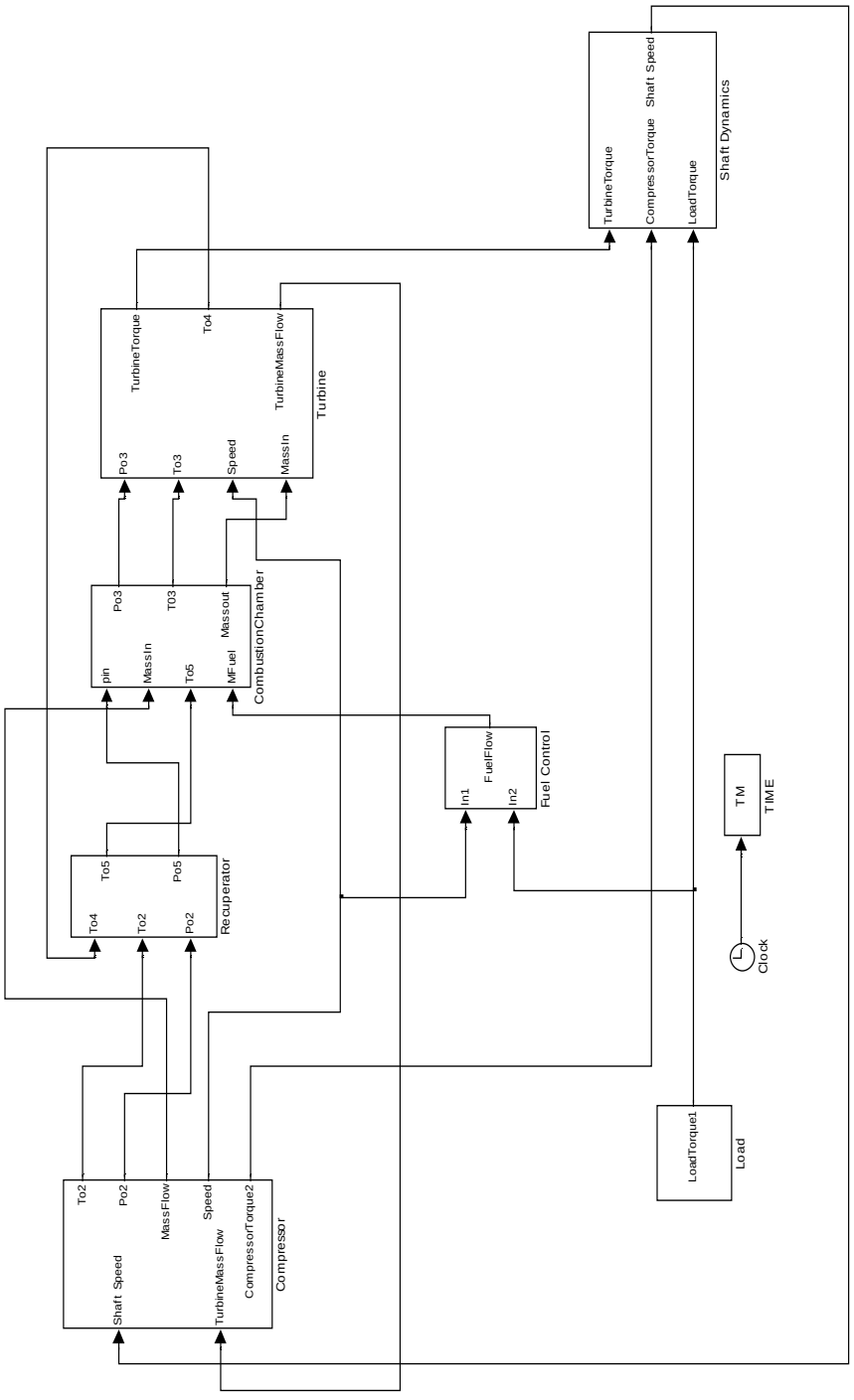

Figure A.1 Simulink block diagram for the Mercury 50 stationary gas turbine

Appendix B Matlab/Simulink Code For Data Acquistion

Matlab Code

```
%   DATA ACQUISITION PROGRAM FOR MERCURY 50


%%%%%%%%%%%%%%%%%%%%%%%%%%%%%%%%%%%%%%%%%%%%%%%%%%%%%%%%%%%%%%%%%%%%%%%%%%%%%%%%
%%%
The code tests the availability of the MXOPC server and waits for
an error if no error is detected (i.e., the connection has been
established for the Mercury 50 stationary gas turbine)the data
can be transmitted
%%%%%%%%%%%%%%%%%%%%%%%%%%%%%%%%%%%%%%%%%%%%%%%%%%%%%%%%%%%%%%%%%%%%%%%%%%%%%%%%
%%%
mxopc ?
hr=mxopc('open','RSLinx OPC Server','localhost',1000)
hr=mxopc('BrowseRoot');
hr=mxopc('BrowseFolders')
hr=mxopc('BrowseDown','M50');
hr=mxopc('BrowseDown','Online');
hr=mxopc('Browsedown','N11');
%
%
%
StartTime=clock;
%
for n=1:30000
%%%%%%%%%%%%%%%%%%%%%%%%%%%%%%%%%%%%%%%%%%%%%%%%%%%%%%%%%%%%%%%%%%%%%%%%%%%%%%%%
% Data Acquisition is started by specifying the signals to be
recorded to the MXOPC server for the Mercury 50 stationary gas
turbine
%%%%%%%%%%%%%%%%%%%%%%%%%%%%%%%%%%%%%%%%%%%%%%%%%%%%%%%%%%%%%%%%%%%%%%%%%%%%%%%%
    [v1,hr]=mxopc('ReadInt','[M50]N11:1');
    [v2,hr]=mxopc('ReadInt','[M50]N11:19');
    [v3,hr]=mxopc('ReadInt','[M50]N11:20');
    [v4,hr]=mxopc('ReadInt','[M50]N11:22');
    [v5,hr]=mxopc('ReadInt','[M50]N11:23');
    [v6,hr]=mxopc('ReadInt','[M50]N11:24');
    [v7,hr]=mxopc('ReadInt','[M50]N11:25');
    [v8,hr]=mxopc('ReadInt','[M50]N11:26');
    [v9,hr]=mxopc('ReadInt','[M50]N11:27');
    [v10,hr]=mxopc('ReadInt','[M50]N11:28');
    [v11,hr]=mxopc('ReadInt','[M50]N11:29');
    [v12,hr]=mxopc('ReadInt','[M50]N11:30');
    [v13,hr]=mxopc('ReadInt','[M50]N11:31');
    [v14,hr]=mxopc('ReadInt','[M50]N11:32');
    [v15,hr]=mxopc('ReadInt','[M50]N11:33');
    [v16,hr]=mxopc('ReadInt','[M50]N11:34');
    [v17,hr]=mxopc('ReadInt','[M50]N11:43');
    [v18,hr]=mxopc('ReadInt','[M50]N11:46');
    [v19,hr]=mxopc('ReadInt','[M50]N11:51');
    [v20,hr]=mxopc('ReadInt','[M50]N11:54');
    [v21,hr]=mxopc('ReadInt','[M50]N11:57');
    [v22,hr]=mxopc('ReadInt','[M50]N11:60');
```

```
    [v23,hr]=mxopc('ReadInt','[M50]N11:64');
    [v24,hr]=mxopc('ReadInt','[M50]N11:65');
    [v25,hr]=mxopc('ReadInt','[M50]N11:66');
    [v26,hr]=mxopc('ReadInt','[M50]N11:71');
    [v27,hr]=mxopc('ReadInt','[M50]N11:73');
    [v28,hr]=mxopc('ReadInt','[M50]N11:74');
    [v29,hr]=mxopc('ReadInt','[M50]N11:76');
    [v30,hr]=mxopc('ReadInt','[M50]N11:79');
    [v31,hr]=mxopc('ReadInt','[M50]N11:80');
    [v32,hr]=mxopc('ReadInt','[M50]N11:81');
    [v33,hr]=mxopc('ReadInt','[M50]N11:82');
    [v34,hr]=mxopc('ReadInt','[M50]N11:87');
    [v35,hr]=mxopc('ReadInt','[M50]N11:88');
    [v36,hr]=mxopc('ReadInt','[M50]N11:89');
    [v37,hr]=mxopc('ReadInt','[M50]N11:91');
    [v38,hr]=mxopc('ReadInt','[M50]N11:92');
    [v39,hr]=mxopc('ReadInt','[M50]N11:103');
    [v40,hr]=mxopc('ReadInt','[M50]N11:104');
    [v41,hr]=mxopc('ReadInt','[M50]N11:107');
    [v42,hr]=mxopc('ReadInt','[M50]N11:189');
    [v43,hr]=mxopc('ReadInt','[M50]N11:199');
    [v44,hr]=mxopc('ReadInt','[M50]N11:225');
    [v45,hr]=mxopc('ReadInt','[M50]N11:291');
    [v46,hr]=mxopc('ReadInt','[M50]N11:292');
    [v47,hr]=mxopc('ReadInt','[M50]N11:293');
    [v48,hr]=mxopc('ReadInt','[M50]N11:295');
    [v49,hr]=mxopc('ReadInt','[M50]N11:308');
    [v50,hr]=mxopc('ReadInt','[M50]N11:310');
    %%%%%%%%%%%%%%%%%%%%%%%%%%%%%%%%%%%%%%%%%%%%%%%%%%%%%%%%%%%%
    % Once the data has been recorded the connection is closed
    %%%%%%%%%%%%%%%%%%%%%%%%%%%%%%%%%%%%%%%%%%%%%%%%%%%%%%%%%%%%
    mxopc('Sleep',1000);
    Nmissed=mxopc('Sleep')
    Nmiss(n)=double(Nmissed);
    n
end

StpTime=clock;
tt=1:length(s295);
figure
plot(tt,s295)                    %A test signal is plotted
title('TRIT for the Actual Run')
grid

%%%%%%%%%%%%%%%%%%%%%%%%%%%%%%%%%%%%%%%%%%%%%%%%%%%%%%%%%%%%
```

Appendix C Matlab/Simulimk Code For Prognostics

Mercury 50 Gas Turbine

%%% The code involves the usage of the Matlab statistical and wavelet toolboxes

Matlab Code For Statistical Method

```
% Tuple Formation

% Parameter Definition


clc
orient landscape

%load turfeb2
% Load the Data
%load turapr5
%Enter Parameters and their descriptions
signal_y = ((double(temp46)-6240)/89856);
%signal to be plotted on the y-axis
signal_z = double(temp199);
%signal to be plotted on the z-axis
signal_description_y = char('Fuel Flow [lb/hr]');
%description of y-axis variable
signal_description_z = char('Power [kW]');
%description of z-axis variable
order = 1;
%order of regression line
predict_length = 1000;
%Length Beyond the data that the program predicts
point_freq = 1;
%Sets how often points are plotted
circ_freq = 50;
%Sets how often circles are plotted
window_size = 500;
%moving meanwindow size

%Plot to check for times
%plot(1:length(signal_y),signal_y,1:length(signal_z),signal_z)
%comment rest of program and uncomment this line to use
%figure

%Select Times For Data
s_up = 2305;
%turbine ramp up start time (use line 19 to find)
sstart = 4000;
%start of steady state time (use line 19 to find)
sstop = 8000;
%stop of steady state time  (use line 19 to find)
```

```
s_down = 10801;
%end of shut down phase     (use line 19 to find)

%Select Region

%region = input('Enter 1 for Start up, 2 for Steady State, 3 for
Shut Down 4 for Manual Entry of Time ')
region = 4;

if region == 1
    start = s_up;
    stop = sstart;
end
if region == 2
    start = sstart;
    stop = sstop;
end
if region == 3
    start = sstop;
    stop = s_down;
end
if region == 4
    start = sstart;
    stop = sstop                                %sstart+(sstop-
sstart)/2;
end

%Statistics
std_y = std(signal_y(start:stop));
std_z = std(signal_z(start:stop));
mean_y = mean(signal_y(start:stop));
mean_z = mean(signal_z(start:stop));
ry = std_y*2;
rz = std_z*2;


%plots circles
hold on
plot3(start:point_freq:stop,signal_y(start:point_freq:stop),signa
l_z(start:point_freq:stop),'.g')
corry=signal_y;
corrz=signal_y.*lin;
for i = start:circ_freq:stop+predict_length
th = 0:pi/50:2*pi;
yunit = ry * cos(th) + corry(i);
zunit = rz * sin(th) + corrz(i);
plot3(ones(1,length(zunit)).*i,yunit,zunit,'k');
end
xlabel('time [s]')
ylabel([signal_description_y])
zlabel([signal_description_z])
legend('Data','Correlation Prediction')
axis([-inf,inf,1040,1180,2000,2200])
grid on
```

```
% MOVING MEAN
for i = window_size:length(signal_y)
    temp_data_y = corry(i-window_size+1:i);
    mean_data_y(i-window_size+1)=mean(temp_data_y);
    std_y(i)=std(temp_data_y);
    temp_data_z = corrz(i-window_size+1:i);
    mean_data_z(i)=mean(temp_data_z);
    std_z(i)=std(temp_data_z);
end

figure
hold on
plot3(start-window_size:point_freq:stop,signal_y(start-
window_size:point_freq:stop),...
    signal_z(start-window_size:point_freq:stop),'g.',...

start:stop+window_size,mean_data_y(start:stop+window_size),mean_d
ata_z(start:stop+window_size),'r--')

%plots circles

for i = start:circ_freq:stop+window_size
y=mean_data_y(i);                                %y-coordinate of
center of circle
z=mean_data_z(i);                                %z-coordinate of
center of circle
th = 0:pi/50:2*pi;
yunit = ry * cos(th) + y;
zunit = rz * sin(th) + z;
plot3(ones(1,length(zunit)).*i,yunit,zunit,'k');
end

%%%%%%%%%%%%%%%%%%%%%%%%%%%%%%%%%%%%%%%%%%%%%%%%%%%%
xlabel('time [s]')
ylabel([signal_description_y])
zlabel([signal_description_z])
legend('Data','Sliding Mean Tuple Center','Tuple')
axis([-inf,inf,1040,1180,2000,2200])
grid on

% REGRESSION (MINIMIZED LEAST SQUARES)

%Calculation of Trend Line

t = [start:stop];
tp = [start:stop+predict_length];
y = mean_data_y(start:stop);
z = mean_data_z(start:stop);
pyy = polyfit(t,y,order);
pzz = polyfit(t,z,order);
py = polyval(pyy,t);
pz = polyval(pzz,t);
pyp = polyval(pyy,tp);
pzp = polyval(pzz,tp);
```

```
% Plot of Data and Trend Line
figure
hold on
plot3(start:point_freq:stop,signal_y(start:point_freq:stop),signa
l_z(start:point_freq:stop),'.g')
plot3(tp,pyp,pzp);

% %plots circles
 for i = start:circ_freq:stop%+predict_length
 y=pyp(i-start+1);
%y-coordinate of center of circle
 z=pzp(i-start+1);
%z-coordinate of center of circle
 th = 0:pi/50:2*pi;
 yunit = ry * cos(th) + y;
 zunit = rz * sin(th) + z;
 %plot3(ones(1,length(zunit)).*i,yunit,zunit,'k');
 end
xlabel('time [s]')
ylabel([signal_description_y])
zlabel([signal_description_z])
%legend('Data','Minimized Least Squares Tuple Center','Tuple')
grid on
 axis([4000,9200,.15,.23,3000,3400])
```

Matlab Code For The Wavelet Method

```
 %%% Wavelet toolbox has been used

% Forecast of TRIT using Wavelets

clear all
clc
 load wavelet1   %%% load turbine inlet temperature
 S=signal(1:14400);
 [cA1,cD1] = dwt(S,'db2'); % take the wavelet transform of the
signal
 t=1:length(cA1);
 p=polyfit(t,cA1,2);       % perform least square fit
 y=polyval(p,7201:10999);
 cA2=[cA1 y];
%
 A1 = upcoef('a',cA2,'db2',1); % inverse wavelet tarnsform
%
 tt=1:length(A1);
 ttt=1:length(signal);
%
 figure (1)   % plot signal approximations and the signal

 plot(tt(1:100:length(tt)),A1(1:100:length(tt)),'--
',ttt(1:100:length(ttt)),signal(1:100:length(ttt)))
 axis([0,25000,2000,2050])
 xlabel ('Time (sec)')
 ylabel ('TRIT (K)')
```

```
%
 figure (2)   % plot the approximation coefficients
 plot(1:length(cA1),cA1)
 axis([0,8000,2840,2900])
 xlabel ('Time (sec)')
 ylabel ('Wavelet Coeff')

 figure (3)      % plot the signal approximations
 plot(1:length(A1),A1)
 axis([0,25000,2000,2050])
xlabel ('Time (sec)')
ylabel ('Approximation (F)')
%
 figure (4)   %%% plot the signal
 plot(1:length(signal),signal)
 axis([0,25000,2000,2050])
 xlabel ('Time (sec)')
 ylabel ('TRIT (K)')
```

GE 7EA gas turbine

Matlab Code for both the statistical method and the wavelet method

The following code uses the statistical and the wavelet toolboxes

```
%% load signalconcatenated (i.e load the required signal)
 %%%%%%%%%%%%%%%%%% Filtering
   for i=1:(length(tst4)-1)
       tstt1(1,i)=tst4(1,i+1)-tst4(1,i);
   end
% %  %%%%%%%% thresholding the filtered signal
  for i=1:length(tstt1)
      if tstt1(1,i)<6;
         tstt2(1,i)=tstt1(1,i);
          else tstt2(1,i)=0;
      end
  end
  for i=1:length(tstt2)
      if tstt2(1,i)>(-6);
          tstt3(1,i)=tstt2(1,i);
          else tstt3(1,i)=0;
      end
  end
% %
% % %   %%%%%%%%%%% Forecasting
% %  %%%%%%%%%%% wavelet method (use the wavelet toolbox)
  tstt4=tstt3(1:22000);
  %%%%%%%%%%%%%%% wavelet
   [cA1,cD1] = dwt(tstt4,'db4');
   ta=1:length(cA1);
   p=polyfit(ta,cA1,2);
   yy=polyval(p,length(cA1)+1:((length(tstt3))/2));
   cA2=[cA1 yy];
   A1 = upcoef('a',cA2,'db4',1);

  %%%%%%%%%%%%%%%%%%%%%%%%%%%%%%%%%%%%%%%%%%%% statistics
```

```
  tt=1:length(tstt4);
  p = polyfit(tt,tstt4,3);
  ttt=1:length(tstt3);
  yy=polyval(p,ttt);
% % %%%%%%%%%%%%%%%%%%%%%%%%%%%%%% statistical end


% % % % % %  %%%%%
plots%%%%%%%%%%%%%%%%%%%%%%%%%%%%%%%%%%%%%%%%%%%%%%%%%%%%%%%%
   figure (1)   (plots signal versus time)
   plot(1:length(pcd),pcd), grid on
   ylabel('Turbine Inlet Temperature')
   xlabel('Time (minutes)'),axis([0 60000 0 1000])

% % % % % %  %%%%%%%%%%%%%%%
   figure(2)  (plots concatenated signal versus time)
   plot(1:length(tst4),tst4),grid on
   ylabel('Turbine Inlet Temperature (C)')
   xlabel('Time (minutes)'),axis([0 32400 0 1000])

% % % % % %  %%%%%%%%%%%%%%%%%%%
   figure (3) (plots filtered signal versus time)
   plot(1:length(tstt3), tstt3),grid on
   ylabel('Turbine Inlet Temperature (C)')
   xlabel('Time (minutes)'),axis([0 32400 -10 10])

% % % % % %  %%%%%%%%%%%%%%%
   figure (4) (plots coefficients versus time)
  plot(1:length(cA1),cA1),grid on
  ylabel('Wavelet coeffecients (Turbine Inlet Temperature (C))
   xlabel('Time (minutes)'), axis([0 16500 -10 10])

% % % %   %%%%%%%%%%%%%%%%%%%%%%%
   figure (5) (plots spproximations versus time)
   plot(1:length(A1),A1),grid on
   ylabel('Signal approximation for Turbine Inlet Temperature
   xlabel('Time(minutes)'),axis([0 32400 -10 10])

% % % %   %%%%%%%%%%%%%%%%%%%%%%%
   figure (6) (plots forecast versus time)

plot(ttt,A1,1:100:length(ttt),,tstt3(1:100:length(tstt3))),grid
on
   ylabel('Turbine Inlet Temperature (C)')
   xlabel('Time (minutes)')
    axis([0 32400 -20 20]),legend('Forecast,Experimental data')
% % % % % % %%%%%%%%%%%%%%%%%%%%%%%
```

Appendix D Statistical and Wavelet Method Coefficients

Signal No.	Signal Description	Statistical Coefficients			
		a_{j_0}	a_{j_1}	a_{j_2}	a_{j_3}
1	T_{TT}	0.077	3.60e-5	3.40e-9	9.0e-14
2	T_G	0.16	-2.40e-4	1.10e-7	1.30e-9
3	T_{EX}	-0.078	3.8e-6	2.14e-8	4.14e-12
4	A_{GV}	-0.36	2.87e-5	4.04e-8	2.20e-12
5	A_{TV}	0.58	1.86e-4	1.58e-8	-3.19e-12

Table D.1. Regression coefficients for the statistical method for the five signals studied

Signal No.	Signal Description	Wavelet Coefficients		
		a_{j_0}	a_{j_1}	a_{j_2}
1	Turbine inlet temperature (T_{TT})	0.043	-2.53e-5	2.38e-8
2	Generator temperature (T_G)	0.20	-4.48e-4	1.33e-11
3	Exhaust temperature (T_{EX})	-0.11	1.92e-5	1.01e-7
4	Generator maximum vibration (A_{GV})	-0.14	4.96e-5	3.40e-9
5	Gas turbine maximum vibration (A_{TV})	0.90	-3.50e-4	2.82e-8

Table D.2. Regression coefficients for the wavelet method for the five signals studied

REFERENCES

Aboufadel, E., and Schlicker, S., *"Discovering Wavelets"*, Wiley Interscience: New York, 1999.

Addison, P., "*The Illustrated Wavelet Transform Handbook*", Institute of Physics Publishing: Philadelphia, 2002.

Agrawal, R., and Yunis, M., "A Generalized Mathematical Model to Estimate Gas Turbine Starting Characteristics", *Journal of Engineering for Power*, vol. 104, no. 1, pp. 194-201, January 1982.

Ailer, P., Santa, I., Szederkenyi, G., and Hangos, M., "Nonlinear Model-Building of A Low-Power Gas Turbine", *Periodica Polytechnica Ser. Transp. Eng*., vol. 29, no. 1-2, pp. 117-135, October 2001.

Atlas, L., Bloor, G., Brotherton, T., Howard, L., Jaw, L., Kacprzynski, G., Karsai, G., Mackey, R., Mesick, J., Reuter, R., and Roemer, M., "An Evolvable Tri-Reasoner IVHM System", proceedings of the IEEE Aerospace Conference, vol. 6, pp. 63023-63037, Big Sky, MT, March 2001.

Barlas, I., Zhang, G., Propes, N., and Vachtsevanos, G., "Addressing Uncertainty and Confidence in Prognosis", proceedings of the ASNE Intelligent Ship Symposium, Philadelphia, PA, April 2003.

Bassily, H., and Wagner, J., "A Stochastic Approach to Dynamic System Modeling with Application to Gas Turbines", proceedings of the ASME IMECE Conference, IMECE 2005-79385, Orlando, FL, November 2005.

Bettocchi, R., Spina, P., and Fabri, F., "Dynamic Modeling of Single Shaft Industrial Gas Turbine", proceedings of International Gas Turbine and Aeroengine Congress, 96-GT-332, Birmingham, UK, June 1996.

Boyce, M., "*Gas Turbine Engineering Handbook*", Gulf Publishing Company: Houston, 2005.

Brotherton, T., Jahns, G., Jacobs, J., and Wroblewski, D., "Prognosis of Faults in Gas Turbine Engines", proceedings IEEE Aerospace Conference, vol. 6, pp. 163-171, Big Sky, MT, March 2000.

Byington, C., Roemer, M., and Galie, T., "Prognostic Enhancements to Diagnostic Systems for Improved Condition-Based Maintenance", proceedings of the IEEE Aerospace Conference, vol. 6, pp. 2815-2824.

Crosa, G., Pittaluga, F., Trucco, A., Beltrami, F., Torelli, A., and Traverso, F., "Heavy-Duty Gas Turbine Plant Aero Thermodynamic Simulation Using Simulink", proceedings of the 1996 ASME Turbo Asia Conference, pp. 1-8, Jakarta, Indonesia, November 1996.

Camporeale, S., Fortunato, B., Mastrovito, M., "A High-Fidelity Real-Time Simulation Code of Gas Turbine Dynamics For Control Applications", proceedings of the ASME Turbo Expo Conference, vol. 2A, pp. 169-182, Amsterdam, The Netherlands, June 2002.

Camporeale, S., Fortunato, B., Dumas, A., " Dynamic Modeling and Control of Regenerative Gas Turbine", proceedings of the International gas Turbine and Aeroengine Congress and Exhibition, 98-GT-172, Stockholm, Sweden, June 1998.

Daubechies, I., "*Ten Lectures on Wavelets*", Society for Industrial and Applied Mathematics: Philadelphia, 1992.

Feng, C., Yu, Z., and Kusiak, A., "Selection and Validation of Predictive Regression and Neural Network Models Based on Designed Experiments", *IIE Transactions,* vol. 38, no.1, pp. 13-23, January 2006.

Greitzer, F., and Ferryman, T., "Predicting Remaining Life of Mechanical Systems", proceedings of the ASNE Intelligent Ship Symposium, Philadelphia, PA, April 2003.

Gulen, S., Griffin, P., and Paolucci, S., "Real-Time on Line Performance Diagnostics of Heavy-Duty Industrial Gas Turbines", *Journal of Engineering for Gas Turbine and Power,* vol. 124, no. 4, pp. 910-921, October 2002.

Guo, J., Chen, Q., Hu, W., Xu, S., "Nonlinear Generalized Predictive Control Based on Inverse System Using Wavelet Networks", proceedings of the International Conference on Wavelet Analysis and Its Applications, vol. 2, pp. 883-889, China, May 2003.

Howell, J. R., and Buckius, R. O., *"Fundamentals of Engineering Thermodynamics",* McGraw-Hill: Columbus, 1987.

Huang, D., and Jin, Y., "Application of Wavelet Neural Networks to Nonlinear Predictive Control", proceedings of the IEEE International Conference on Neural Networks, vol. 2, pp. 724-727, Houston, TX, June 1997.

Jardim, R., Barata, M., Assis, L., Alavro, J., and Garcao, A., "Application of Stochastic Modelling to Support Predictive Maintenance for Industrial Environments", proceedings of the IEEE International Conference on Systems, Man and Cybernetics, vol. 1, pp. 117-122 , Beijing, China, October 1996.

Kacprzynski, G., Roemer, M., Modgil, G., and Palladino, A., "Enhancement of Physics of Failure Models with System Level Features", proceedings of the IEEE Aerospace Conference, vol. 6, pp. 2919-2925, Big Sky, MT, March 2002.

Kikstra, J., and Verkooijen, A., "Dynamic Modeling of a Cogeneration Nuclear Gas Turbine Plant Part 1: Modeling and Validation", *Journal of Engineering for Gas Turbine and Power*, vol. 124, no. 3, pp. 725-733, July 2002.

Korakiantitis, T., Hochstein, J., and Zou, D., "Prediction of the Transient Thermodynamic Response of A Closed Cycle Regenerative Gas Turbine", proceedings of the International Gas Turbine and Aeroengine Congress and Exposition, 93-GT-136, Cincinnati, OH, May 1993.

Krikelis, N. J., and Papadakis, F., "Gas Turbine Modeling Using Pseudo-Bond Graphs", *International Journal of System Science*, vol.19, no. 4, pp. 537-550, April 1988.

Langston, S., "New Horizons", *ASME Power and Energy Magazine*, vol. 2, no. 2, June 2005.

Lebold, M., McClintic, K., Campbell, R., Byington, C., and Maynard, K., "Review of Vibration Analysis Methods for Gearbox Diagnostics and Prognostics", proceedings of the 54th Meeting of the Society for Machinery Failure Prevention Technology, pp. 623-634, Virginia Beach, VA, May 2000.

McAlpin, R., Tally, P., Bernstein, H., and Holm, R., "Failure Analysis of Inlet Guide Vanes", *Journal of Engineering for Gas Turbines and Power*, vol. 125, no. 1, pp. 236-240, January 2003.

Montgomery, D., and Friedman, D., "Prediction Using Regression Models with Multicollinear Predictor Variables", *IIE Transactions*, vol. 25, no. 3, pp. 73-85, May 1993.

Nava, P., Quercioli, V., and Mammoli, T., "Dynamic Model of a Two Shaft Heavy-Duty Gas Turbine with Variable Geometry", proceedings of International Gas Turbine and Aeroengine Congress, 95-GT-348, Houston, TX, June 1995.

Orsagh, R., Roemer, M., Sheldon, J., and Klenke, C., "A Comprehensive Prognostics Approach for Predicting Gas Turbine Engine Bearing Life", proceedings of ASME Turbo Expo, vol. 7, pp. 777-785, Vienna, Austria, June 2004.

Pawlowski, R., and Greitzer, F., "Embedded Prognostics Health Monitoring", proceedings of the International Instrumentation Symposium, vol. 48, pp. 301-310, San Diego, CA, May 2002.

Rowen, W. I., "Simplified Mathematical Representations of Single Shaft Gas Turbines in Mechanical Drive Service", proceedings of International Gas Turbine and Aeroengine Congress, 92-GT-22, Cologne, Germany, June 1992.

Sarvanamuttoo, H. I. H., Rogers, G. F. C., and Cohen, H., *"Gas Turbine Theory"*, Pearson Education: Upper Saddle River, 2001.

Schneider, A., Landgren, G., and Bhavaraju, M., "Analysis and Prediction of Transmission Unit Performance Using Advanced Regression Models", *IEEE Transactions on Power Apparatus and Systems*, vol. 104, no. 5, pp. 1084-1094, May 1985.

Schwabacher, M., "A Survey of Data Driven Prognostics", proceedings of the American Institue of Aeronautics and Astronautics Conference, AIAA 2005-7002, Arlington, VA, September 2005.

Sekhon, R., Bassily, H., and Wagner, J., "Real Time Prognostic Strategies with Application to Stationary Gas Turbines", proceedings of the ASME IMECE Conference, IMECE 2006-14068, Chicago, IL, November 2006.

Sekhon, R., Bassily, H., Wagner, J., and Gaddis, J., "Stationary Gas Turbines – A Real Time Dynamic Model with Experimental Validation", proceedings of the American Control Conference, WEC13.1, pp. 1838-1844, Minneapolis, MN, June 2006.

Sulieman, H., McLellan, P., and Bacon, D., "A Profile-Based Approach to Parametric Sensitivity Analysis of Nonlinear Regression Models", *Technometrics*, vol. 43, no. 4, pp. 425-433, November 2001.

Sun, Z., Wang, R., Jiang, X., and Xu, M., "Application of Wavelet Transform to Recursive Prediction of Vibration Signals", *Journal of Harbin Institute of Technology*, vol. 12, no. 5, pp. 483-493, October 2005.

Kim, J., Song, T., Kim, T., and Ro, S., " Model Development and Simulation of Transient Behavior of Heavy Duty Gas Turbines", *Journal of Engineering for Gas Turbines and Power*, vol. 123, no. 3, pp. 589-594.

Thomson, B., “Basic Transient Effects of Aero Gas Turbines”, proceedings of AGARD, no. 15, paper no. 2, pp. 2-1 to 2-15, Ustaoset, Norway, September 1974.

Veer, T., Haglerod, K., and Bolland, O., “Measured Data Correction for Improved Fouling and Degradation Analysis of Offshore Gas Turbines”, proceedings of the ASME Turbo Expo, vol. 7, pp. 823-830, Vienna, Austria, June 2004.

Vroemen, B., Essen, H., Steenhoven, A., and Kok, J., “Nonlinear Model Predictive Control of A Laboratory Gas Turbine Installation”, proceedings of the International Gas Turbine and Aeroengine Congress and Exhibition, 98-GT-100, Stockholm, Sweden, June 1998.

Walsh, P., and Fletcher, P., *"Gas Turbine Performance”*, Blackwell Publishing: Malden, 2004.

Wang, P., and Vachtsevanos G., “Fault Prognosis Using Dynamic Wavelet Neural Networks”, *Journal of Artificial Intelligence and Intelligent Design, Analysis and Manufacturing,* vol. 15, no. 4, pp. 349- 365, September 2001